Author:
Wang, Wei-Ting

Title:
Effect of Direct Deposition of Dry Particle Tougheners on the Processability and Forming Quality of Carbon Fibre Epoxy

EFFECT OF DIRECT DEPOSITION OF DRY PARTICLE TOUGHENERS ON THE PROCESSABILITY AND FORMING QUALITY OF CARBON FIBRE/EPOXY PREPREGS

Wei-Ting Wang

A dissertation submitted to the University of Bristol in accordance with the requirements for award of the degree of Doctor of Philosophy in the Faculty of Engineering

November 2019

Word Count: 30,182

Effective of Direct Deposition of Dry Particle Tougheners on the Processability and Forming Quality of Carbon Fibre/Epoxy Composite Prepreg – WeiTing Wang - 2019

ABSTRACT

Prepreg-based high performance composite parts require the use of a material with not only good mechanical properties of both fibre reinforcement and polymer matrix, but also good processability and formability into desired shapes without quality issues. Among various mechanical properties of interest, delamination resistance has been one of the major requirements for aerospace composite components, especially for the primary load bearing parts. Interlaminar toughening by interleaving methods is an effective way to improve the delamination resistance. One of the most cost-effective toughening methods is incorporating thermoplastic microparticles within the matrix, which can significantly improve the fracture toughness of the laminate by crack deflection and particle bridging. Most previous studies have mainly focused on the toughening effect and mechanisms of laminates interleaved with various particle materials. However, their impact on the processability of composites has not been well investigated yet.

In this work, a method of directly depositing dry polyamide particles on prepreg materials was used as an alternative to conventional interlaminar toughening methods. The aim of this work was to investigate the effect of particle's physical parameters (e.g. sizes, shapes and amount) on both the toughening effect and the material processability and formability.

This thesis includes three parts. The first part presents the fracture toughness of laminated composites interleaved with a range of toughening materials. The effect of physical characteristics of the particles and processing conditions on interlaminar fracture toughness were discussed. The second part investigates the processability of the particle-toughened laminates in diaphragm forming and autoclave curing, which includes an in-depth investigation on the interply friction and the compaction behaviour of uncured prepreg stacks with interleaving particle toughеners. Finally, L-shaped composite beams interleaved with different toughеners were manufactured to validate the effect of the toughening materials on the forming and curing qualities in a diaphragm forming process followed by autoclave curing. The correlation between forming/curing and material characterisation results was discussed.

This work demonstrated that the direct particle deposition method is a very effective toughening method which could improve both the interlaminar fracture toughness and the processability of prepregs. It was also found that careful selection of a suitable particle type considering its impact on material processability would be important, otherwise the toughening effect might counteract the manufacturing quality.

DEDICATIONS

To my parents Ken-Pen Wang and Yeng-Pen Chen.

ACKNOWLEDGEMENTS

Many people have been contributed to my PhD study. First, I would like to express my sincere gratitude to my supervisors Dr Byung Chul Kim and Dr HaNa Yu. I really appreciate your help and support on teaching me new skills in the first year of my PhD, and the guidance when I face crucial stages during the research. I also like to thank Professor Kevin Potter, who provided useful feedback on my publications.

Second, I would like to acknowledge ACCIS CDT and the support from EPSRC. This postgraduate course not only gave me the opportunity to involve in diverse engineering fields, learning different skills, also allow me to involve in the multicultural working environment. This is a very valuable experience to me. I would like to thank my CDT14 colleagues and Rico Kuehlewind, you all helped me a lot on the exams that I was not good at in the taught year.

Apart from the PhD research, I would like to thank my supervisor Dr Kim who offered me some work on other short projects, which was good learning chance. Professor Paul Waver and Sarah Hallworth who offered me to be the photographer/videographer in ACCIS, which I was really enjoyed.

Finally, I specially would like to say thank you to my parents Ken-Pen Wang, Yeng-Pen Chen, and my girlfriend Chih-Ying Huang, for your support throughout my study in the UK.

DECLARATION

I declare that the work in this dissertation was carried out in accordance with the requirements of the University's *Regulations and Code of Practice for Research Degree Programmes* and that it has not been submitted for any other academic award. Except where indicated by specific reference in the text, the work is the candidate's own work. Work done in collaboration with, or with the assistance of, others, is indicated as such. Any views expressed in the dissertation are those of the author.

SIGNED: ..... DATE:.....

CONTENTS

LIST OF TABLES

LIST OF FIGURES

1 INTRODUCTION

1.1 Background

Fibre reinforced composite is an ideal material for weight critical high-performance parts due to their high specific stiffness and strength. Nowadays, for some latest civil aircraft, 50% or more of the total weight is made of composite materials. In the meantime, as the commercial composite market is growing rapidly, aerospace manufacturers and airliners are looking for solutions to reduce the costs for production and operation. From a material perspective, developing stronger and tougher composites allows for reducing the maintenance costs for repairs and part replacements. From a manufacturing perspective, improved processing efficiency such as production rate and manufacturing quality is also important to reduce the cost and meet the growing demand in the market.

Although automation technologies have been widely adopted in composites production, there are still fundamental limitations. Currently, ply-by-ply lay-up is still a widely used processing method for composite part manufacture. Although automation technologies have been used, the lay-up process is still time-consuming especially for the parts with relatively complex geometries. The processing time could be reduced by adopting forming techniques such as diaphragm or hot drape forming; however, the manufacturable part geometries are limited. Furthermore, the processing window is known to be sensitive to the stacking sequences and manufacturing conditions. Especially, the interleaving thermoplastic microparticle layer on prepreg surface could increase the interply friction [1], which limits the processing rate and manufacturable part geometries due to the ply wrinkling in the forming processes. The particle layer may also affect the bulk factor of uncured preform [2]. The impregnation in prepregging process can be affected by the inclusion of particles due to the increased resin viscosity, particularly when using nanoparticles. This could increase the required manufacturing time or more processing steps to create the particle rich layer on the prepreg surface. These impacts inevitably increase cycle time and manufacturing costs, which is undesirable to the cost-sensitive commercial aerospace composite markets.

This PhD thesis was to provide an in-depth investigation on the processability of laminated composites interleaved with various of different thermoplastic particles and a nonwoven veil. Their influence on the formability and curing quality were experimentally studied through interply friction and compaction tests, as well as manufacturing trials. Based on the results, a guideline to choose an optimal toughening material and processing condition was provided.

1.2 Literature review

1.2.1 Toughening composite laminate using interleaving methods

Despite the many advantages of using high performance fibre reinforced composites for weight critical parts, one of the main concerns is their poor damage tolerance, which can cause large area delamination resulting in a catastrophic failure.

The interlaminar toughness of laminated composites can be improved by introducing through-thickness reinforcement (e.g. z-pinning and tufting) [3,4], or by modifying the matrix material, which has been the main focus in many previous studies. The aim of matrix modification is to increase the required energy for crack propagation by pinning or deflection crack [5,6], usually involves incorporation of rigid particles [7,8] or ductile materials such as elastomers [9,10] or thermoplastics [11–13] with thermoset resin matrix at a molecular level, which provides significant improvement of the fracture toughness of the matrix. However, an effective toughener for bulk resin does not always offer a similar improvement when used within laminated composites, as the interlaminar resin layer thickness is usually too small to fully develop plastic deformation at the crack tip [14]. This local deformation is an important energy absorption mechanism preventing crack propagation in a bulk polymer. Sela et al. [15] reported that a slightly thicker resin layer can be beneficial to the interlaminar fracture toughness. They also proposed that toughening critical regions locally could be useful to reduce stress concentration near the structurally discontinuous locations such as joints in various of composite applications [16].

1.2.1.1 Toughening by interleaving particles

Interleaving a composite laminate with thermoplastic micro-particles is known as an effective interlaminar toughening method [17–22], as the inclusion of secondary particle material allows for crack deflection [6] and bridging [23] promoting the fracture energy absorption mechanism during crack propagation.

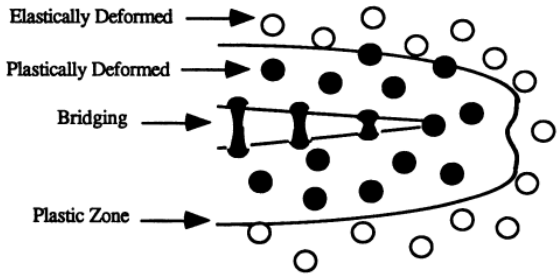

Figure 1-1 Schematic diagram of thermoplastic toughening mechanisms in bulk resin [13]

Particle bridging (Figure 1-1) is commonly observed when ductile materials are used as particle tougheners in bulk polymers. This mechanism allows for stable crack propagation and reduces stress concentration at the crack tip [12,23]. Particle bridging effect requires a good particle-matrix bonding [24]. This adhesion can be achieved by promoting chemical bonding or creating molecular entanglements between the two materials. Nichols *et al*. [25] stressed that the development of the interphase between poly-butylene-terephthalate (PBT) and epoxy molecules is more important than the dispersion of PBT in the epoxy. This molecular entanglement is also referred to as a semi-interpenetrating network (semi-IPN), which can significantly affect the fracture toughness of a modified epoxy resin system [26].

The development of semi-IPN structure requires both material phases in a gel state, which is temperature dependent. Kim et al. [26] have mixed polyamide 6 particles with an epoxy resin at different temperatures, and then introduced the curing agent to initiate consolidation. They found the Mode-I fracture toughness, G_{IC}, was improved when the mixing temperature was close to the melting point of polyamide 6, but the modulus and yield strength remained unaffected. They found that the morphology of fractured particles changed depending on the mixing temperature. They also reported the

chemical reaction between an amine cured epoxy and polyamide 6 particles contributed to the interfacial bonding strength. Park et al. [27] interleaved a 120°C amine cured carbon/epoxy prepreg laminate with 20 μm polyamide 6 particles, and found the particles were debonded from the resin and the G_{IC} was not affected by varying the particle amount. Paris [28] reported the G_{IC} of M21/T700 composite was approximately 0.36 kJ/m^2 when consolidating at normal 180 °C curing temperature. However, this value was nearly doubled by implementing a higher curing temperature (210°C). Although the exact polyamide type used for the particles in M21 resin was not mentioned from the manufacturer, the toughness improvement could attribute to the melting point of the particles. The crack shifted from the interlaminar region to the fibre layer was observed when change the processing temperature [29].

Zeng et al. [22] investigated the toughening of dicyanate matrix composites using polyamide 6 particles. They observed that the Mode-I fracture toughness was unaffected, but Mode-II fracture toughness affected by the amount of particles. Groleau et al. [17] premixed polyamide 12 particles into three different composites whose resin matrices had different levels of ductility. The particles and matrix formed good bonding. For the highly cross-linked brittle resin systems they used, the particle deformation and bridging were the main mechanisms that improved the Mode-II fracture toughness. This mechanism would require micro-crack initiation at toughening particles in order to resist delamination. They concluded that the interlayer thickness was important to Mode-II fracture toughness. However, this depends on the amount of particles or the particle size, which was not rigorously investigated in their work. Hillermeier et al. [20] modified epoxy tackifier incorporated with polyamide 6 particles. The modified tackifier was applied to the carbon fabrics surface by dry and wet spray methods. The Mode-II fracture toughness was improved by approximately 30% for the sample with the tackifier using wet spray method, because of the more uniform toughening layer. Yasaee et al. [18] studied the toughening effect of composites interleaved with polyamide 6 and polyamide 12 particles. They reported that these particle-toughened samples exhibited lower G_{IC} propagation, which was attributed to the limited fibre bridging effect due to the particle layers at the interlaminar regions.

Toughening by interleaving particles has been patented [30,31] and special prepreg resin systems taking advantage of such a mechanism are commercially available; for example, Hexcel M21 and Toray 3900-2 prepreg resin include polyamide particles as tougheners [21,28].

Table 1-1 Summary of laminated composites toughened by interleaving materials in some literatures

Test methods	Toughener			Composite manufacture method	Results	Reference
	Toughener material	Manufacturing method	Particle size, areal weight, interlayer			
Impact strength	PEI	Premixed	-	CF/Epoxy, VARTM	Impact +59%	He, 2013 [32]
	PC				Impact +39%	
	PBT				Impact +29%	
CAI, indent	Thermoplastic particles	Spread on prepreg	~40 μm, 2 gsm* Interlayer 20-30 μm	CF/EP, UD	Average threshold energy of delamination +29.9 ~ 39.8%	Gao,2005 [33]
DCB, ENF	Polyamide 6	Spread on prepreg	20 μm, 4-25.5 gsm*	CF/EP, woven	G_{IC} ±0 Small G_{IIC} improvement with particle amount	Park, 1997 [27]
	Kevlar short fibres		6 mm long		G_{IIC} +370%	
	Polyamide + Kevlar fibres				G_{IIC} +310%	
DCB, ENF	Polyamide-6 particles	Spread on prepreg	20 μm	GF/EP, UD	G_{IC} +50%	Yasaee, 2012 [18]
	Polyamide-12 particles		30 μm		G_{IC} +75%	
DCB, ENF, CAI	Rubber based particles	Premixed	~50 μm	CF/EP, UD	G_{IC}+70%, G_{IIC}+250% CAI+38%, damage area -82%	Gilbert, 2003 [19]
ENF, ILSS	Polyamide-6	Spread on prepreg using tackifier	22 μm	CF/EP, woven, RTM	G_{IC} ±0, G_{IIC}+30%, ILSS slightly reduced, compression ±0%	Hillermeier, 2001 [20]
DCB	Polyamide particles	Toughened prepreg system	-	CF/EP, UD	G_{IC} +160-350%	Hojo, 2005 [21]
ELS	Polyamide-12 particles	Premixed, powder prepregging	20, 30, 50 μm Interlayer 8-60 μm	CF/EP, UD/fabric	Brittle resin system G_{IIC} +45%	Groleau, 1996 [17]
DCB, ENF	Polyamide-6 particles	Premixed	20 μm	CF/dicyanate resin	G_{IC} ±0%, G_{IIC} + 200%	Zeng, 1993 [22]
DCB, ENF	Rubber particles, core-shell particles	Adhesive film	50 μm, 0.3 μm	Woven prepreg	G_{IC} +100 ~ 200%	Hayes, 2002 [34]
DCB, ILSS, CAI	Polysulphone particles (rigid polymer)	Spread on prepregs	40, 80 μm	CF/EP, BMI, Cyanate	G_{IC} +84%, ILSS ±0%, CIA +17%, damage area -59%	MeGrail and Jenkins, 1993 [35]

*gsm = g/m^2

The fabrication of commercial particle toughened prepreg systems involves pre-mixing particles with the liquid resin, followed by powder prepregging [17] or single/double pass impregnation methods [19] to create a particle rich surface on the prepreg. In this process, the amount of the employed particles is inevitably limited due to the increased resin viscosity. In lab-scale manufacturing methods, directly applying particles on the prepreg surface have been used [18,20,27,33,35,36]. However, the uniformity of particle layer could be difficult to control, which could affect the toughening effect [20]. A summary of composites toughened by interleaving materials is shown in-Table 1-1.

1.2.2 Forming defects

Manufacturing quality of a composite part is closely related to the processing characteristics of the composite material. Particularly for the prepreg-based manufacturing processes, the viscoelastic behaviour of the epoxy matrix during the process is one of the most critical aspects. Introducing toughening particles in the resin matrix can change the behaviour of the resin matrix during processing. Such a change could negatively affect the processing conditions.

In the overall manufacturing processes, composite material is subjected to a various of deformations in different stages. Preforming and curing are the two processes that will induce the most significant shape change and deformation of material. If the chosen materials cannot adapt to such a change properly, defects can be generated during the processes, which causes quality issue and can further influence the structural integrity and mechanical performance of composite parts [37–39]. Therefore, it is necessary to understand the defect generation mechanisms in order to minimise or even overcome this issue.

Ply-by-ply lay-up is known as a time-consuming process. Although automation technologies such as automated tape laying (ATL) and automated fibre placement (AFP) are introduced to the commercial aerospace manufacturer, the processing speed and achievable geometries are still limited especially for directly lay-up on a 3D tool surface.

In general, forming is a mass production technique that can create a complex shape from a flat sheet material in a short time. This technique is also used in composites

industry, which usually refer to single/double diaphragm forming (SDF/DDF) and stamp forming [40], but with some modifications. In these methods, a flat prepreg stack is created first, then is deformed into a desired shape using external pressure, which generates a 'preform' prior to a follow-up consolidation process.

The difference between forming methods is shown in Figure 1-2. SDF uses a single diaphragm and vacuum pressure to create the preform. DDF has the same approach as SDF but the prepreg stack is sandwiched by two diaphragms, which helps to handle a large preform and to position materials that has weak interlaminar bonding such as dry fabrics or thermoplastic prepregs before melting. The stamp forming deforms the material using mechanical force from the upper mould. In terms of manufacturing cost, diaphragm forming has a great advantage over stamp forming in manufacturing large composite parts, as using upper mould will require a large hydraulic press and significant energy for heating in the process, also the tooling costs can be expensive.

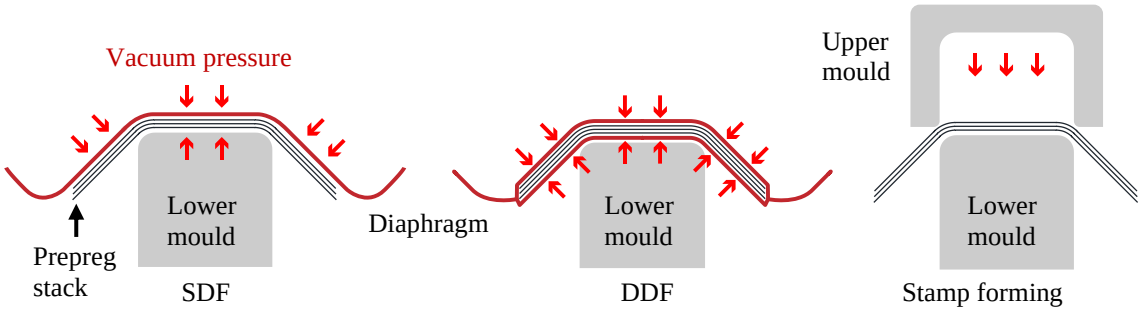

Figure 1-2 Single diaphragm forming (SDF), double diaphragm forming (DDF) and stamp forming.

Forming a flat prepreg stack into a desired 3D shape requires sufficient material deformation caused by the generated in-plane and out-of-plane shear stresses during the process [40–43]. However, the friction between fibres or plies generates local tensile and compressive forces in the prepreg stack. When the compressive force developed within the stack is greater than its buckling strength, ply wrinkling can be generated during forming [44].

Understanding interply shear behaviour is important to achieve high forming quality, because it is unavoidable phenomena when creating a 3D geometry with 2D materials. Figure 1-3 demonstrates a simple forming case; folding a stack of prepregs over a radius

to create a L-shaped part. Ideally each ply should be able to slip against its adjacent ply by a small distance to accommodate the change of the arc length over the laminate thickness (Figure 1-3a), but if the interply slip resistance is too high, wrinkling can occur at the inner plies due to the developed compressive force (Figure 1-3b).

Avoiding critical process conditions was the main goal of most of the previous researches. This was usually through characterising the interply [1,43,45,46] and in-plane [47–50] shear properties for simulation [48,51–54] to determine the processing window.

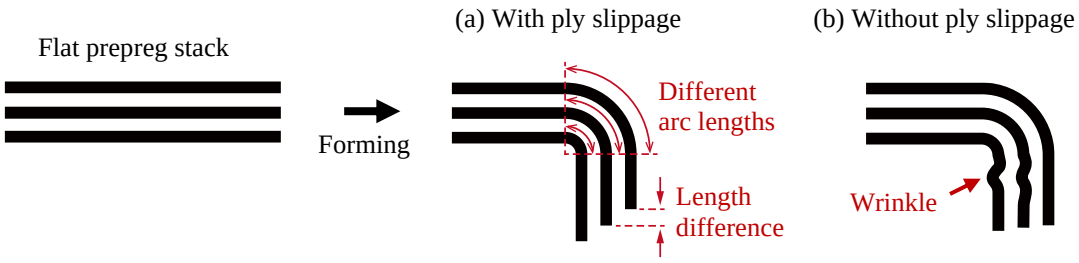

Figure 1-3 Cross-section view of the deformation mechanism of prepreg stack

In processing prepreg materials, because the surface of fibres is usually covered by the uncured resin, the frictional resistance mainly comes from the resistance of shearing the resin layer at ply interfaces and between fibres. Equation 1-1 describes the dynamic friction of two surfaces separated by a thin viscous layer without considering the surface roughness. The τ is shear stress, η(T) is temperature dependent viscosity of the resin, γ is shear rate, which is defined by the thickness of the viscous fluid layer, h, and the lateral velocity, v.

$$\boldsymbol{\tau = \dot{\gamma}\eta(T) = \frac{v}{h}\eta(T)} \qquad \textbf{Equation 1-1}$$

As shown in the Equation 1-1, the processing temperature and rate have significant influence for both thermoplastic and thermoset prepreg systems [45,49,50,55–60]. Insufficient temperature or high processing speed can negatively impact the formability, resulting in undesirable wrinkles [61,62]. Although processing at an elevated temperature helps to promote interply shear deformation, it weakens the integrity of the

fibres along the transverse direction and may increase the instability of the plies [63], which risks ply buckling or splitting of unidirectional fibre bed in the preform.

The interply friction is also affected by the condition of the ply interface. The stacking angle between two unidirectional plies in contact has shown to affect the frictional properties [64,65]. Erland et al. [66] reported that such an effect is due to the fluid dynamics of the viscous resin at the interlayer during the ply slippage, as described below. When the fibre orientation is the same for both plies, the lubrication effect of the resin layer contributes to decreasing the out-of-plane shear stiffness at the initial ply slippage. However, while the slippage progresses, the applied normal pressure promotes more fibre-fibre contact. Although the fibre deformation and the resin redistribution under pressure were ignored in the assumption, the result was agreed with their experiment finding to some extent. They found that 0°-0° ply contact exhibited greater shear stiffness than angled ply contact, as the former case can achieve a higher fibre packing density (Figure 1-4).

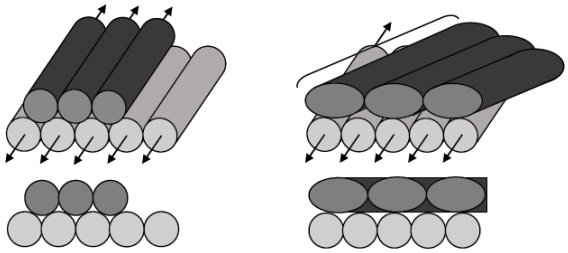

Figure 1-4 Fibre packing between 0°-0° and 0°-45° interfaces [66]

Since interlaminar toughening became more popular toughening method, more researchers have studied on the influence of the introduced interleaving materials on the interlaminar shear properties. Larberg et al. [1] investigated the interply friction behaviour of a few different thermoset prepregs including M21/T700 prepreg, which is a carbon/epoxy prepreg system that has a particle-rich resin layer on the surface. At processing temperatures resulting in a similar resin viscosity range, particle toughened prepreg exhibited a higher interply frictional force compared to standard prepreg systems, and the effect of shear rate on frictional coefficient varied. This implies that the toughening particles at the interlayer affects the interply shear behaviour and may impact its formability to a greater extent than standard prepreg systems. The later study

showed a laminate interleaved with carbon nanotubes also significantly increases interply friction [67].

1.2.2.1 Defects during consolidation

Many thermoset matrix composites used for aerospace applications are cured using autoclave to achieve a high fibre volume fraction and a low void content, as the uniform and high air pressure allows resin redistribution at the initial curing stage before consolidation begins. However, the internal resin flow accompanying with fibre movement sometimes causes corner thinning, or generates ply wrinkles when the part has a sharp corner or curvature [68–72].

The fibre bed compaction behaviour is dependent on the fibre architecture in a laminate such as the format of textile, number of layers, fibre orientations and lay-up methods. These parameters define the final packing configuration of fibre bed and the density of fibre bed [73–76], which affects the resin flow within the laminate under external pressure.

Resin flow in a laminate can be explained by shear flow and squeeze flow [77]. Normally shear flow is used to describe the flow of resin with high viscosity, where the fibre position can be moved by the flow; while in a squeeze flow model, which is commonly used for low viscosity resin such as thermoset matrix. The model includes fibre bed compaction behaviour, fibre bed permeability and resin flow model (based on Darcy's Law). A better fibre alignment leads to less structural relaxation of the fibre bed. Li et al. [78] investigated the compression behaviour of different unidirectional fibre beds impregnated with low viscosity fluids. They reported that a laminate formed with cross-plies was more difficult to compress than that of with 0° lay-up. A 'compressibility index' was used in their work to determine the level of compaction between different stacking sequences.

Many of new generation prepreg systems are toughened with thermoplastic microparticles. As discussed in Section 1.2.1, these tougheners are located between fibre layers to enhance the delamination resistance of composites, but could change the compaction behaviour of a preform when the preform is under compressive pressure [2,69,79–82]. Hall et al. [79] investigated the temperature effect on the thickness change and in-plane expansion of uncured IM7/M21 laminate during compaction. They found

that interply shear and resin bleed were the main cause of the thickness reduction in cross-ply laminates; while in all 0° stacking sequence, fibre bed spreading was obvious, which resulted in significant in-plane expansion. Both behaviours were highly dependent on testing temperature. The material configuration in such a toughened prepreg system leads to a complex deformation response, which requires a combination of different models in order to describe the mechanism.

Hallander et al. [82] studied the manufacturing quality of a complex shaped composite spar. They found different level of corner thinning effect when the spar was partially interleaved with nonwoven veils or carbon nanotubes. Although the relationship between the interleaving tougheners and the level of corner thinning was not discussed in detail in their work, this observation implies interleaving materials could influence the thickness change of composites. Nixon-Pearson et al. [2] have compared two different prepreg systems; IM7/8552 without particle tougheners and IMA/M21 with particle tougheners only located at the interlaminar region. They observed that the particle layers in IMA/M21 separate fibre plies isolating their interaction under compression, which differently affected the compaction of the preforms depending on the stacking sequences. Belnoue et al. [80] developed a hyper-viscoelastic model to describe the resin flow behaviour under compaction, which showed good agreement with the experimental results in Nixon-Pearson's work. Their later work [69] experimentally demonstrated the consolidation-induced wrinkles in a tapered laminate have a notable relationship with the bulk factor of a laminate. Severe defects can be generated only with 5% of thickness change in a tapered laminate.

1.2.2.2 Minimise forming defects

Some previous works have investigated methods of minimising forming defects in manufacture without changing the basic processing parameters (i.e. temperature and rate). Truslow [83] investigated forming process for the Boeing 777 rib chord. A few techniques, were used in the diaphragm forming process to prevent ply buckling, which were generally external supports such as clamps, rigid bars or wires. However, the methods used were relatively complicated compared to the conventional diaphragm forming method.

Optimisating the stacking sequence for improving the formability of a prepreg preform has been investigated by Johnson et al. [84]. They suggested a ‘compatibility factor’ as a formability index calculated by their analytical model. They demonstrated that reducing the number of transitions from ±45° plies to 0° plies contributed to minimising the level of forming wrinkle of the beam geometry used in their work. This finding seemed to agree with previous studies done by Lightfoot et al. [85] and Hallander et al. [86], where ply wrinkles occurred more easily when the stacking sequence has 45°-0° interfaces. Sjölander et al. [51] showed that some wrinkles can be removed by cut off certain plies when forming a complex spar, as this created discontinue fibres that reduced in-plane shear stress during forming. However, this may negatively affect the mechanical performance of the part, and can generate different types of wrinkle.

The interply friction characteristics can be changed by including additional materials at ply interfaces. Potter [87] reported that the required bending force for an uncured UD laminate was decreased when the surface of each ply was coated with a layer of thermoplastic microparticles. This is caused by the reduced surface tack of prepreg that resulted in lower defect ranking. However, the particle-resin interaction and tackiness reduction mechanism were not further investigated. Hallander et al. [67,82] investigated the feasibility of locally tailoring the interply friction and in-plane shear characteristic of a prepreg stack by coating carbon nanotubes and thermoplastic nonwoven veils on prepreg surface, or applying pre-consolidation only to selected interfacial areas. This resulted in an improved forming quality of the complex spar geometry used in their work. These findings indicate that the forming behaviour can be affected when inclusion of additional materials at certain interfaces in a prepreg stack, which shown potential to improve composite forming quality.

1.2.3 Summary of review and research objectives

Methods of including thermoplastic microparticles in thermoset laminated composites have been widely applied to improve their poor interlaminar fracture toughness. Many composites manufacturing related works studied the commercially available particle-toughened prepreg systems, which are being limited used for special cases on the market, and the details of material information is nearly unavailable. Furthermore, most

of previous studies have focused mainly on the toughening effects without in-depth analyses on the impact on the material processibility.

The main focus of this research is to provide a more comprehensive study on the impact of interleaving materials on the laminated composites. The selected interleaving materials are a range of different thermoplastic microparticles, they have different physical characteristics such as shapes, sizes and surface morphologies. Their toughening effect were also discussed.

The main body of his PhD thesis includes six chapters. Chapter 2 presents the study on Mode-I fracture toughness of IM7/8552 composites toughened by a range of different polyamide particles. The toughening mechanisms and the effect from processing conditions are discussed. Chapter 3 to Chapter 6 presents processability related investigations. Chapter 3 provides the development details of a test rig developed in this work for processability characterisation. The design concept is to improve the quality of test results. This helps to further understand the mechanisms of interleaving materials behaviours in a preform during different processing stages. Chapter 4 investigates the interply friction of uncured prepreg plies coated with different toughening materials at the interface. The test parameters used was for simulating different processing scenarios, which includes single diaphragm forming, double diaphragm forming, as well as cold forming conditions. Chapter 5 presents the compaction behaviour of preforms interleaved with the toughening materials. The investigation focuses on the rearrangement of toughening materials under high compaction pressure. Finally, Chapter 6 demonstrates composite processing quality by manufacturing thick L-shaped composite beams using a single diaphragm forming method and autoclave curing. The samples were interleaved with selected toughening materials and formed at different temperatures. The observed manufacturing quality is correlated with the characterisation studies in the previous chapters.

2 FRACTURE TOUGHNESS OF CARBON/EPOXY COMPOSITES INTERLEAVED WITH POLYAMIDE PARTICLES

Fracture toughness is a mechanical property that indicates the damage tolerance of laminated composite materials, which is important for high performance composites in aerospace applications. There are several approaches to improve the toughness of composites, but incorporating laminate with thermoplastic particles is known as a cost-effective method to. In this method, the particles are included at the interlaminar region, the particles absorb crack propagation energy that resulting in higher toughness. However, the toughening effect can be affected by many parameters, which includes the types, sizes and the amount of particles, as well as the used processing conditions.

In this chapter, the Mode-I fracture toughness of carbon fibre/epoxy composites were experimentally studied. The composites were interleaved with a range of polyamide microparticles that have various sizes, shapes and surface morphologies, and then consolidated using different temperatures. Differently from conventional methods of pre-mixing the particles with the matrix resin before the prepreging process, the particles were directly deposited on the prepreg surface before lay-up. The toughening effect and failure mechanisms were investigated and discussed in this chapter.

2.1 Experimental

2.1.1 Materials

The prepreg material used in this work was HexPly® IM7/8552 (Hexcel, US), which is made of a 180°C amine-cured epoxy resin system and intermediate modulus carbon fibres, IM7 (Tohotanex, JP). The resin system was modified with poly-ethersulfone (PES) [88]. The 0° and 90° tensile moduli are 164 GPa and 12 GPa [89], respectively. Five types of polyamide particles with different sizes and shapes were used in this work, as listed in Table 2-1.

The material ID was given based on the material type and particle diameter. The particle surface morphology was categorised by smooth (-s), rough (-r) and arbitrary shape (-a). The PA12-d5s and PA12-d10s are spherical particles and have smooth particle surfaces, while the PA6-d13r has a higher surface area due to its rough surface. The PA6-d16a and PA12-d30a have irregular shapes, as shown in Table 2-1. Polyamide 12 has a melting point similar to the recommended curing temperature of the 8552 resin, while the polyamide 6's is higher.

Table 2-1 Overview of the polyamide particles used in this work

Material	Polyamide 12			Polyamide 6	
ID	**PA12-d5s**	**PA12-d10s**	**PA12-d30a**	**PA6-d13r**	**PA6-d16a**
Product name	SP500	SP10	AM376010	TR1	AM306010
Supplier	Toray, JP		Goodfellow, UK	Toray, JP	Goodfellow, UK
SEM (1000x) 30 μm	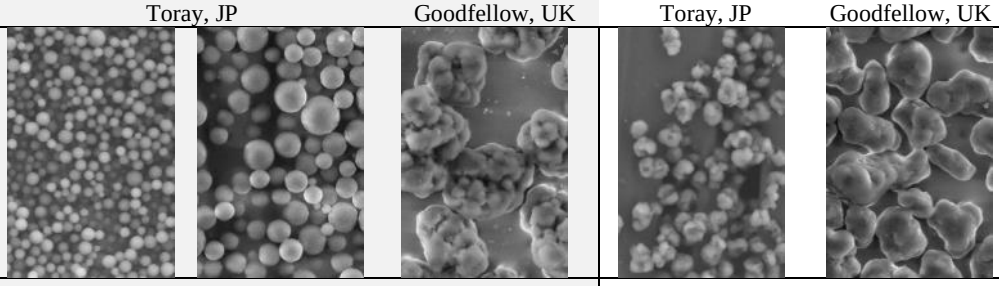				
Size* (μm)	~5	6-14	25-30	10-16	15-20
Particle shape	Smooth spherical	Smooth spherical	Irregular, quasi-spherical	Rough, quasi-spherical	Irregular shape
Melting Point (˚C)**	165-171	165-171	180	-	210-220
Tensile Strength**	-	-	50-55 MPa	78 MPa	75 MPa

*From manufactures
**Limited information about the particle properties was available from the manufacturers' catalogues.

2.1.2 Sample preparation

Polyamide particles were dehydrated in a dehumidifier chamber at 80°C for 24 hours before use. Two particle deposition methods were used. In the first particle deposition process (Figure 2-1a), the particles were spread on a silicon rubber sheet that has micro dimples with a periodic pattern first. A straight steel bar was used to scrap the particles over the surface, which removed excess particles and left some in the patterned dimples. Then, a prepreg sheet was place on top of the particle coated rubber surface and pressed using a roller. The particles were transferred to the prepreg surface due to its tacky surface. The second method was using two plastic films (20 μm thick) as spacers to keep a distance between the scraper and prepreg surface, as shown in Figure 2-1b. As a result, a relatively thick layer of particles could be formed on the prepreg surface.

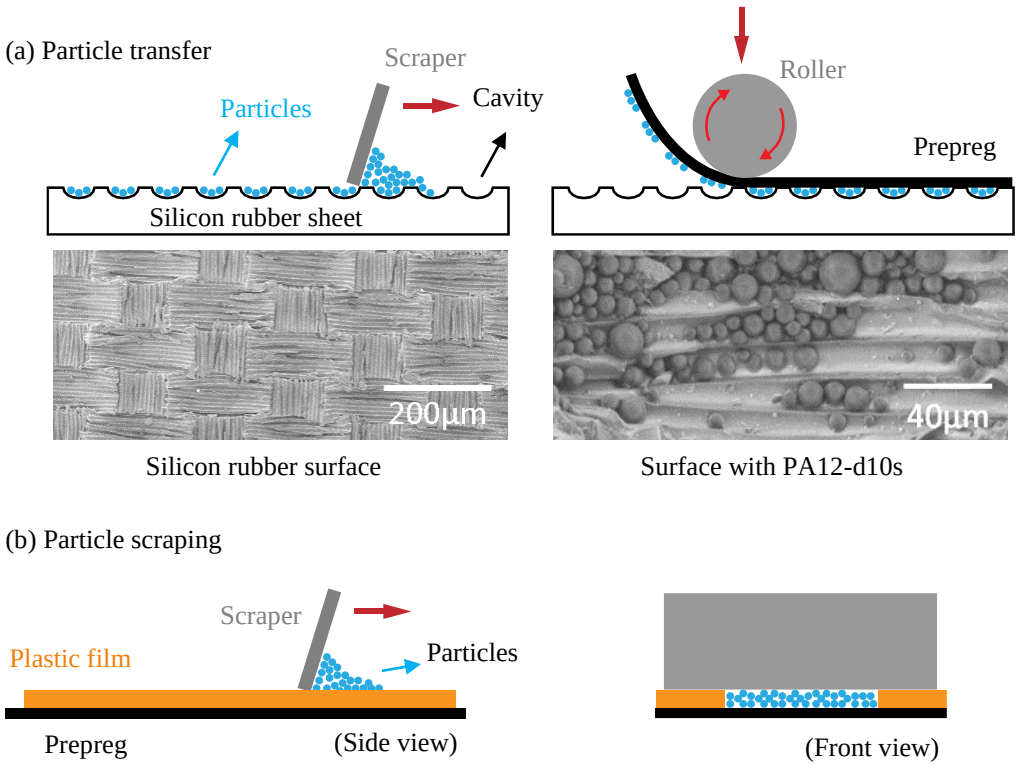

Figure 2-1 Schematic of particle coating methods

The first particle transfer method was more suitable to deposit a small amount of particles (< 5 g/m^2) with a good uniformity. However, a high particle areal weight was difficult to achieve, which could attribute to the small cave size on the surface of this

specific type of silicon rubber sheet. In contrast, the scrapping method allowed for achieving a high particle areal weight, but the coating quality is highly dependent on the flatness of prepreg surface. Fine particles such as PA12-d5s and PA12-d10s were difficult to be coated on prepreg with this method, because such fine particles easily agglomerated so that the particle layer was scrapped away easily.

Double cantilever beams (DCB), shown in Figure 2-2, were made from 30 layers of unidirectional prepregs with the dimensions of 340 mm × 120 mm. The particles were uniformly distributed only on the surface of the interlayers in the middle of the laminate (the 15th and 16th plies) using the particle deposition method aforementioned, as shown in Figure 2-2.

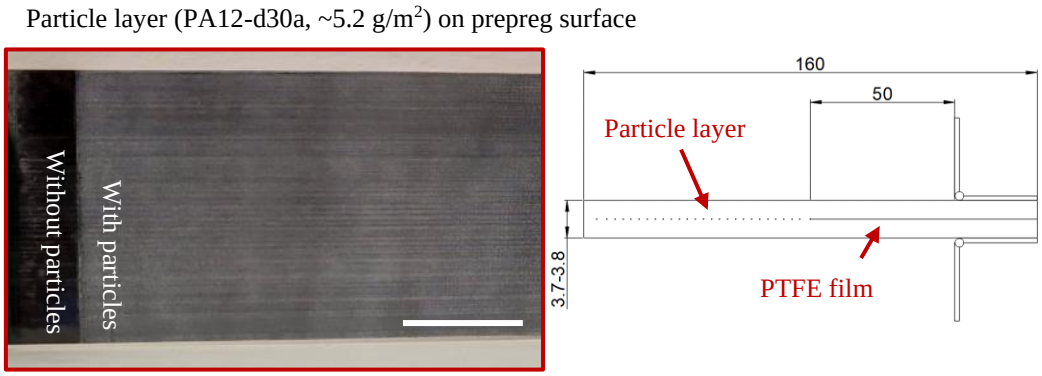

Figure 2-2 Schematic of the manufacturing method for the DCB test samples with a photo of the prepreg surface coated with particles.

The actual particle areal weight was calculated by measuring the weight of the ply before and after the particle deposition. A 12 μm thick PTFE film was inserted between the two layers to create a 50 mm long initial crack, as shown in Figure 2-2.

The curing cycle used in this work was a cycle recommended by the material suppliers; 1 hour dwell at 110°C and 2 hours curing at 180°C. After curing, the panels were cut into coupons with dimensions of approximately 160 mm × 20 mm × 3.7 mm, and hinges were bonded on both sides where the PTFE film was inserted, at the position as required by ASTM D5528 [90]. The side edges of the test coupon were coated with white paint, and grid lines were marked for crack propagation length measurement.

2.1.3 Measurement of the interlayer thickness

The particle tougheners included in the interlayers resulted in thickening of the interlayer [91,92]. In order to investigate such thickening effect of different particles, the edges of the double cantilever beam (DCB) samples were polished and observed using an optical microscopy, as shown in Figure 2-3. The interlayer thickness was measured using an image analysis software. Due to the variation of the thickness, the values were averaged from total 12 measurements in three photos taken from different locations along the specimen length.

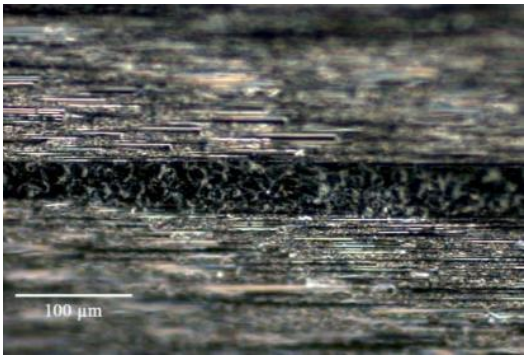

Figure 2-3 Microscopic image of the cross-section of the particle toughened interlayer for thickness measurement (PA6-d16a, 27.8 g/m^2).

2.1.4 Measurement of the Mode-I interlaminar fracture toughness

Mode-I fracture toughnesses were measured following ASTM D5528. A universal material testing machine (Shimadzu, JP) with a 1 kN load cell was used at a cross-head speed of 1 mm/min. Each test included two steps; a 3-5 mm long sharp crack tip was formed first by opening the precrack and the specimen was unloaded, and then in the second step, the specimen was reloaded until the crack growth reached about 30 mm from the initial crack tip created in the first step. Crack propagation during test was captured by a high-resolution video camera (iMETRUM, UK) at a sampling rate of one frame per second (Figure 2-4). The crack length was manually measured using the image analysis software.

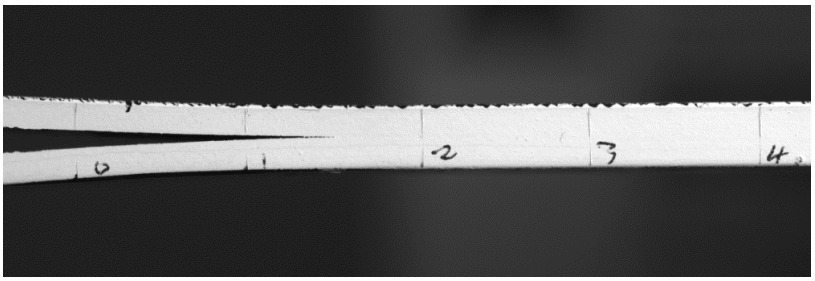

Figure 2-4 Crack propagation on a DCB captured by video camera

The G_{IC} value was calculated using the modified beam theory (MBT) [90], which is described as;

$$G_{IC} = \frac{3P\delta}{2b(a+|\Delta|)} \qquad \textbf{Equation 2-1}$$

where P, δ, b, a and Δ are the peak load, cross-head displacement at the peak load, specimen width, crack length and correction factor for the DCB arm, respectively.

2.1.5 Fractography analysis

To observe the fractured surface and the crack propagation path, the tested DCB samples were cut into a few pieces, as showed in Figure 2-5. After the longitudinal cut, the cut surface was polished to reveal the side of the crack tip. A scanning electron microscope (TM3030Plus, Hitachi) was used for this observation.

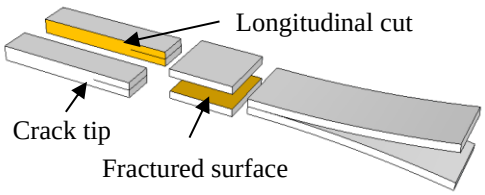

Figure 2-5 Illustration of the observed surfaces (yellow) from the cut sample using SEM.

2.2 Experimental results

2.2.1 Toughened layer thickness

The cross-sectional SEM image showed that with the range of particle areal weight applied to the laminates in this work, the particles were well impregnated with the epoxy resin after curing in the interlayer (Figure 2-6a). As shown in Figure 2-6b, the interlayer thickness increased proportionally to the amount of particle at low areal weights (< 20 g/m^2). It was found that the interlayer thickness increase was influenced by the average particle size, which can be seen from PA12-d5s, PA12-d10s and PA12-d30a toughened samples in the range of low areal weights (< 20 g/m^2). However, a further increase of the particle amount resulted in different trends of thickness change for different particles. The most significant thickening effect was observed when a high areal weight (> 20 g/m^2) of PA6-d13r was applied. Although its particle size was not the greatest among the particles, the interlayer thickness was greater than the slightly smaller PA12-d10s particles. This might be resulted from the difference in the particle surface morphology affecting the particle packing behaviour, which is further discussed in Section 2.3.1.

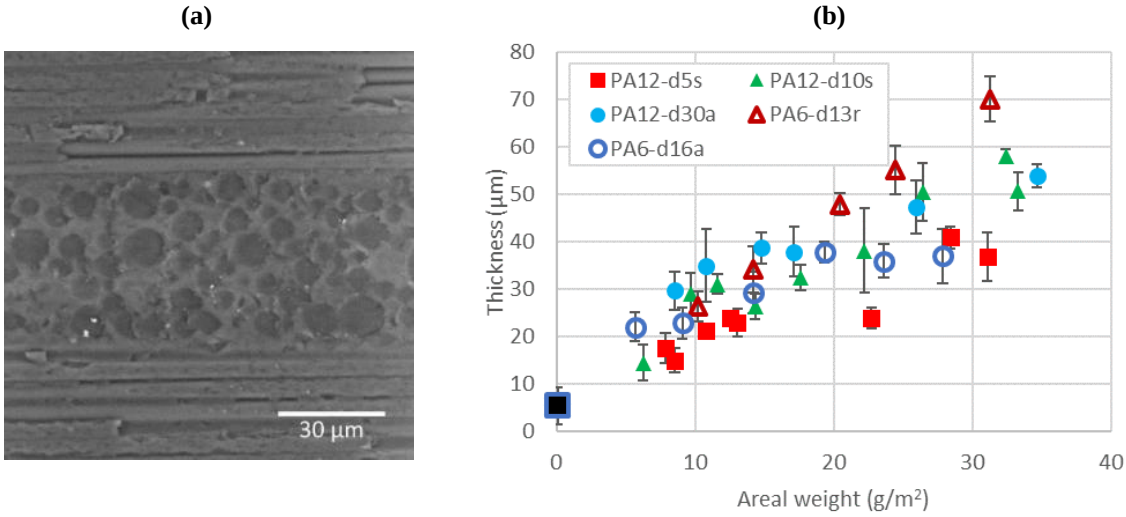

Figure 2-6 Interlaminar resin layer including the particle toughenes: (a) SEM image of PA12-d10s (32 g/m^2) toughened interlayer, (b) Interlayer thickness change of the DCB samples interleaved with different particle areal weights.

2.2.2 Mode-I DCB test

Most of the polyamide 6 and polyamide 12 particle-toughened samples exhibited stable crack propagation during the DCB test, as shown in Figure 2-7. As shown in Figure 2-7a, the polyamide 12 particles were much more effective in toughening than the polyamide 6 particles in general. The increase of particle areal weight contributed to increasing the crack opening load (Figure 2-7b), while the same trend was not observed in the polyamide 6 particle-toughened samples (Figure 2-7c).

Another difference found from the load-displacement curves was that the polyamide 12 particle-toughened samples exhibited more ductile response; a rather 'blunt' load peak was observed when the crack was initiated (Figure 2-7a). This became more outstanding when the amount of polyamide 12 particles was greater than a certain level. For example, the transition from 'sharp' to 'blunt' peak was clear in PA12-d10s, when the particle areal weight increased from 6.25 g/m^2 to 9.66 g/m^2 (Figure 2-7b). However, this response was not seen in the samples toughened with polyamide 6 particles (Figure 2-7c) where the load drop was rather linear right after reaching a sharp peak load, resulting in no difference from the non-toughened specimen. The difference of the load-displacement curves between polyamide 6 and polyamide 12 particles is described in Figure 2-7d. The reason for this difference will be further discussed in Section 2.3 in depth.

Figure 2-8a shows the crack growth resistance curve (R-curve) for different toughening particles and all the G_{IC} initiation (G_{IC_init}) values of the tested samples. The increased particle amount resulted in G_{IC} improvement in all the polyamide 12 particle-toughened samples, while the small particles (PA12-d5s and PA12-d10s) were more effective than the large particle (PA12-d30a) at the similar areal weight. Although the PA12-d30a particles started being effective when the particle amount was higher than 10 g/m^2, the PA12-d5s and PA12-d10s particles significantly improve the fracture toughness even when it was below 10 g/m^2; the G_{IC} was almost twice that of the non-toughened specimens at 10 g/m^2.

As shown in Figure 2-8b, by interleaving the IM7/8552 composite with a very small amount (5 g/m^2 or less) of PA12-d5s or PA12-d10s, the G_{IC_init} can be significantly improved to a similar level to that of the composites made with M21 matrix based prepreg (approximately 0.3-0.36 kJ/m^2 [28,29]). In contrast, the samples interleaved

with polyamide 6 particle layers showed almost no improvement. Although the highest G_{IC} values for PA6-d16a and PA6-d13r were observed when the particle areal weight was about 14 g/m^2, the values were almost the same as that of the non-toughened sample (0.24 kJ/m^2). The larger particle (PA6-d16a) seemed to provide a slightly higher G_{IC} than the smaller particle (PA6-d13r). However, the particle size didn't influence the fracture toughness significantly.

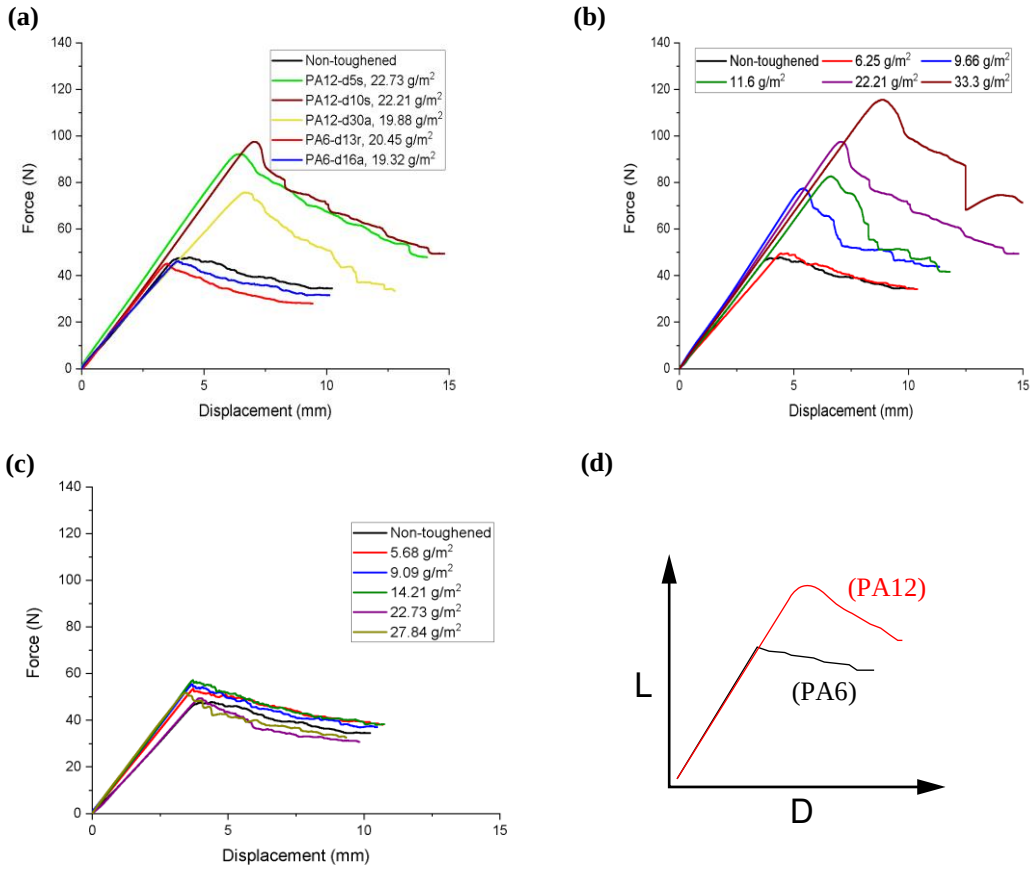

Figure 2-7 Load-displacement curves in the DCB tests of the samples interleaved with: (a) different particles with areal weights close to 20 g/m^2, (b) PA12-d10s, (c) PA6-d16a, and (d) typical load-displacement response between PA12 and PA6.

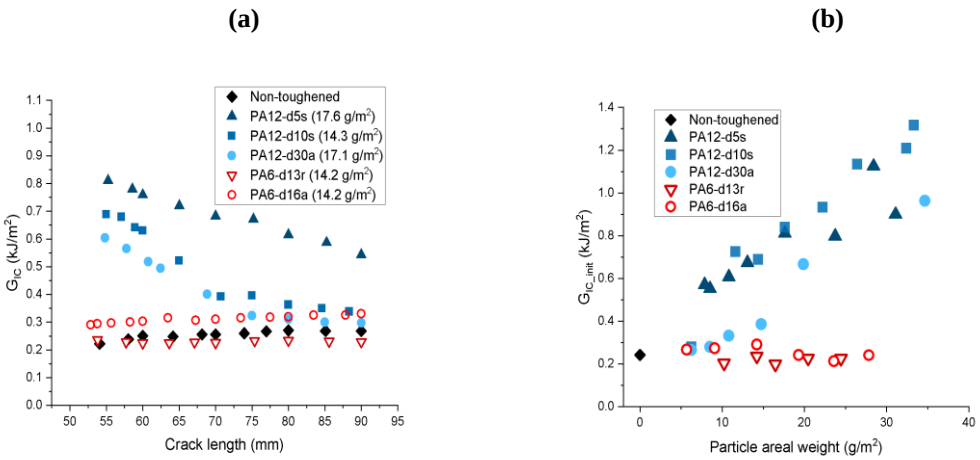

Figure 2-8 (a) The R-curves of the samples interleaved with different polyamide particles (particle areal weight: approximate 15 g/m^2), (b) the initiation GIC of the samples interleaved with different areal weight of polyamide particles.

2.3 Discussions

2.3.1 Particle amount vs. interlayer thickness

Interleaving particles increase the interlayer thickness. Figure 2-6 shows that the interlayer thickness is related to the particle size to some extent. Figure 2-9a and Figure 2-9b show the cross-sections of DCB samples interleaved with PA6-d13r and PA12-d10s, respectively. Although the average size of those two particles is similar, the packing density of the smooth PA12-d10s particles was much higher than the rough PA6-d13r particles at the interlaminar region. It was inferred that a greater size variation of the PA12-d10s particles (as shown in the SEM image in Table 2-1) contributed to increasing the particle packing density, as the smaller particles can easily fill the gaps between the larger particles [93], which can be seen in the Figure 2-9a and Figure 2-9b. For the PA6-d13r, particle layer thickness increased linearly with the particle areal weight (Figure 2-6b). This could be attributed to its rough surface and relatively uniform size preventing particle-particle movement, which results in a lower packing density (Figure 2-9a).

2.3.2 Particle amount vs. fibre volume fraction

As shown in Figure 2-10, the particle tougheners at the interlayers might increase the laminate thickness significantly, depending on their areal weight. This can affect the structural performance of the laminate.

By assuming that the polyamide particles do not affect the modulus of the interlayer epoxy matrix due to its similar modulus and the fibre volume fraction of each fibre layer is constant, the in-plane tensile modulus of the unidirectional laminate can be easily calculated; the increased thickness of the interlayer and the fixed amount of carbon fibres result in reduction of the overall fibre volume fraction.

Figure 2-11 shows the reduced tensile modulus at fibre direction calculated using the rule of mixture, for PA12-d10s particle as an example. The interlayer thickness used in this calculation is from the data in Figure 2-6. The interlaminar fracture toughness is also plotted, which is from the data in Figure 2-8. As shown in Figure 2-11, although 10 g/m^2 of the particle areal weight approximately doubled the G_{IC}, the tensile modulus is significantly decreased by 14.2%. If the tensile stiffness needs to remain the same, more plies will be needed, which increases the structural weight considerably. But, an increased thickness with a slightly lower fibre volume fraction might be beneficial to increase the bending stiffness.

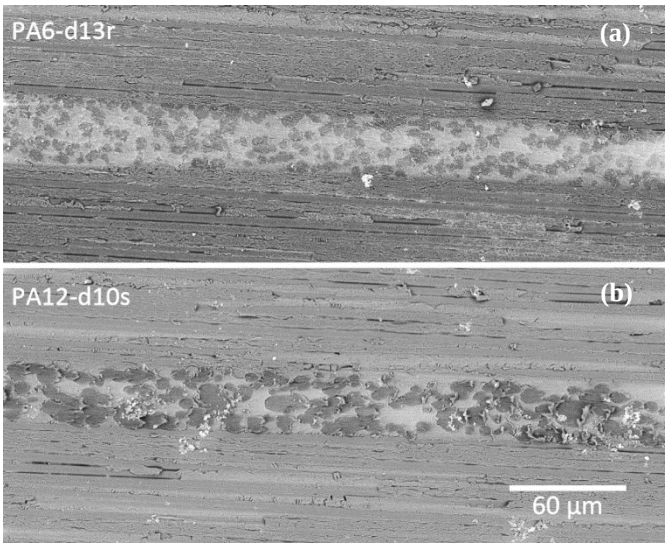

Figure 2-9 SEM images of the cross-section of the laminates interleaved with (a) PA6-d13r (16.5 g/m^2) and (b) PA12-d10s (17.6 g/m^2) particles

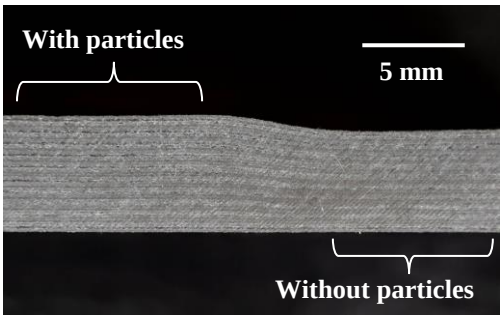

Figure 2-10 Cross-section view of a cured IM7/8552 laminate made of 40 plies (left: all interlayers interleaved with PA12-d30a particles at 9 g/m^2, right: without particles)

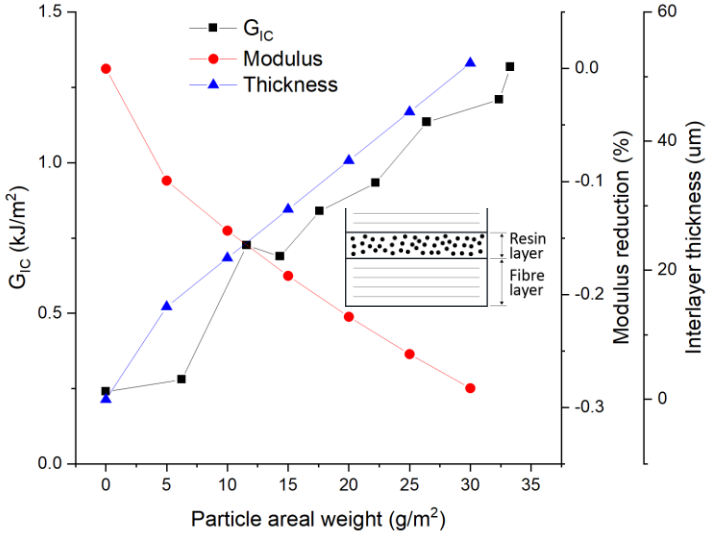

Figure 2-11 Effect of the PA12-d10s particle amount on the tensile modulus, GIC and the interlayer thickness of a unidirectional IM7/8552 laminate composite.

2.3.3 SEM observation

Laminates interleaved with polyamide 6 and polyamide 12 particles exhibited completely different fractured surface morphology, as shown in Figure 2-12 and Figure 2-13. With polyamide 12 particles (Figure 2-12), the crack went through the particles causing fracture of the particles, as shown in Figure 2-12a. Due to the yielding, the particles effectively bridged the cracked surface preventing its rapid propagation. As

shown in Figure 2-12b, the PA12-d10s particles were plastically deformed necking at the centres of the particles before final fracture, which implies that strong particle-matrix bonding, as the curing temperature was close to or higher than the melting temperature of the polyamide particles.

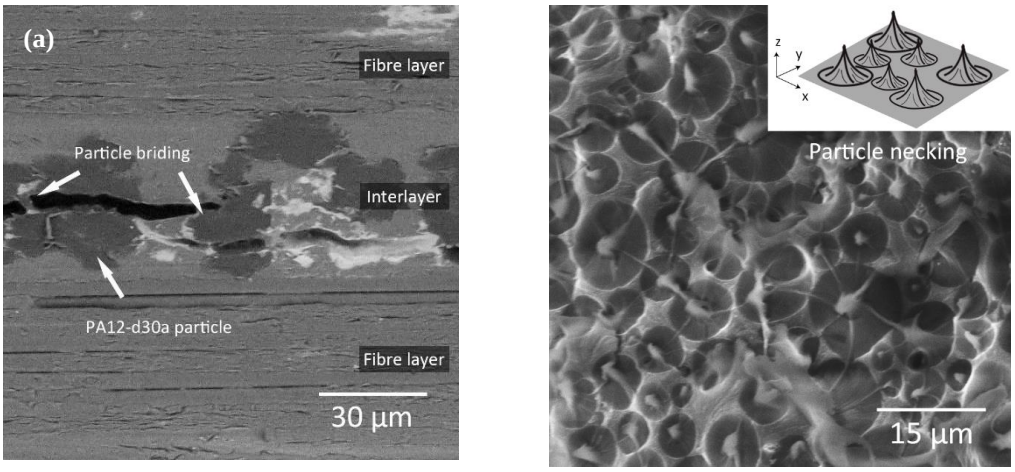

Figure 2-12 SEM images of polyamide 12 toughened samples: (a) longitudinal cut surface of sample toughened with PA12-d30a and (b) fractured surface of the sample toughened with PA12-d10s.

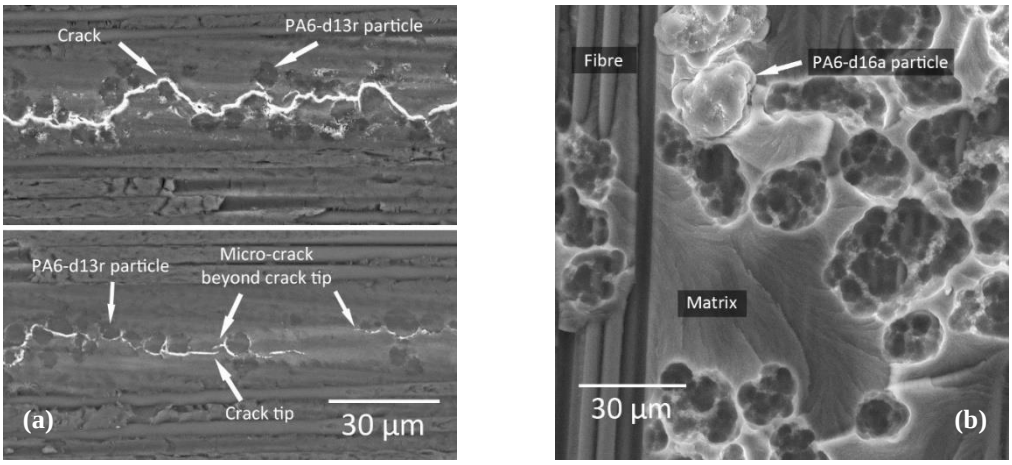

Figure 2-13 SEM images of polyamide 6 toughened samples: (a) longitudinal cut surface of sample toughened with PA6-d13r (top: the crack path after the propagation, bottom: the area near the crack front) and (b) fractured surface of the sample toughened with PA6-d16a.

Similar particle bridging was reported by Cardwell *et al*. [23] where the polyamide 12 particles were used to toughen a neat epoxy resin. In their study, the curing temperature (120°C) was far below the melting point of particle, but the 16 hours long curing enabled the amine group to react with liquid resin before gel.

However, particle bridging was not observed in the specimens toughened with the polyamide 6 particles. As shown in Figure 2-13a, the crack path followed the particle-matrix interface, and crack deflection was the main role of the polyamide 6 particles. The PA6-d16a particles were pulled out from the resin layer on the fractured surface (Figure 2-13b), which implies that the particle-matrix bonding strength was too weak to withstand the crack opening stress, causing no plastic deformation in the load-displacement curve (Figure 2-7d).

2.3.4 Toughening effect

The failure mechanism of the polyamide 6 particle-toughened samples was similar to the case where impenetrable rigid particles are used as toughgeners. Nakamura and Yamaguchi [7] investigated the toughening effect of epoxy including silica particles. They concluded the larger particles are more effective to impede crack propagation by diverting the crack tip along a longer path, leading to higher energy absorption, which could explain the higher G_{IC} values of the samples toughened with PA6-d16a particles compared to those toughened with PA6-d13r particles.

However, in the polyamide 12 particle toughened samples, most of the fracture energy was absorbed by the plastic deformation of the particles. Since the toughening effect was mainly dependent on the amount of bridged particles at the failure surface, the smaller particles (PA12-d5s and PA12-d10s) resulted in higher G_{IC} values than the larger particles (PA12-d30a) at a similar particle areal weight, because small particles can form a denser particle layer compare to large particles, as shown in Figure 2-8b.

2.3.5 Effect of processing conditions

Although both polyamide 6 and polyamide 12 have similar chemical and mechanical properties (Table 2-1), their toughening effect was completely different depending on the processing condition. In order to investigate the effect of the curing temperature in relation to the different melting points of the two polyamide types, additional DCB test samples with different polyamide 12 particle areal weights were manufactured using the same fabrication method but cured at 140°C for 5 hours, which was able to achieve approximately 75% of degree of cure [94].

In contrast to the load-displacement curve shown in Figure 2-7b, the test results showed there was no obvious ductile behaviour, as shown in the a. In Figure 2-14b, the initiation G_{IC} had no relationship with the particle areal weight.

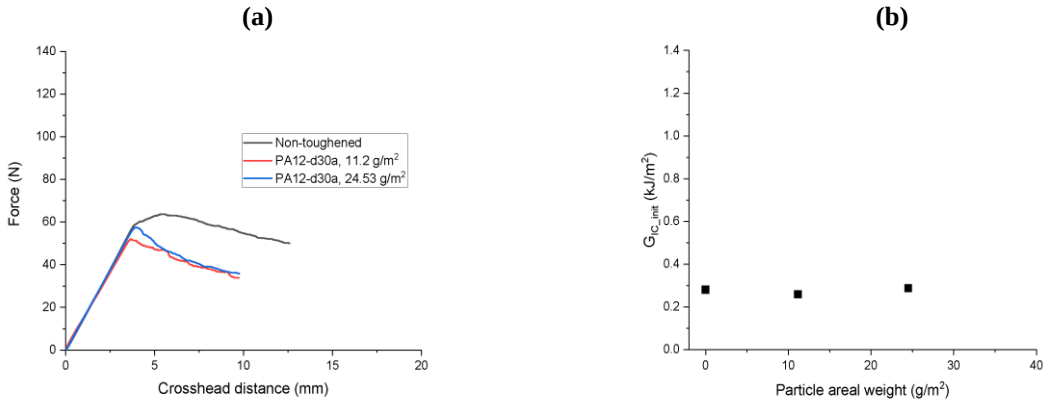

Figure 2-14 DCB test results of the sample interleaved with PA12-d30a cured at 140°C for 5 hours: (a) load-displacement curve and (b) initiation GIC values for different particle areal weights.

As shown in Figure 2-15, the fractured surfaces were completely different from that of the specimens cured at 180°C (Figure 2-15a) and 140°C (Figure 2-15b). The sample cured at 140°C has a failure surface similar to the sample toughened with polyamide 6 particles, which showed particle-matrix debonding (Figure 2-15b). The load-displacement curve in the DCB test (Figure 2-14a) also showed a similar response (Figure 2-7c), as no particle bridging occurred during the crack propagation. This result

suggests that the curing temperature can significantly change the particle-matrix interfacial strength and influence the interlaminar toughing mechanism.

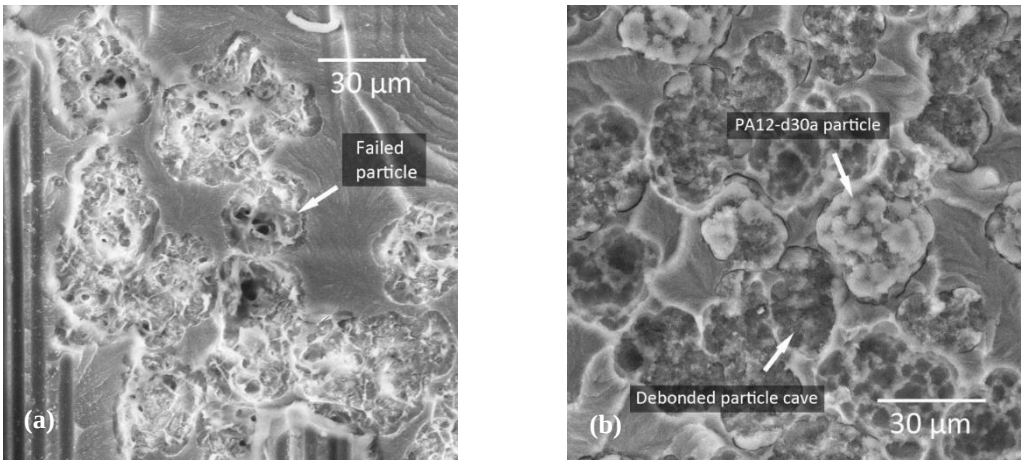

Figure 2-15 SEM images of the fractured surfaces of the samples that were toughened with PA12-d30a and cured at: (a) 180°C and (b) 140°C.

Based on the discussion in literature about the semi-IPN [25,26], it was deduced that the superior toughening effect of polyamide 12 particle was due to its melting point close to the curing temperature of the prepreg resin matrix, which allows for better adhesion between the particle and the matrix during curing. Although this interfacial strength can be promoted with longer processing time at lower temperature [23], this approach may not be cost-efficient in high volume production. Therefore, it is important to choose a thermoplastic particle toughener that has a melting point close to or below the curing temperature of the prepreg matrix system.

2.4 Conclusion

In summary, this chapter investigated the interlaminar toughening effect of a range of different polyamide particles for carbon fibre/epoxy composites. The results showed that the toughness can be significantly improved by direct particle deposition onto the prepreg surface, which could be more effective than the conventional resin-particle pre-mixing and prepreging method in terms of cost and toughening effect.

It was found that the particles' size and shape as well as the deposition amount affect the interlaminar toughness. However, the most important factor was the curing condition such as the difference between the curing temperature and the melting point of the particle, which determines the particle-matrix bonding strength. Well-established particle-matrix bonding of the polyamide 12 toughened samples resulted in failure with significant plastic deformation of particles (particle bridging), which led to high initiation and propagation G_{IC}. The degree of toughening effect depended on the density of particle bridging, so the more polyamide 12 particles, the greater G_{IC}. In contrast, the failure in the polyamide 6 particle-toughened samples occurred at the particle-matrix interface. The ductility of the particle was unable to contribute to fracture energy absorption. Consequently, the G_{IC} was very close to that of non-toughened samples. The effect of the particle surface morphology on the interfacial bonding strength was minimal.

The importance of interfacial bonding strength in toughening was further demonstrated by applying a lower curing temperature to the samples toughened with the polyamide 12. The G_{IC} was significantly reduced, and no obvious ductile response was observed in the load-displacement curve. SEM images revealed the dominant failure mechanism was particle-matrix interface that was similar to the polyamide 6 toughened samples.

When sufficient interfacial bonding can be achieved, smaller particles were more effective, which appeared to be related to the increased particle bridging density. Finally, in the range of particle areal weight used in this work (5 - 35g/m^2), more polyamide 12 particles resulted in higher G_{IC}. However, its impact on other mechanical properties such as in-plane mechanical properties due to the reduced fibre volume needs to be considered.

If a commercial prepreg with a particle toughened resin system is used, it is difficult to achieve both high stiffness and high interlaminar toughness (or damage tolerance) at the same time. Direct particle deposition method used in this work has a great advantage in that the particle tougheners can be selectively applied to only where needed.

3 TEST RIG DEVELOPMENT FOR PROCESSABILITY CHARACTERISATION

3.1 Introduction

The interply friction and bulk factor are two important factors that influence the manufacturing quality of composite. Since there are no standardised test methods for evaluating those material characteristics, many previous researchers have devised their own test devices and test methods. However, the design and configuration of the test rig can affect accuracy of the test result, and this has not been well addressed in the relevant literatures.

This chapter first provides a brief review of the test methods used in the previous studies, and then presents a test rig that was developed to improve the accuracy of measurement in this work. Its special design allows for measurement of both the interply friction between prepreg sheets and the bulk factor of a prepreg stack in the same rig.

3.2 Interply friction measurement

Friction measurement is widely used to characterise material's surface properties in many aspects. The test measures the transverse force required to make slippage between two surfaces in contact sliding against each other, with an external force normal to the interface. However, the test configuration varies depending on the test material, which leads to a variety of test standards and commercially available test devices [95].

Prepreg surface friction is dominated by the viscosity of its uncured resin matrix, which is highly temperature dependent. Some studies [96,97] characterised the prepreg friction using a conventional rheometer with parallel disc plates. A prepreg sample was cut into small pieces to fit in the test area. The advantage of this method is that the temperature and normal force can be precisely controlled and monitored precisely, however its critical disadvantage is that measurement is for rotational friction force. The test set-up causes a variation of the rotational speed as well as the fibre orientations along the radial direction of the disc, which makes it difficult to analyse the effect of them separately from the temperature effect. For example, in Groves' [96] work the interply shear behaviours between two 0° plies and 0°/90° plies were similar. However, it is different from the findings in later studies that used linear friction test configurations [64,66].

To create a similar condition to the actual forming process, a linear-motion test method would be more ideal. Several studies using such a test method for thermoplastic and thermoset prepreg systems have been reported in the literatures [1,45,48,57,58,64,98].

3.2.1 Review of test rig designs

Interply friction test requires to control three parameters: pulling force, normal force and testing temperature. However, getting accurate test results will require not only the precise control of test conditions, but also to minimise measurement errors from the designed test configuration.

In general, the designs of existing interply friction test rigs can be sorted into horizontal and vertical configurations. The horizontal sliding test set-up is commonly used for plastic or textile materials. This experiment usually follows the ASTM D1894 [99] standard. The advantage of such a configuration is the normal force can be simply applied using weights, but a motion control device moving horizontally or a device converting the force direction from a vertical tensile testing machine would be required together with a force sensor. Since a vertical testing machine is more widely used for mechanical tests, the following review only compares the vertical friction test configuration.

Table 3-1 List of specifications of interply friction test rigs

Design	Normal force*	Surface alignment	Heating**	Testing area (mm)***	Measurement		Prepreg matrix	Ref.
					Pull force/ Ply slippage	Normal force		
a	SP	-	IM	100×51	Testing machine	-	PP	Lebrun [59]
b	GC	-	IM	25.4×50.8	Testing machine	Strain gauge	PEEK	Morris [100]
c	SP	Constrained		100×100 Const.	Testing machine	-	PP	Sachs [101]
d	Pneu.	Linear bearings	IM	80×80	Testing machine	Load cell	PP	Vancloo-ster [102]
e	Pneu.	Self-alignment	IM	50×50 Const.	Testing machine	Load cells	PP	Sachs [101]
f	Pneu.	Alignment pins	IM	102×108	Testing machine	Pressure gauge	Epoxy	Martin [58]
g	Pneu.	Self-alignment	HC	50×50 Const.	Testing machine/ Extensometer	Pressure gauge	Epoxy	Erland [45]

*Normal force - SP: springs; GC: G-clamp; Pneu: Pneumatic system
**Heating system - IM: imbedded heater; HC: heat chamber
***Testing area - Const.: constant pressure area during test

Figure 3-1a is a simple test configuration used by Lebrun et al. [59]. The sample is formed by sandwiching three plies of prepreg, the mid-ply is fixed and the outer plies were pulled by a tensile testing machine. The normal pressure is applied using four calibrated springs at each corner of the aluminium pressure plate. Heaters are attached on the outer surface of each pressure block and a thermocouple is placed in between the blocks to measure the testing temperature. The advantage of this test rig is its simplicity, which requires less parts to build.

However, a very precise adjustment of the spring length will be required to achieve a uniform normal pressure distribution. The other concern is the change of the testing area while ply is pulling out, which might increase the normal pressure with time and affect the test result.

The test configuration (Figure 3-1b) used by Morris et al. [100] is similar to the former one. Three plies are also sandwiched together, but the regions outside the testing area are separated using release films. The pressure plates, heaters and prepreg plies are placed together, and a G-clamp is used to apply the normal force, which is monitored by a calibrated strain gauge that was integrated with the clamp. The normal force control could be precise if the G-clamp can achieve a fine adjustment of the displacement.

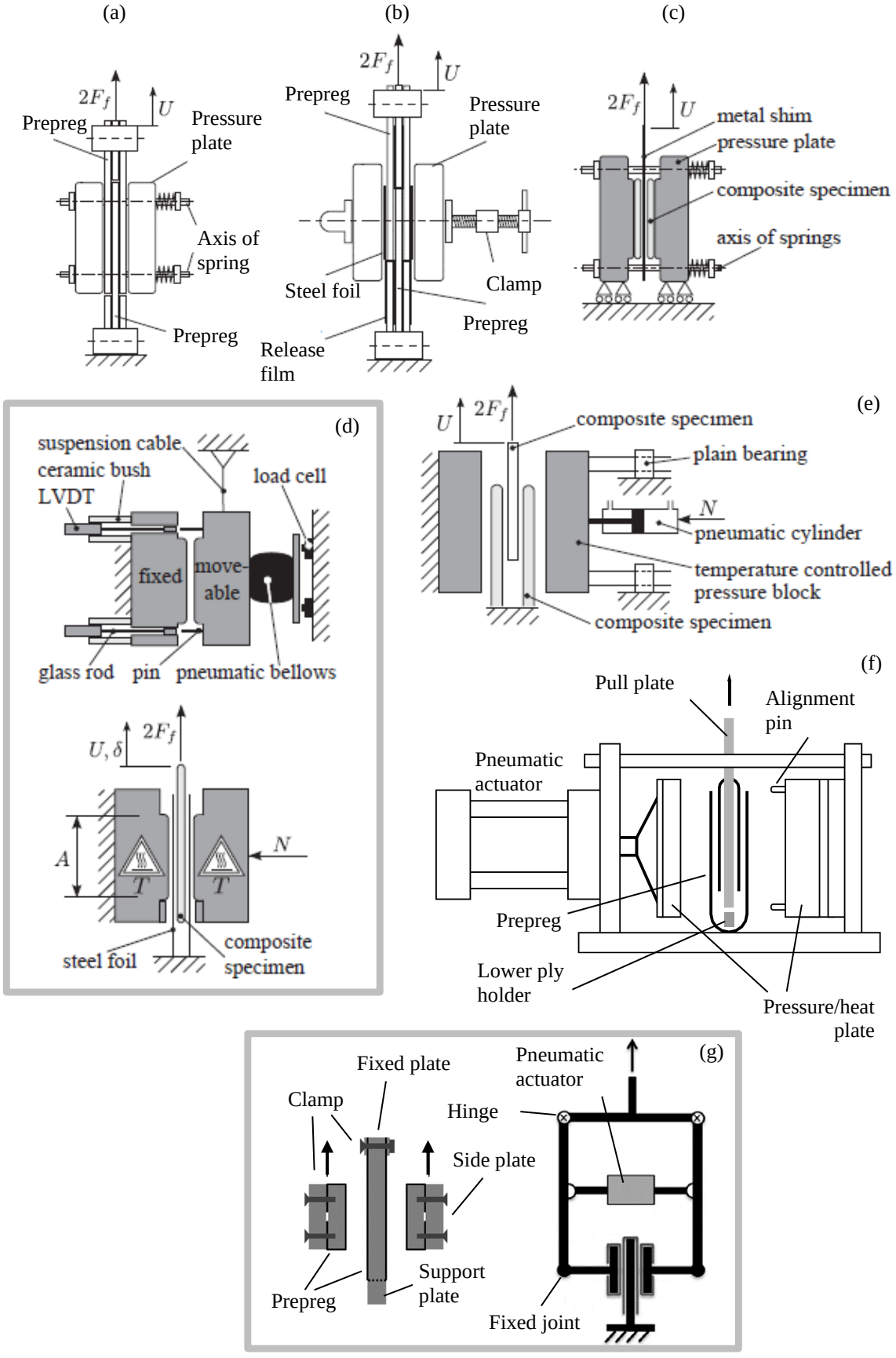

Figure 3-1 Schematics of interply friction test rig configurations [45,58,101]. ((a) - (e) are from the doctoral thesis of Sachs [43], (f) is regenerated from [58])

However, since all the components may not be well-aligned, the pressure distribution would depend on the flatness level of the plies and components. Furthermore, such a displacement control has a critical problem that the normal force will be changed if there is a resin squeeze-out or a thickness change during the test. The regions with release film may be thicker than the testing area, which could lead to underestimation of the pressure level at the testing area.

Figure 3-1c shows the test configuration designed by Clausthal University of Technology in Germany. Unfortunately, all the information about this design is from the description in Sachs' thesis [43], rather than the original developer. Two plies are attached on each pressure plates using double sided adhesive tapes, and the middle ply is place in between the parallel plates to be pulled. The contact area remains constant because the middle ply has a larger size than the fixed plies. The pressure plates are constrained to horizontal movement only, which could provide a better surface alignment than the configuration designed by Lebrun et al. in Figure 3-1a, if the used linear guide is rigid and has a high precision. However, uniform testing pressure may be difficult to achieve due to the normal force is applied by springs. Using adhesive tape to fix the prepreg may not be ideal because the surface resin can loose its tackiness under high temperature and tool-ply slippage can significantly affect the test result.

Figure 3-1d is the configuration in Sachs' study [101]. Three plies are stacked together as a test sample. Since the overlapped area is slightly larger than the pressurised area, which can keep the size of the testing area the same during pull-out of the middle ply. The pressure plates have embedded heaters and thermocouples. The normal pressure is applied by pneumatic bellows only on a side, the generated force is monitored by the load cells placed between the bellows and the test rig frame. The advantage of this design is that the normal force could be controlled relatively precisely. However, the critical disadvantage is that the movable pressure block is suspended by a cable providing no resistance to transitional and rotational movements of the block.

The configuration designed by Vanclooster is shown in Figure 3-1e. The sample is formed by stacking three plies together, which is similar to the setups described above, however the downside is that the testing (pressurised) area changes while the middle ply is pulled out during test. A pneumatic actuator is used to apply the normal pressure through a guided compaction block, and the other block has a fixed position. This way a

fine adjustment of normal force could be achieved. A heater and thermocouples are attached on the compaction blocks. The use of linear guides can ensure a good parallel alignment of the compaction blocks.

Martin et al. [58] developed a test rig to determine the friction between thermoset prepregs. As shown in Figure 3-1f, two plies are used for each test; one is folded and wrapped around the pull plate, the other is also folded but clamped on the table of the rig. This configuration could minimise ply slippage during test, since the loading on the prepreg should be symmetric. The testing temperature is controlled by the embedded heaters in the pressure plates and a thermocouple placed in the pull plate. The pull plate is connected to a universal testing machine using a cable. The normal force is provided by a pneumatic actuator from one side. The positions of two pressure plates are aligned by the alignment pins. The test configuration may have a similar issue to the design in Figure 3-1e, because the testing area decreases and the centre position changes during test, which can lead to an ununiform pressure distribution. However, pulling the pull plate using a cable may minimise the stress developed due to the small misalignment between the contact surfaces, which is further discussed in the Section 3.2.5.1.

Erland et al. [45] used a test rig with different design to the others, as shown in Figure 3-1g. A similar rig configuration has also been reported by Larberg et al. [1]. This rig has a fixed plate at the middle, and two side plates located on the both sides, which are connected with a C-shaped frame pulled by a testing machine. Prepreg plies are wrapped on all the plate in the way shown in the figure and clamped by flat rigid bars with bolts. A pneumatic actuator is used to apply the normal force to the testing area by closing the C-shaped frame. The test is performed in a heat chamber, and the temperature is monitored by a thermocouple attached on one of the side plates. Extensometer is used to measure the ply slippage and rotation of the side plates. This test configuration also allows for finer adjustment of the normal force using the pneumatic system. The long arms of the C-shaped frame and many joints could cause concerns on the overall rigidity, which may increase the compliance of the test rig. Another concern is that the prepreg gripping effect may be reduced when testing at an elevated temperature due to the reduced resin viscosity. Tool-ply slippage could affect the interply slippage measurement. In addition, the heat chamber could achieve a more uniform temperature distribution on samples, but the required heating time could be very long.

The review on the existing test rig designs in this section describes differences in sample preparation methods, ways to apply a normal force, temperature control, and potential issue of normal pressure distribution and the local displacement measurement. For the temperature control, including a heating system in compaction plates/blocks would be more time efficient. Placing thermocouples close to the sample can detect testing temperature more accurately. For the method to apply normal pressure, using a pneumatic system could achieve finer adjustment of the force output, which is more suitable for simulating different processing conditions. Inclusion of a force sensing device can increase the control accuracy of normal pressure. However, the friction force within the test rig (e.g. internal friction of linear guide and bearings) need to be considered, if the measured force output is not directly acting on the testing area.

There are some missing details from the available information. First, the compliance of the test rig could affect the measurement of ply slip distance. Among the reviewed designs in this section, only Erland et al. [45] included an additional measurement device that can directly measure the ply slippage, while the others purely relied on the displacement reading of the test machine. There is also lack of details on the prepreg gripping method. Most of the works seemed to use a simple rigid bar to hold the prepreg plies. At room temperature, the prepreg position might be easily fixed by the adhesion of its highly tacky surface. However, at an elevated temperature, such a method may lose the gripping effect due to the low viscosity surface resin, which potentially causes tool-ply slippage on the fixed plies. This can lead to overestimation of ply slip distance.

3.2.2 Requirements for test rig

In this work, the test rig design focused on increasing the accuracy of measurement and minimising the variation caused by the test set-up. The requirements were:

- The prepreg plies are supported by a flat and rigid surface to maintain the contact area during test.
- A reliable ply fixation method is used to make the slippage happen only at the interply region.
- The contact area does not change during the test.

- The rig has a rigid structure to minimise deformation or bending during the test to guarantee the parallelism of the contact surfaces.
- The rig has a device that can apply uniform pressure on the contact area and maintain the pressure level during the testing accurately.
- The rig has a heating system to control the test temperature without using a heating chamber.
- A non-contact measurement device is used to directly track the slip distance between the plies in contact.

3.2.3 Design of interply friction and compaction test rig

A vertical test configuration was used in this work, which is easy to pull-out the ply on a universal testing machine. Its schematic is shown in Figure 3-2. Two fixed prepreg plies were wrapped on each of the aluminium compaction blocks. The block on the left was at a fixed position, and the other was able to be moved horizontally. The normal pressure was applied by a force acting on this moving block during test. Another pair of prepregs were attached on both sides of a central support, which was pulled by the tensile testing machine. The friction force and slip distance were recorded.

3.2.4 Rig Configuration

Figure 3-3a shows the rig configuration for interply friction test. The movable support (1) is connected to a 1 kN load cell on a screw driven universal testing machine (Shimadzu, JP), which controls the pull-out displacement of the prepreg. The test rig is mounted onto the base of the testing machine (Figure 3-3b). The base is made with three 12 mm thick aluminium plates that joined by four precision linear shafts (5) (MISUMI, JP).

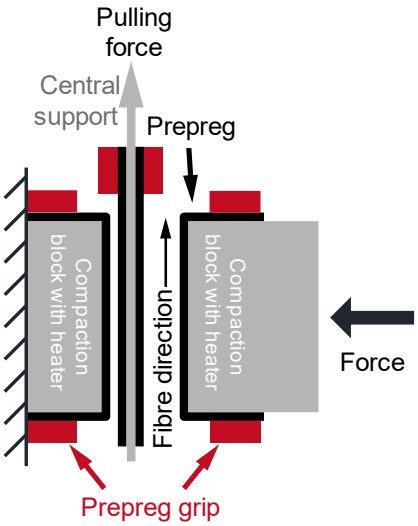

Figure 3-2 The concept of test rig design

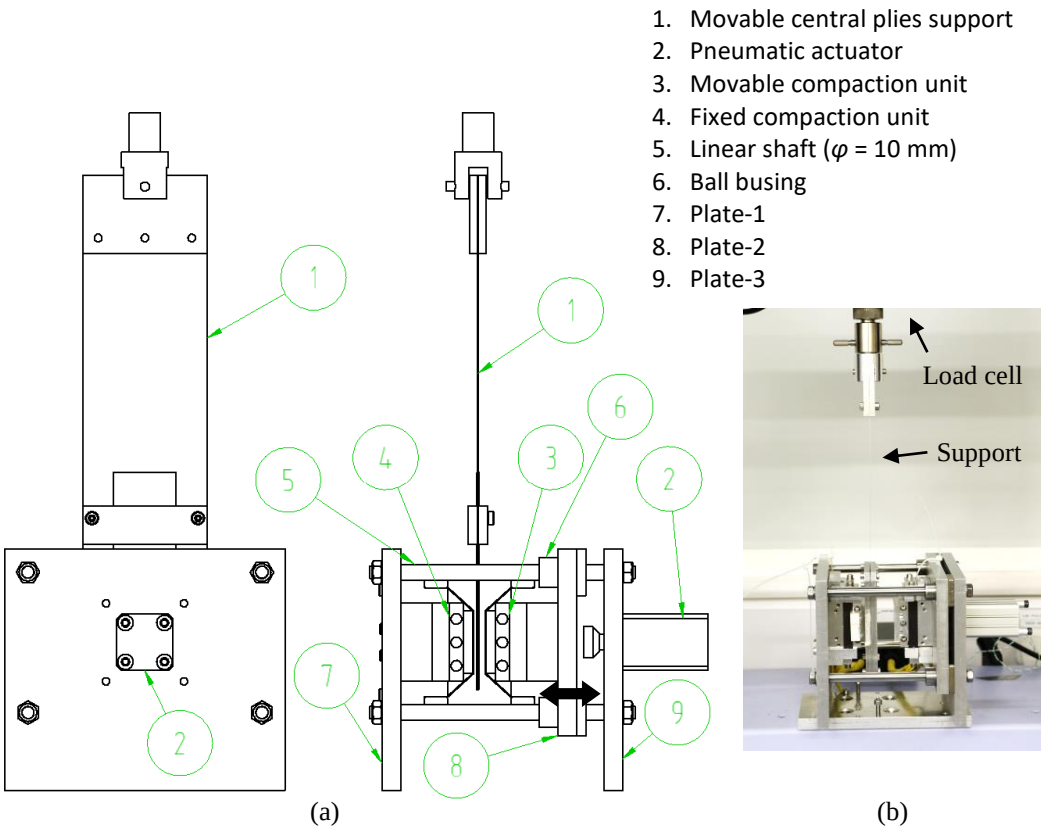

Figure 3-3 (a) Interply friction test rig. (b) Test rig fastened on a universal testing machine

As shown in Figure 3-3a, a compaction block (4) is attached on the fixed Plate-1 (7). Plate-2 (8) has the second compaction block with four precision ball bushings (6) (MISUMI, JP), which allows for the plate-2 to slide freely along the shafts (4)

minimising the plate tilting- or rotation-induced uneven normal pressure (Figure 3-4). Each compaction block have three 20 W cartridge heaters (RS Components, UK), and K-type thermocouple embedded at 1 mm depth from the contact surface of the compaction block. The temperature is controlled by a proportional integral derivative controller (Watlow, US) with a 120 V power supplier, which provides an accuracy of ±1°C. The temperature variation on the surface of compaction was negligible.

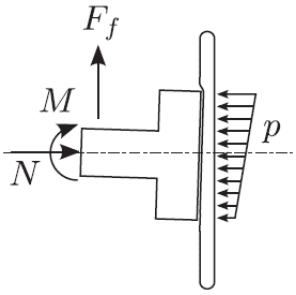

Figure 3-4 Uniformed pressure distribution caused by the deformation of compaction blocks during loading. (Regenerated from the doctoral thesis of Sachs [43])

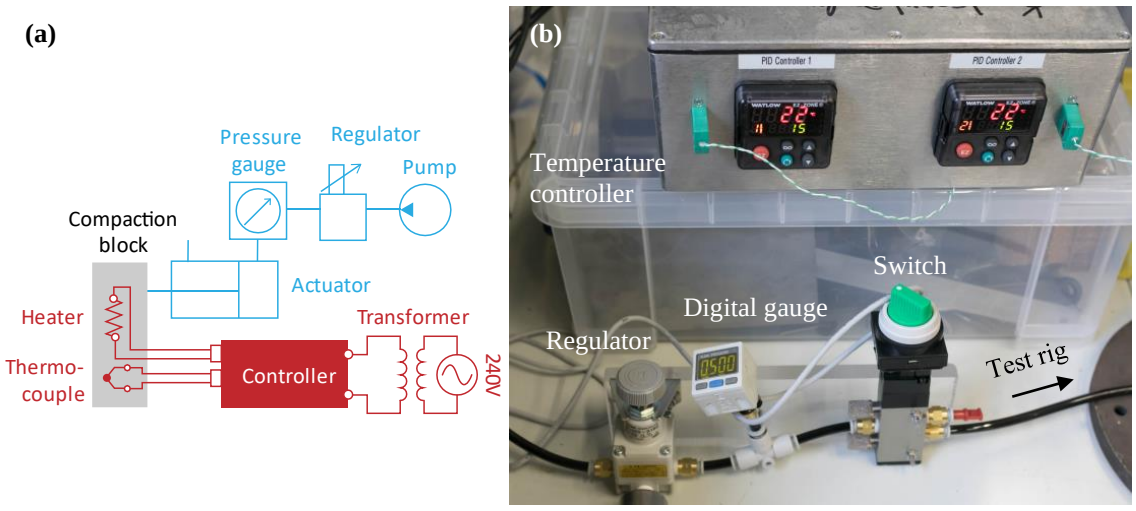

Figure 3-5 (a) A schematic of pneumatic and heating systems of the test rig. (b) Heater and pneumatic controllers.

Plate-3 (9) is a fixed plate with a pneumatic actuator (2), which applies the force to the compaction block on plate-2 (6). The pneumatic actuator (CQSY-B20-30DC, SMC, JP) has a cylinder diameter of 20 mm and stroke length of 30 mm. This specific pneumatic

actuator was designed to have high output force accuracy by creating a few microns gap between the piston and cylinder wall to minimise internal friction. The input air supply to the actuator is controlled by a precision pressure regulator (IR1020, SMC, JP) with a digital gauge (ISE30A, SMC, JP), which has a pressure sensing accuracy up to 0.001 MPa. A schematic of the heating and pneumatic system is shown in Figure 3-5.

3.2.5 Prepreg grip configuration

The theoretical interply slip distance required for creating a L-shaped preform from a flat prepreg stack (Figure 3-6) can be calculated by Equation 3-1:

$$L - l = \frac{2\pi\,(R-r)}{4} = \frac{\pi}{2} \times (R - r) = \frac{t\pi}{2} \qquad \text{Equation 3-1}$$

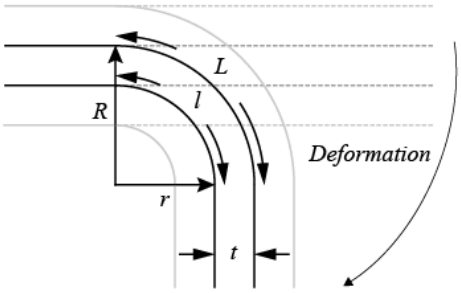

Figure 3-6 Radian difference between two adjacent plies

where the *R* and *r* are the outer and inner radii; *L* and *l* are the arc lengths of outer and inner plies at the corner; *t* is the uncured ply thickness. Assuming the ply has a thickness of 0.13 mm, the ply slip distance of each interlayer is approximately 0.2 mm, which means any unnecessary ply slippage in gripping regions can significantly affect the displacement measurement and underestimate the maximum friction force. The details of the grip design and configuration are discussed in the next sections.

3.2.5.1 Central support

Figure 3-7a shows the configuration of the central support unit, which is used to support the moving plies. The A stainless steel sheet (3) is made of a 300 mm × 80 mm stainless steel shim with a thickness of 0.2 mm. A load cell adapter (1) is connected to the stainless steel sheet (3) using a steel pin (2). Two prepregs with the dimensions of 140 mm × 40 mm, which is called 'moving plies' (5), are attached on both sides on the bottom end of the stainless steel sheet (3), and a pair of 10 mm thick aluminium bars are the prepreg holder (4) to grip the moving plies (5). The gripping effect is not affected by the testing temperature because the prepreg holder (4) is away from the heated testing area and the thermal expansion coefficient and conductivity of the stainless steel are low.

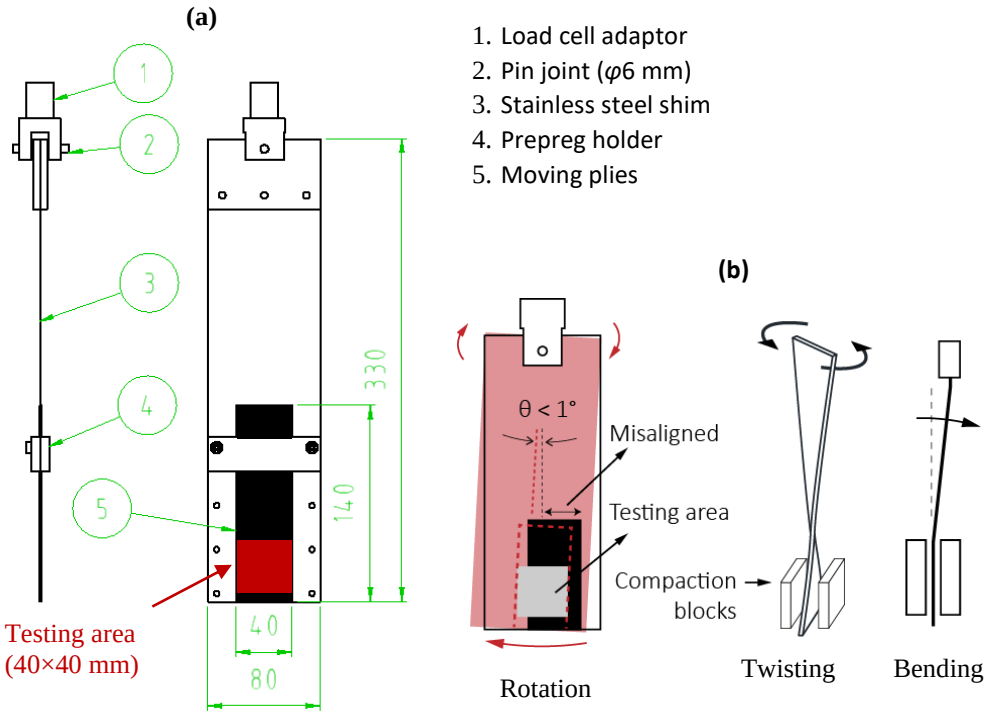

Figure 3-7 (a) Central plies support. (b) Rotation and twist freedoms of the central support.

As shown in Figure 3-7b, sometimes misalignment can occur when installing the rig on testing machine, or the attached moving plies (5) are not perfectly aligned to the centre.

In order to minimise the misalignment effect, the steel rod pin (2) is used to allow small rotation of the stainless steel sheet. Since the thin stainless steel sheet (3) is flexible, if the two moving plies (5) are slightly misaligned to the compaction surface, the stainless steel sheet (3) allows twisting and bending when the compaction blocks are closed. The length of the stainless steel sheet was long and thin enough not to develop a significant amount of stress due to the twisting and bending.

3.2.5.2 Compaction block

The prepreg installed on the compaction block are called as ‘fixed ply’. The gripping issue of the fixed plies was found as shown in Figure 3-8. When installing the prepreg, it was not easy to perfectly fix the ply around the compaction block by hand. Since the friction between the compaction block and the prepreg is reduced because of the low resin viscosity when conducting the test at an elevated temperature, the ply can be pulled out from the clamping device and slip on the compaction block. In order to prevent this, a tensioning mechanism was designed and attached to the gripping device, as shown in Figure 3-9.

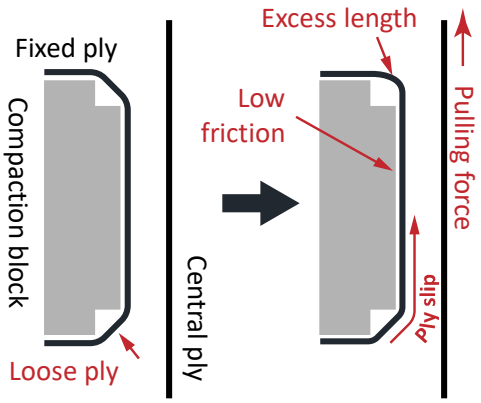

Figure 3-8 Illustration of the fixed ply slip on the compaction block during test

As shown in Figure 3-9a, the compaction block (1), a 11 mm thick phenolic insulator (2) and a spacer (3) are fastened tightly on the aluminium plate-3 with four bolts (9). A fixed ply with a dimension of 140 mm × 40 mm is placed, as shown in Figure 3-9b, both ends are clamped between a L-shaped gripper (4, 7) and an aluminium bar (5) with two bolts, as shown in Figure 3-9c. Once the fixed ply is installed on the compaction

block (1), the fixed ply is tensioned by the bolt with a barrel nut (6) on each grip (4, 7), which makes a flat compaction surface with an area of 40 mm × 40 mm.

Although there is an insulator (2) between the compaction block (1) and spacer (3), the prepreg grip (4, 7) temperature is still affected by the temperature of the compaction block (1), which can cause the slippage of the fixed ply during test due to the reduced resin viscosity on the gripping area. In order to minimise this, a L-shaped grip (4, 7) was used to help locking the fixed ply position while tensioning the fixed ply, as shown in Figure 3-9b.

Another gripping issue found from the preliminarily test is shown in Figure 3-10a. It was common to find a uneven tension across the width of the fixed ply between the two grips, which causes ply bridging (Figure 3-10b, c) when installing the fixed ply on the compaction block (1). A rotational freedom was given to the gripper by using a barrel nut, which allows the grip to self-adjust the ununiform tension (Figure 3-10d, e).

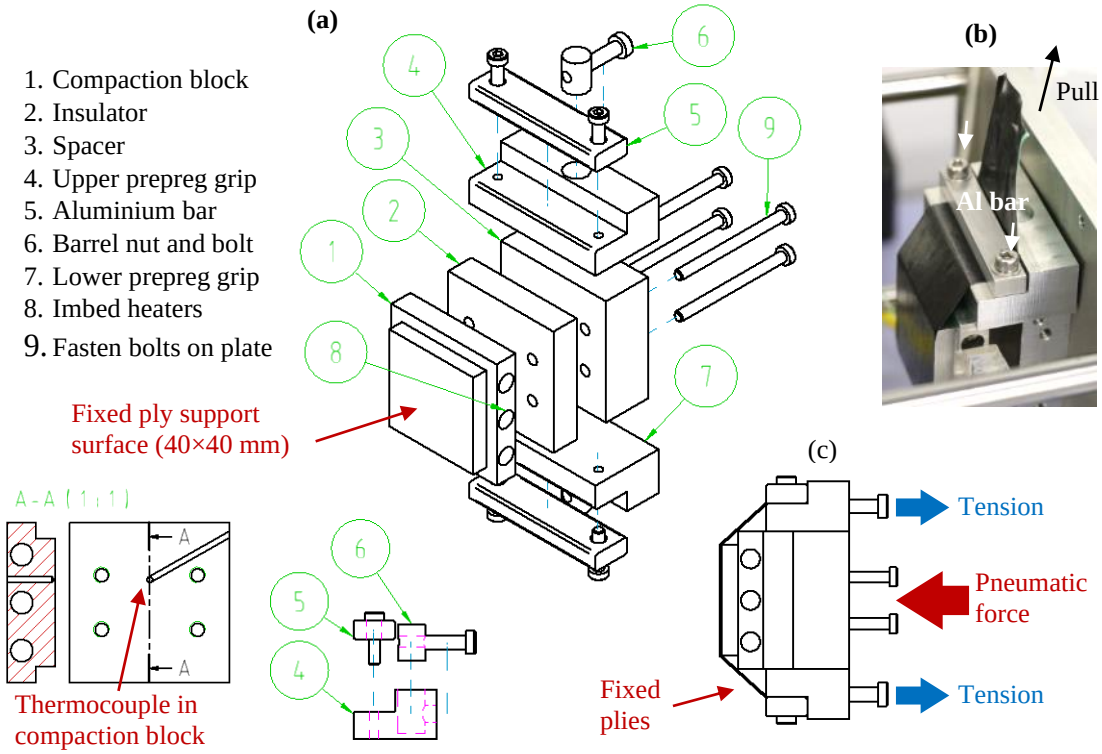

Figure 3-9 (a) Assembly view of compaction unit. (b, c) Schematic drawing photo of a prepreg installed on the compaction unit.

3.2.6 Normal pressure calibration

To apply a normal pressure of 0.1 MPa on the testing area (40 mm × 40 mm), a compaction force of about 160 N was required. This needs approximately 0.5 MPa input air pressure with a pneumatic actuator with a bore diameter of 20 mm. Although the force from the actuator can be preciously controlled by the pneumatic regulator, the friction between the linear shaft and ball bushings as well as the small internal friction within the actuator can affect the final output force. Therefore, the compaction force was calibrated by placing a load cell between the compaction plates (Figure 3-11). Within 0.51 MPa air pressure input, the force output was approximately 160 ± 1 N. Also, when completely releasing the air pressure input from 0.5 to 0 MPa, the remaining output force between the plates was approximately 9 N, which is equivalent to 6 kPa. This difference was caused by the ball busing friction.

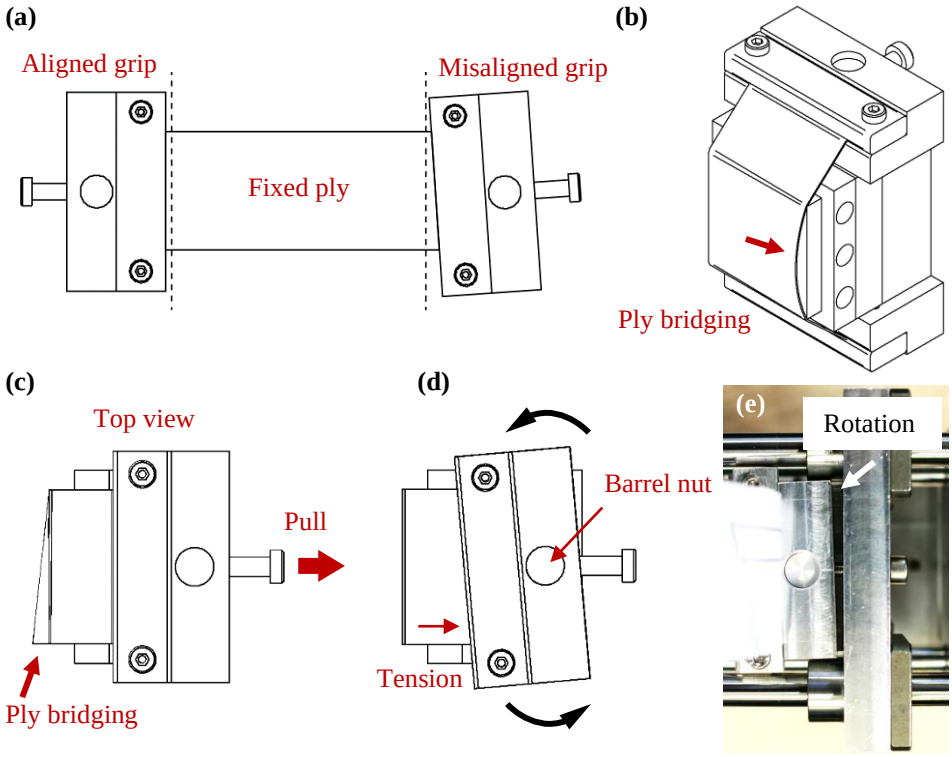

Figure 3-10 (a) Misalignment between the two grips. (b and c) Ply bridging on one side of the ply. (d) Barrel nut allows the grip to balance the ununiform tension by rotation. (e) Photo shows the grip was self-realigned by tension.

3.2.7 Slip distance tracking

Using the crosshead displacement reading from universal testing machine can overestimate the ply slip distance due to the compliance of the test rig. In this work, the ply slip distance was measured using a video gauge system (Imetrum, UK), which provides the tracking accuracy up to 3 μm. The test set-up shown in Figure 3-12a allows for tracking the movement of the central support and the compaction block at the same time (Figure 3-12b, c). The slip distance (δd) is simply obtained by considering the relative position between the targets on the central support and the compaction block. The compaction block could vertically move nearly 30 μm in the test due to the transverse compliance of the linear bushing, but this only happened at a very high loading condition (e.g. 500 N). The deformation in most of testing conditions was neglectable.

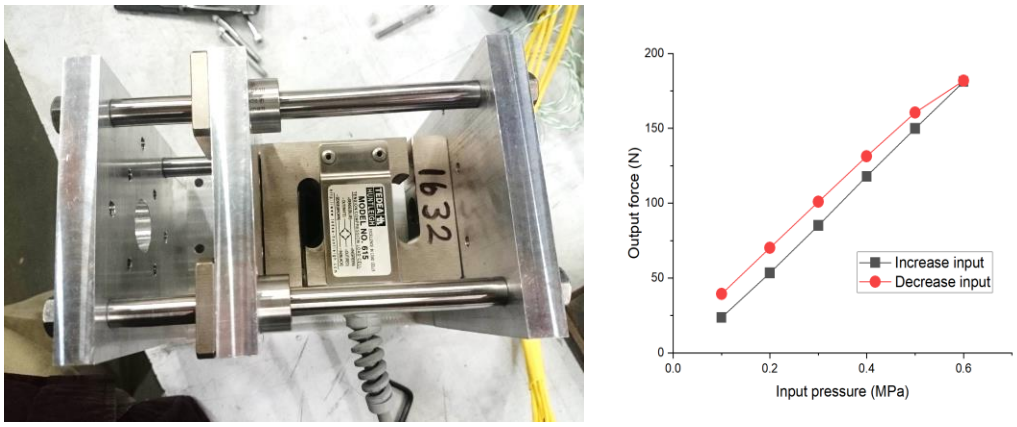

Figure 3-11 The output force calibration

Figure 3-13 shows the interply friction test results obtained by using the crosshead displacement of the testing machine and the video gauge. The peak force (38.8 N) occurred at the slip distances of 0.154 mm and 0.085 mm from the crosshead displacement and video gauge measurement, respectively. This result clearly shows the importance of the direct ply slip distance measurement.

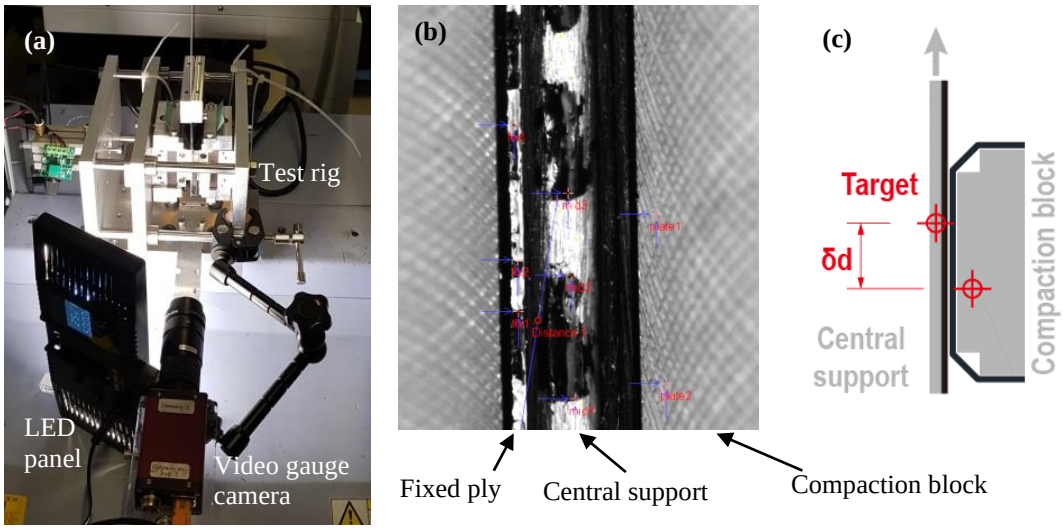

Figure 3-12 (a) The test set-up of measuring ply slip using video gauge camera. (b) Tracking image on video gauge system (c) Schematic drawing shows the slip distance (δd) is obtained from the tracking targets

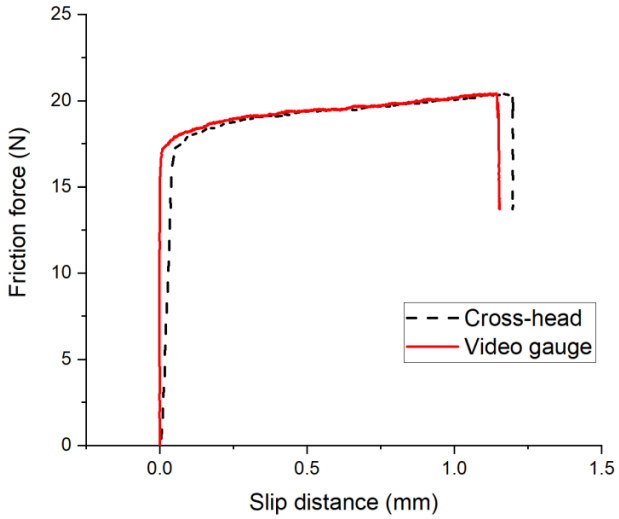

Figure 3-13 The ply slip distance obtained by the crosshead displacement and video gauge.

3.3 Preform bulk factor measurement

In contrast to the interply friction measurement, a compression test set up was much simpler. Normally the test is preformed by a universal testing machine with parallel

compaction discs with an integrated heating system. The only difference is the used stacking sequences, testing temperature, and whether the sample edge is constrained in the test. Three typical test configurations reported in literatures [2,79,103–105] are listed in Figure 3-14.

However, the size of compaction samples is usually much smaller than most of the composite laminates, so it can be challenging to represent the real laminate compaction behaviour through experimental method.

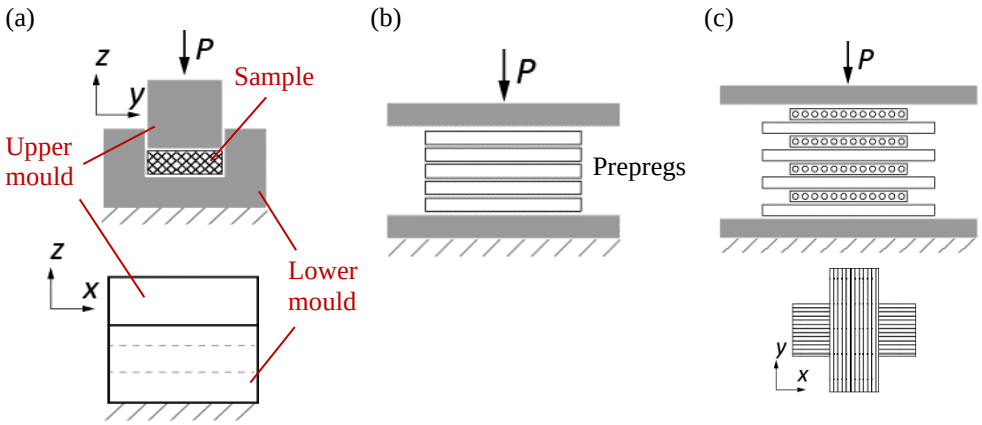

Figure 3-14 Schematic of compaction test configurations from literature

Hubert et al. [103,106] used a U-shaped match die compaction mould, as shown in Figure 3-14a, which has a compaction area of 25 mm × 75mm. The device was mounted on a universal testing machine with a heat chamber to apply the force and heat. The temperature used was over 100°C, which was monitored by two thermocouples attached on both upper and lower moulds. The sample materials were unidirectional thermoset prepregs. All 0° and quasi-isotropic stacking sequences were tested. The sample was not able to expend along the y-direction under pressure due to the walls of the U-shaped bottom mould, but no constraints on the x-direction, so resin could squeeze out from the both ends.

Figure 3-14b is the test configuration used by Lukaszewicz et al. [105]. The test was performed by a universal testing machine with parallel heated discs. The test samples were formed with 8 layers of 0° fibre thermoset prepregs without edge constraints. The test temperature was between 20°C and 40°C, which was considerably lower than a typical curing temperature process for thermoset prepregs.

Hall et al. [79] and Nixon-Pearson et al. [2] used a similar test set-up to Lukaszewicz (Figure 3-14c), but different cross-ply stacking sequences ($[0/90]_8$, $[0_2/90_2]_4$ and $[0_4/90_4]_2$) were used. The samples were laid into a cruciform shape as shown in the Figure 3-14c, which is to minimise over spreading transversely to the fibre direction under compaction. In Nixon-Pearson's work, two sample sizes were used, which gave the centre pressurised area of 15 mm × 15 mm and 30 mm × 30 mm. The force and thickness change of the sample were recorded by the testing machine. The testing temperature was in the range from 30°C to 90°C and different compaction pressures were used with no edge constraints, so resin can easily squeeze out under high temperature and pressure.

In this study, the sample preparation was similar to the description in Nixon-Pearson's [2] work, and the compaction test was performed with the interply friction test rig with a modified configuration.

3.3.1 Test set-up configuration

The compaction test configuration is shown in Figure 3-15. The temperature and pressure control methods were the same as used in the interply friction test process. The only difference was that the compaction force was applied by a pneumatic actuator with a 50 mm bore diameter (CDQ2B50TF-30DZ, SMC, JP) to provide a higher pressure. The sample thickness change was recorded by using a video gauge system.

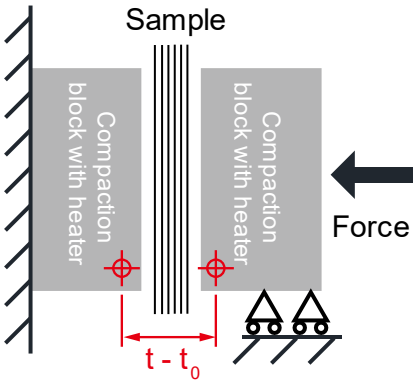

Figure 3-15 The concept of compaction test configuration

Because the actual compaction surface was unable to see, the tracking targets were set on the compaction block as shown in Figure 3-15. The thickness change, $t-t_0$, was measured, where the t_0 is the distance when the compaction blocks are closed without the sample.

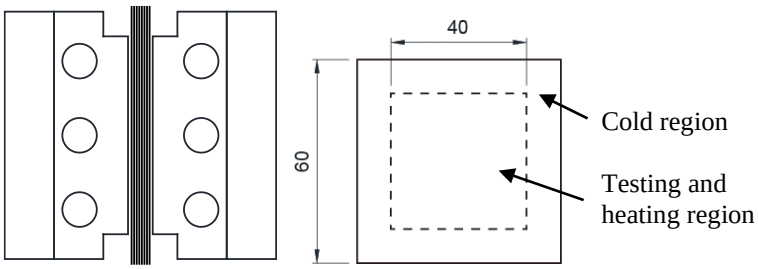

Figure 3-16 Configuration of the compaction test with oversized sample (not in scaled)

3.3.2 Resin bleed control

The laminate thickness is dominated by the volume of fibres and matrix. When curing a composite part under a high pressure in autoclave, some resin bleeding is ideal to remove the voids and control the fibre volume fraction to a right level. However, the problem of the compaction test is that the sample size is much smaller than typical sizes of laminates, significant resin squeeze-out can happen under a high compaction pressure. Therefore, the test will require some control to limit the resin bleeding.

The approach used in this research was to use an oversized laminate sample (60 mm × 60 mm). Each sample was debulked for 10 minutes after the lay-up was completed, and then placed between the compaction blocks (Figure 3-16). Because the laminate has been pre-compacted, the cold region become a barrier to reduce the amount of resin escapes from the hot testing area at the centre.

3.4 Conclusion

This chapter reviewed different test rig designs used for characterisation of interply friction described in literatures, also in-depth discussions and comparisons on how to minimise the variation of testing conditions and to improve the accuracy of measurement. A brief review of compaction test was also given.

Based on the discussion in the review, a custom-designed test rig was developed in this work, which can be used to measure both interply friction and compaction behaviour of an uncured prepreg stack. In the interply friction test, a special prepreg fixture design with a video tracking technique was used to measure the actual ply slippage, which minimised unwanted deformation from test rig and improve the accuracy of measurement. A flexible central support design could avoid local stresses on the testing area due to set-up misalignment. In the compaction test configuration, the compaction force was applied by a pneumatic system to generate the normal force in the interply friction. The thickness change was accurately recorded by the video tracking system. The resin bleed issue was considered in the sample preparation.

4 FORMABILITY OF CARBON/EPOXY PREPREG LAMINATES INTERLEAVED WITH TOUGHENING MATERIALS

Forming is a cost-effective manufacturing method for mass production, as it can create product shapes by deforming flat sheet materials. The level of interply friction is an important indicator of material's formability in many preforming methods for continuous fibre composites due to their laminated structure. Although the processing conditions such as the temperature and applied pressure level affects the interply friction, the behaviour is mainly dominated by the rheological property of the resin interlayer in a stack of prepregs. For high performance composites, the included interlaminar toughening materials can significantly change the resin behaviour, which is the field that has not been well investigated in previous studies. This chapter provides an in-depth analysis on the interply friction of uncured prepregs with a range of different interleaving tougheners under different processing conditions.

4.1 Experimental

4.1.1 Sample preparation

The prepreg and interleaving particles used in the interply friction test are the same as those used in the study on their effect on interlaminar fracture tougheness. The detail of these materials and the particle deposition method are presented in Chapter 2 An

additional interleaving material used in this test was a fine nonwoven veil (Optiveil®, TFP, UK), which is formed with randomly distributed polyester fibres with a length of 5 mm and a diameter of 6 μm. TFP supplied both 4 g/m^2 and 6 g/m^2 veil products, the average thicknesses under a 10 kPa pressure were 30 μm and 50 μm, respectively. A cross-linked polyester binder was used in the fabrication process.

Figure 4-1 Optiveil® polyester veil (TFP, UK)

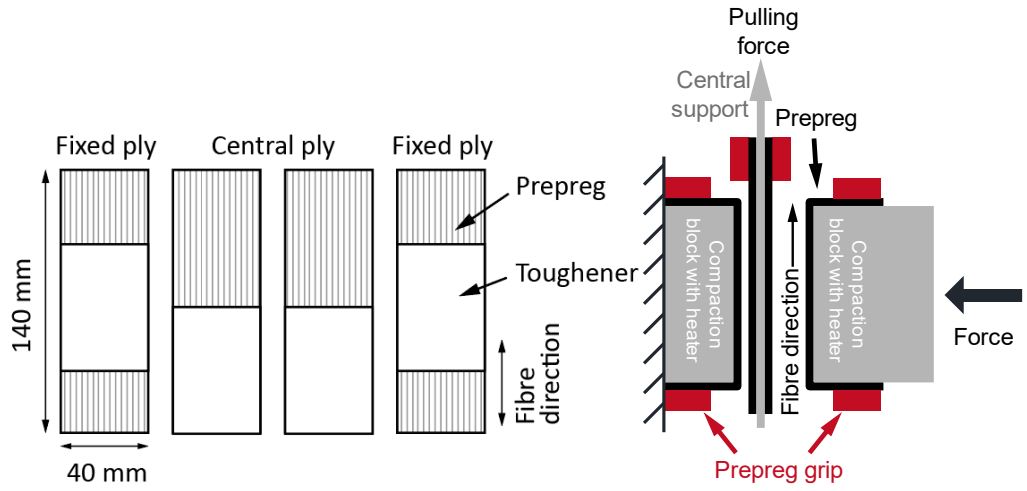

Figure 4-2 Schematic drawing of the test sample configuration

Each test required four plies of prepregs cut into a dimension of 40 mm × 140 mm, as shown in Figure 4-2. The toughening particles were directly applied on the testing area of prepreg surface with an approximate size of 40 mm × 60 mm. The particle amount on each sample was calculated by measuring the weight change before and after particle deposition. Polyester veils were cut into a size of 40 mm × 60 mm and then attached on the testing area. The details of interply friction test rig configuration, sample position and ply slippage measurement method are described in Chapter 3.

4.1.2 Surface analysis

In order to observe the surface condition of a prepreg with the particle layer, a single ply compaction test was carried out. A single prepreg ply was coated with the particles using the same method described in Chapter 2. The coated face was covered with a release film, and then pressed with the compaction blocks of the interply friction test rig, as shown in Figure 4-3. The applied pressure was 0.1 MPa for 3 minutes at room temperature to simulate the debulking process. Then the sample surface was observed using a microscopy and SEM.

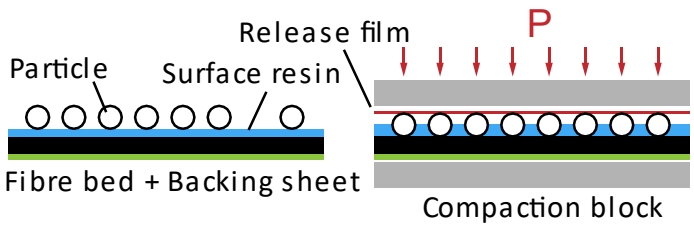

Figure 4-3 Schematic of single ply press

4.1.3 Test condition

In this experiment, the chosen test conditions were similar to a typical procedure of diaphragm forming process. Table 4-1 shows the test parameters in each interply friction test. After installing the prepreg sample in the test rig, 0.1 MPa pre-compaction pressure was applied to the sample for 5 minutes at 25°C, which simulates the debulking process during the lay-up when creating a flat prepreg stack for forming. Then the temperature of the sample was increased to 60°C using the built-in heaters embedded in the compaction block. The heating took about 3 minutes, and during heating the input air pressure to the pneumatic actuator was removed, but very low pressure (about 6 kPa) still remained due to the friction between the linear shaft and ball bushing. Once the temperature reached 60°C, the central plies were pulled by the tensile testing machine at a fixed cross-head speed of 1 mm/min, until the ply slipped by 1.2 mm.

Two pressure levels were used in the friction test stage, to simulate two different forming conditions. As shown in Figure 4-4, for a single diaphragm forming scenario, vacuum pressure applied to the diaphragm deforms the prepreg stack. Since the force is mainly applied on the top side of the preform, the area where ply slippage is required is not subjected to any pressure until the end of forming event; therefore, almost very low normal pressure was applied for the first test case. The second scenario is for double diaphragm forming. In this case, vacuum is applied between the two diaphragms that provides some compaction to the preform. Thus, normal pressure was applied during the test for this scenario. Because the applied pressure level between diaphragms varies depending on the used materials and processing condition, 0.1 MPa was used for the test in the second test case.

Table 4-1 Procedure of the interply friction test

Stage	Pressure	Temperature °C	Time min	Pulling rate mm/min
1. Pre-compaction (Debulking)	0.1 MPa	25	5 mins	-
2. Heating	6 kPa	25 → 60	-	-
3. Testing	6 kPa/0.1 MPa*	60	-	1

* Two different pressure levels were used to simulate a single or double diaphragm forming process.

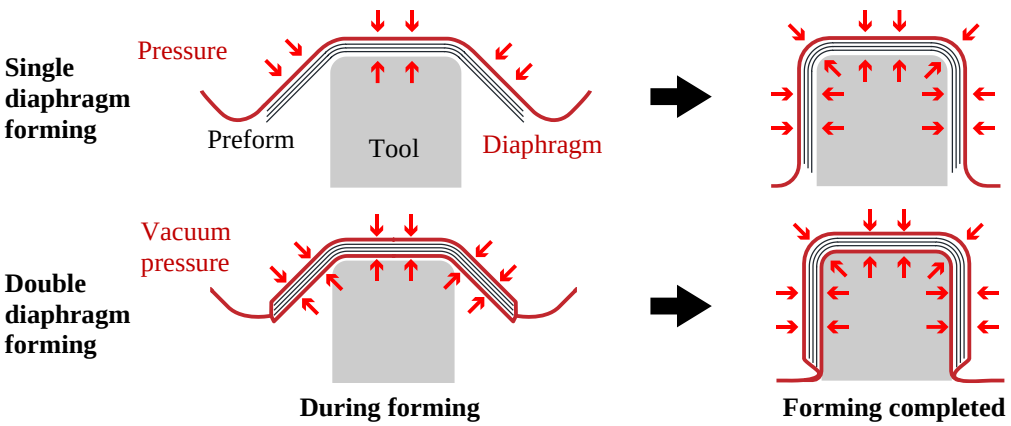

Figure 4-4 The different pressure conditions between single and double diaphragm forming

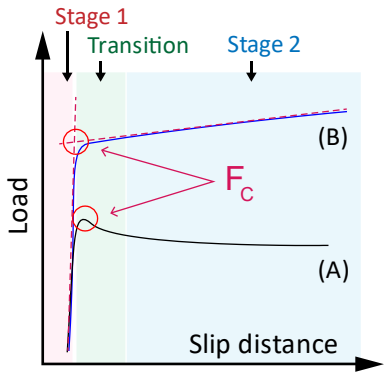

Figure 4-5 The method to determine the critical force, F_C

Figure 4-5 schematic showed the trends of friction force vs. slip distance curves in the interply friction test. The force growth was rapidly in the stage 1 and then stabilised in the stage 2. There was a transition stage in between. The trend of the interply friction force varied depending on the type and areal weight of the applied particles. Some interesting discussions on these behaviours in the transition stage and stage 2 are provided in Section 4.3. The method to determine F_C is demonstrated in Figure 4-5. For the case (A) where the peak in the curve was used as F_C. While in case (B), the F_C was determined by the intersection points between the two lines created by linear regressions of the curves in the stage 1 and 2.

4.2 Results

4.2.1 Effect of microparticle tougheners

4.2.1.1 Low pressure condition

Figure 4-7 to Figure 4-11 showed the force vs. ply slip distance curves tested with a normal pressure of 6 kPa at 60°C for different particle types. For the reference sample (0 g/m^2), some variation of friction force was observed in repeated tests. Such difference might be attributed to the inconsistent quality of the prepreg surface; e.g. the local resin distribution and fibre misalignment. In the initial stage of the test (stage 1),

the force increased with almost no ply slippage before reaching a critical force. After the critical force (F_C), ply slippage began, the force stabilised but increasing gradually with the ply slip distance in the stage 2. Such a slowly developing friction force was reported in literature [1], which could be due to the interaction between the fibres within the two fibre beds that came into contact [66]. As shown in Figure 4-6, when two fibre beds have the same fibre orientation, the fibres on each side are separated by the resin at the interface with some trapped air at the initial stage. While the friction test progresses, the applied pressure would cause resin redistribution in the interlayer resulting in more fibre-fibre contacts. This could increase friction force due to lack of lubrication between fibres from the low viscosity resin.

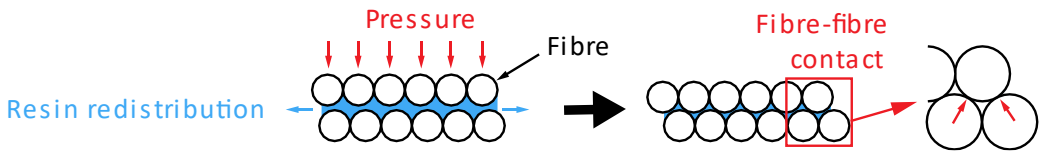

Figure 4-6 Schematic of gradual increased 0° fibre bed contact during ply slippage under normal pressure

In general, all the particle-coated samples showed a lower F_C compared to the reference sample, and the behaviours in the stage 1 were similar; i.e. the force increased without ply slippage. However, the trends in the transition zone and stage 2 were different, depending on the type of particles used. For PA12-d30a and PA6-d16a (Figure 4-7 and Figure 4-8), the force in the stage 2 was nearly unchanged till the end of test. For PA6-d13r (Figure 4-9), the reduction of F_C was limited regardless of particle areal weight, and the F_C appeared as a peak in the transition region. In general, the force increase was not minimal in the stage 2, and a high particle areal weight (20.7 g/m^2) seemed to cause a descending trend of the friction force in the stage 2. The F_C reduction with PA12-d10s (Figure 4-10) was similar to that with the PA12-d30a and PA6-d16a in general, but at a very low particle areal weight (2.6 g/m^2), the force in the stage 2 increased with slip distance. However, when further increasing the amount of particles to 4.8 g/m^2, such behaviour was not observed.

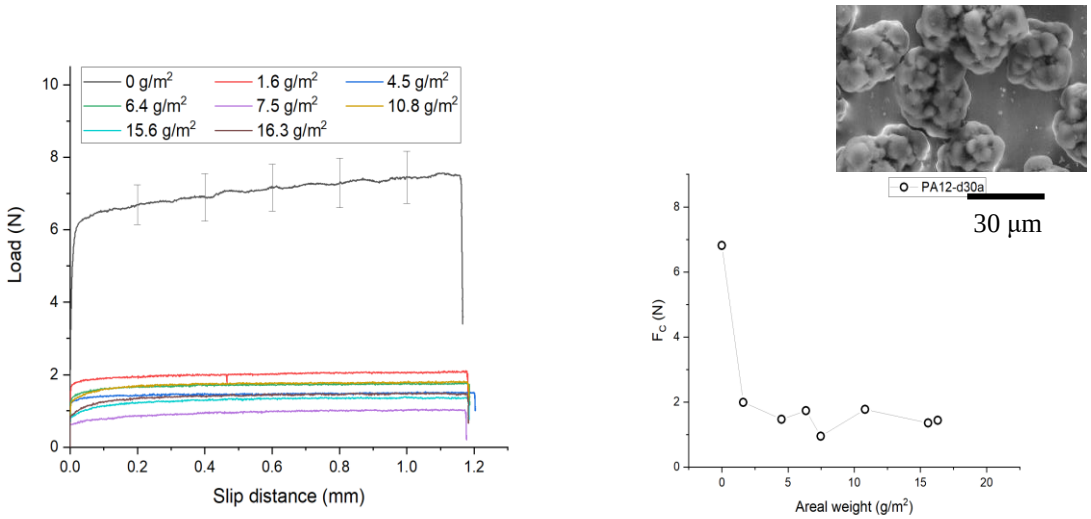

Figure 4-7 Load-slip distance curves and critical forces of samples with PA12-d30a particles tested at 6 kPa, 60°C

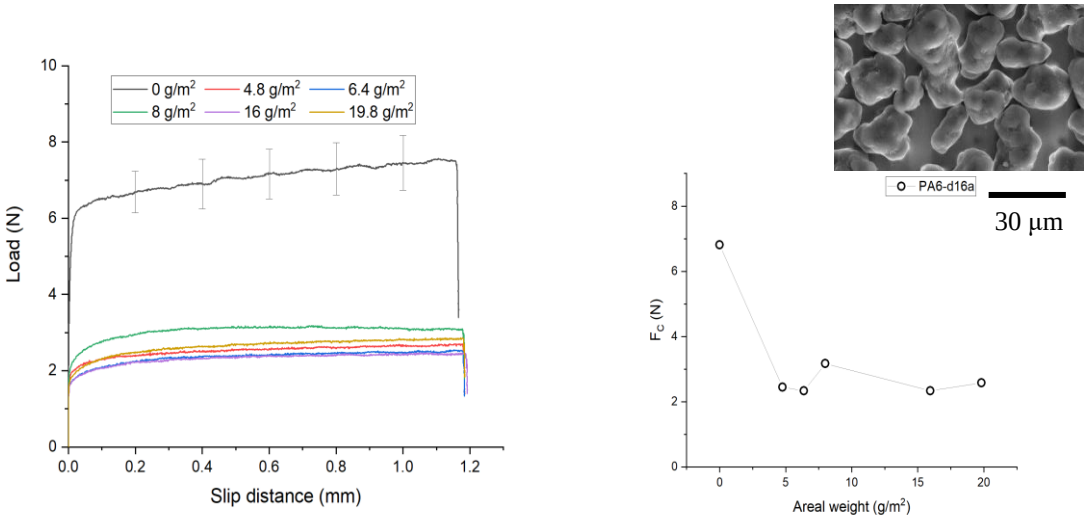

Figure 4-8 Load-slip distance curves and critical forces of samples with PA6-d16a particles tested at 6 kPa, 60°C

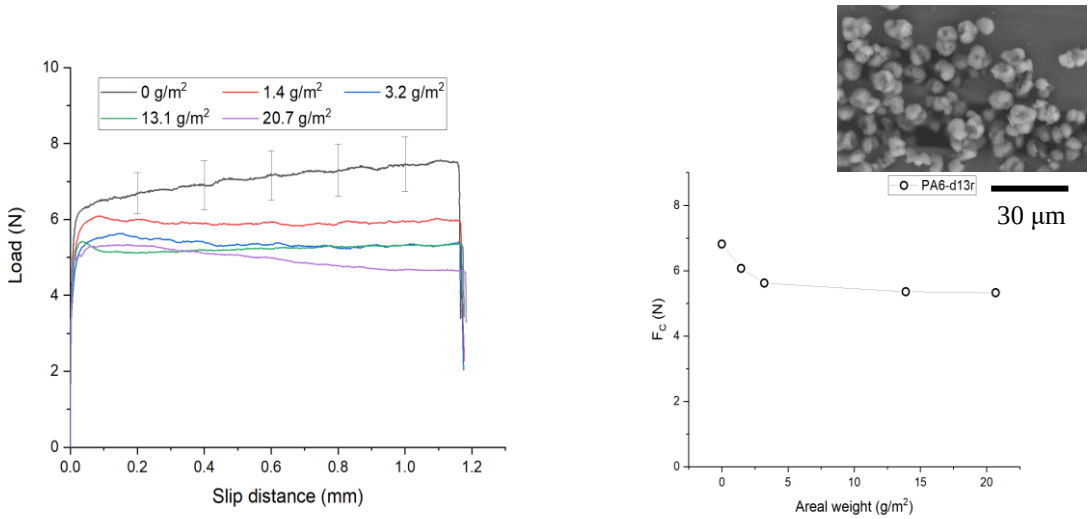

Figure 4-9 Load-slip distance curves and critical forces of samples with PA6-d13r particles tested at 6 kPa, 60°C

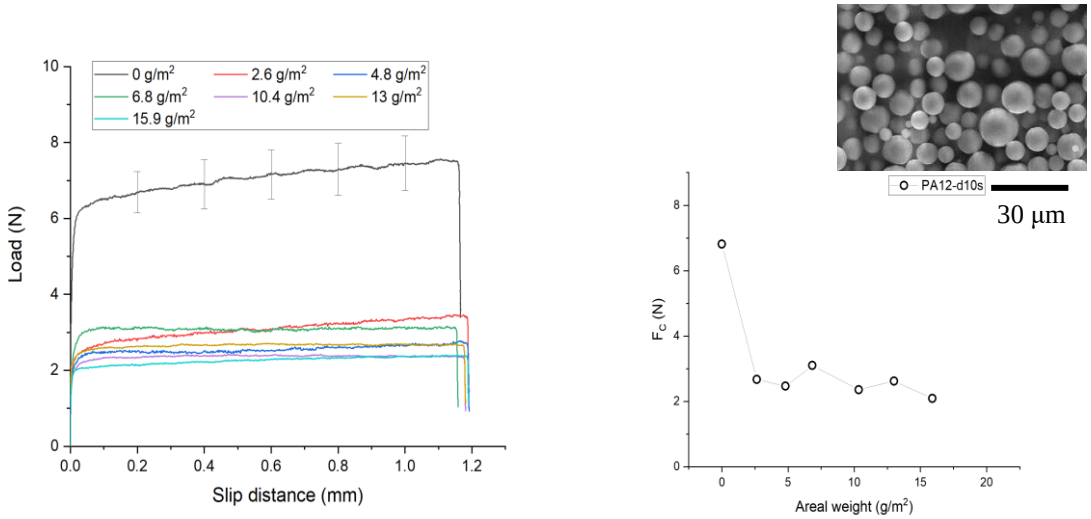

Figure 4-10 Load-slip distance curves and critical forces of samples with PA12-d10s particles tested at 6 kPa, 60°C

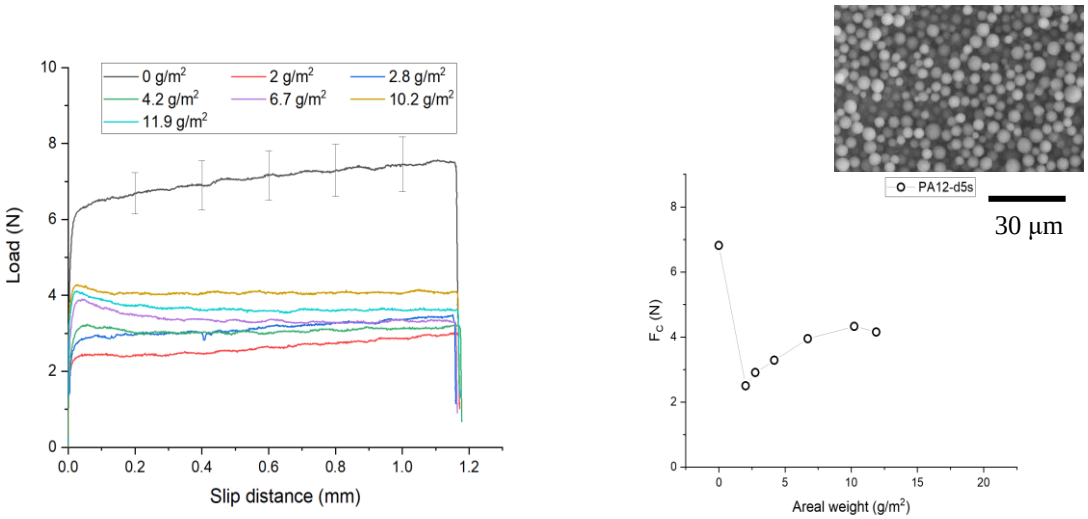

Figure 4-11 Load-slip distance curves and critical forces of samples with PA12-d5s particles tested at 6 kPa, 60°C

PA12-d5s (Figure 4-11) particles showed a rather different response in the force vs. ply slip distance curve. A small amount of particle (2 g/m^2) caused a significant F_C reduction, but with further increase of the particle areal weight, F_C started increasing and a noticeable peak force was found in the transition region. PA12-d5s also showed a gradual force increases in the stage 2 at low areal weight, but such response disappeared when more particles were applied, which is a similar trend as that of PA12-d10s.

4.2.1.2 High pressure condition

Figure 4-12 to Figure 4-16 showed the force vs. ply slip distance curves tested with a normal pressure of 0.1 MPa at 60°C. In general, the stage 1 behaviours of the reference and all the sample coated with particles were the same as the results observed in the low normal pressure test. However, the absolute friction force values were significantly higher.

The PA12-d30a particles (Figure 4-12) induced a different trend in comparison with the results in the low pressure test; a peak force was observed in the transition region. At a lower particle areal weight, the interply friction behaved like a 'stick-slip' response and the transition occurred within a short slip distance. At a higher areal weight, the transition occurred over a longer slip distance, and the F_C appeared slightly later than

the samples with low particle areal weights. In the stage 2, the force values reached a plateau when the amount of particle was less than 10 g/m^2, but further increase of the particle areal weight over 10 g/m^2 resulted in a gradual decrease of the friction force after the transition till the end of test.

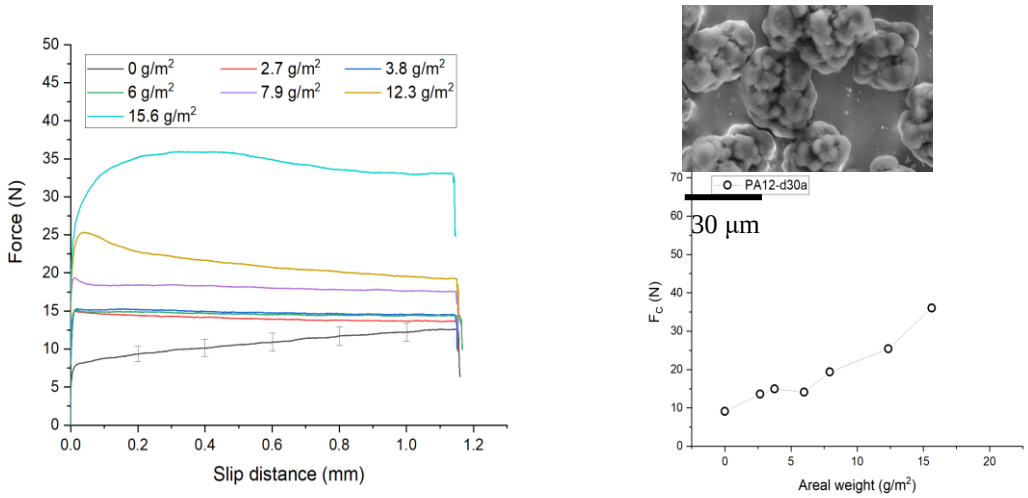

Figure 4-12 Load-slip distance curves and critical forces of samples with PA12-d30a particles tested at 0.1 MPa, 60°C

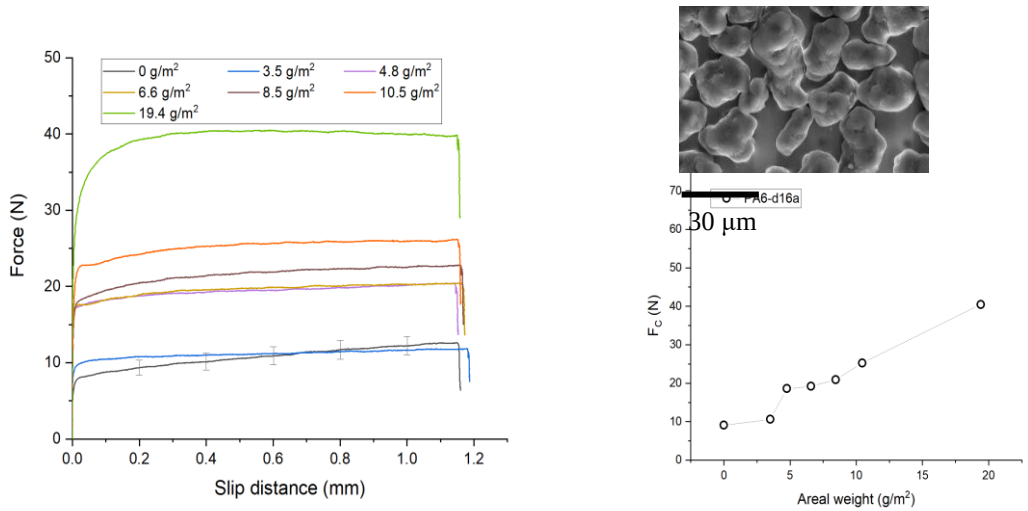

Figure 4-13 Load-slip distance curves and critical forces of samples with PA6-d16a particles tested at 0.1 MPa, 60°C

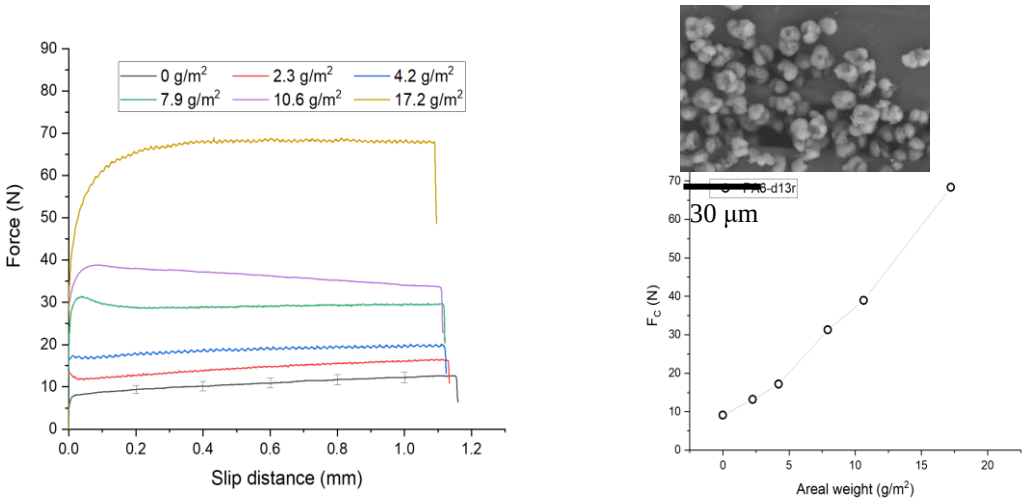

Figure 4-14 Load-slip distance curves and critical forces of samples with PA6-d13r particles tested at 0.1 MPa, 60°C

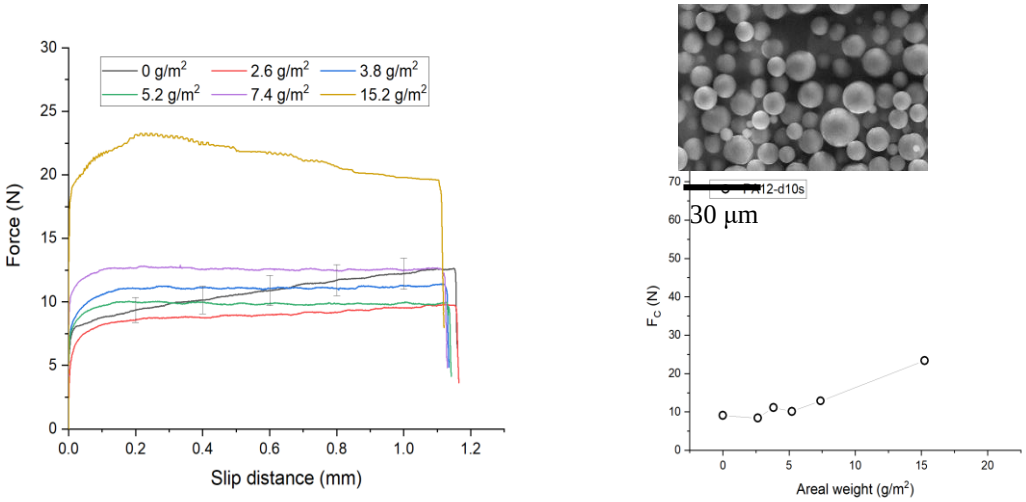

Figure 4-15 Load-slip distance curves and critical forces of samples with PA12-d10s particles tested at 0.1 MPa, 60°C

The PA6-d16a particles (Figure 4-13) induced a rather smooth transition curve without a clear peak force, but with slightly increasing friction force in the stage 2. Similar to the PA12-d30a particles in Figure 4-12, the transition region seemed to be affected by the amount of particle. Below 10.5 g/m^2, the stage 2 started with less than 0.1 mm of ply slip distance, but the 19.4 g/m^2 sample showed a long transition region, where the stage 2 started approximately from 0.4 mm of slip distance.

The sample coated with PA6-d13r (Figure 4-14) also showed a similar migration of the peak F_C in the transition with the increased particle areal weight. At 2.3 g/m^2, the F_C occurred immediately after the start of test. A stick-slip behaviour was found as a clear load drop after the peak force. However, when further increasing the particle amount to about 10 g/m^2, the force reached F_C at nearly 0.1 mm of ply slippage. The transition ended at about 0.4 mm of slip distance at the areal weight of 17.2 g/m^2.

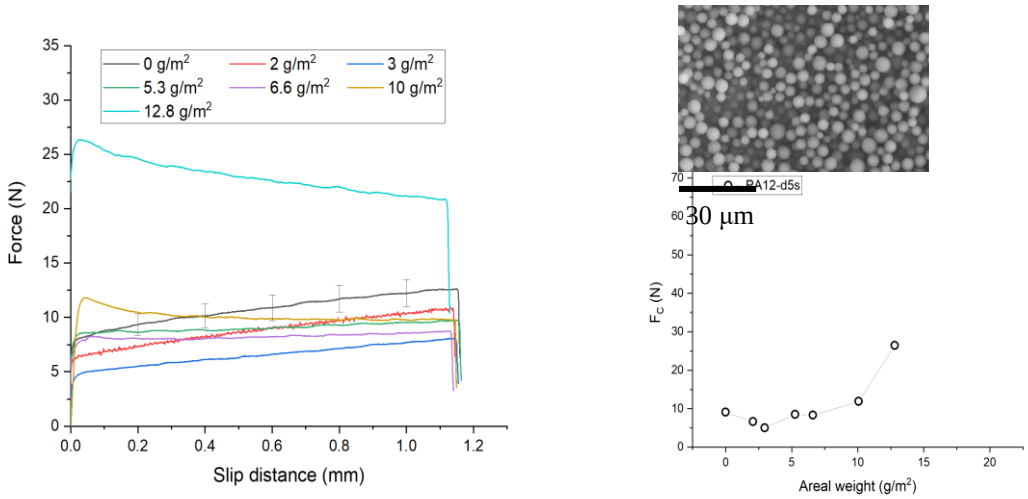

Figure 4-16 Load-slip distance curves and critical forces of samples with PA12-d5s particles tested at 0.1 MPa, 60°C

Figure 4-15 shows the test results of samples coated with PA12-d10s particles. The length of transition region was not significantly affected by the particle areal weight. The transition ended between 0.1 mm and 0.2 mm of slip distance. The friction force reached a plateau in the stage 2 when the particle areal weight was lower than 10 g/m^2, but an obvious load decrease was observed in the 15.2 g/m^2 sample.

For the PA12-d5s particle (Figure 4-16), at low particle areal weights (2 and 3 g/m^2) the curves have a similar trend as the reference sample; i.e. the friction force gradually increased in the stage 2. However, peak forces emerged when further increasing the particle amount to over 5 g/m^2. The trend in the stage 2 was not affected by coating a small amount of PA12-d5s particles, but a higher particle areal weight completely changed the trend; i.e. the friction force gradually decreased as the ply slip distance increased.

4.2.2 Nonwoven veils

Figure 4-17 shows the interply friction between the prepreg sheets with one layer of the 4 g/m^2 polyester nonwoven veil on each surface, which was measured under both 6 kPa and 0.1 MPa at 60°C. At the low pressure condition, the general behaviour was similar to the PA12-d30a and PA6-d16a; i.e. no peak force in the transition, no obvious force change in the stage 2. However, it was observed that ply slippage was initiated early in the stage 1 (started at much lower force level than the samples interleaved with particles), which could be due to the low surface friction between the two nonwoven veils in contact at a low compaction pressure. At the high normal pressure, such ply slippage was not observed in stage 1. The critical friction force was much higher than those of the samples coated with particles at the same areal weight. No peak in the transition region appeared, and the force slightly decreased with increase of slip distance when entering the stage 2.

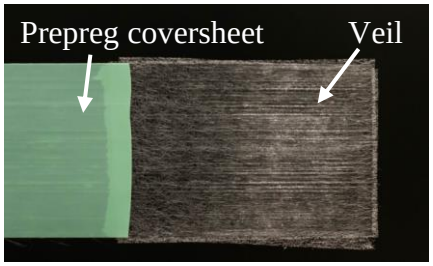

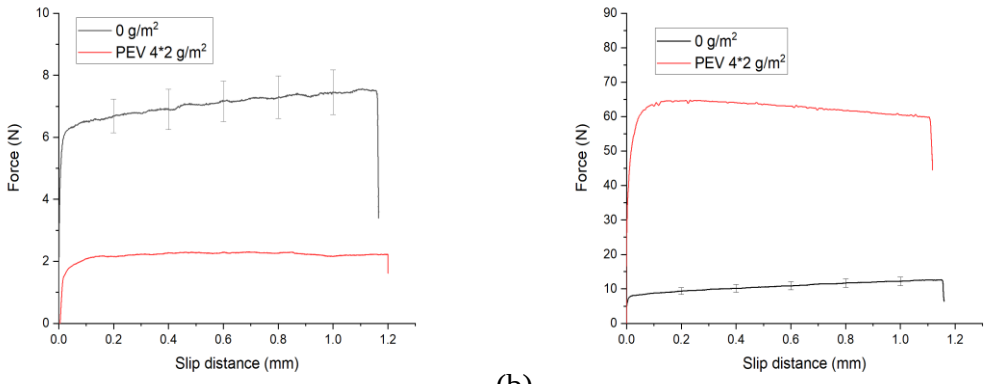

(a) (b)

Figure 4-17 Load-slip distance curves of samples with two layers of polyester veils tested under (a) 6 kPa and (b) 0.1 MPa

4.2.3 Critical forces

Figure 4-18 shows the critical friction force (F_C) from all the friction tests presented from the Figure 4-7 to Figure 4-17. In the low pressure tests (Figure 4-18a) at 60°C, all the interleaving materials caused a reduction of the F_C. The PA12-d30a was the most effective particle with an average F_C of 1.5 N, which is 70% reduction compared to the 6.8 N from the reference sample (0 g/m^2). It could be inferred that its large particle diameter was more effective to separate the resin layer at the interface. Two layers of polyester veils (8 g/m^2) yielded the second highest reduction of 67%, which could be the same reason as described above; the large thickness of each veil causes less resin adhesion at the interface. PA12-d10s and PA6-d16a showed a similar trend; the average reduction was 63% and 62%, respectively. The PA6-d13r was not as effective as the other particles, probably due to its high surface roughness increasing friction during ply slippage; the averaged reduction was only 18%.

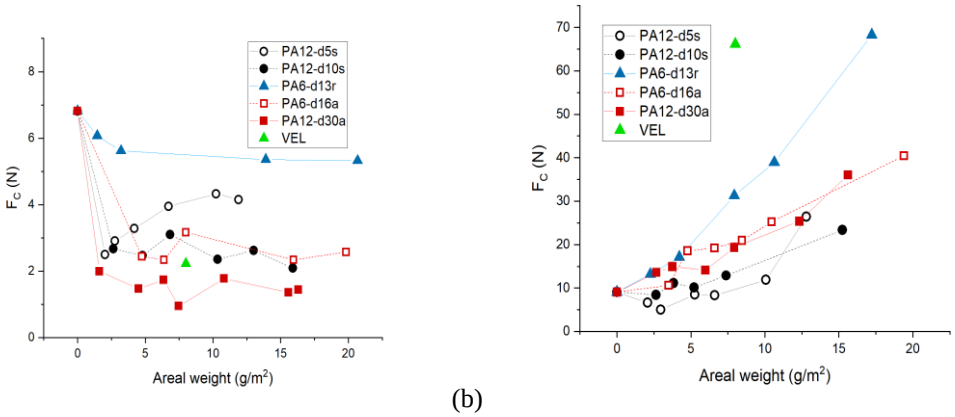

Figure 4-18 Critical force (F_C) of sample with various of coated materials tested at 60°C, (a) 6 kPa and (b) 0.1 MPa

In terms of the general trend in the low normal pressure condition, a considerable reduction of F_C could be achieved by coating a small amount of particles (<5 g/m^2). However, further increase of particle areal weight did not cause a further reduction of F_C. Another interesting part is that the PA12-d5s did not follow the general trend; The F_C decreased by 63% to 2.5 N with 2 g/m^2, but then the F_C increased with the areal weight, yielding the lowest reduction of 37% (4.3 N) at about 10 g/m^2 (The trend

beyond this point was not validated in this work as its small particle size made it difficult to achieve a uniform particle distribution.)

In the tests at 0.1 MPa normal pressure (Figure 4-18b), the average F_C for the reference sample was 9.1 N, which is about 33% higher than the low pressure condition shown in Figure 4-18a. Differently from the low pressure test results, the overall F_C of PA6-d13r, PA6-d16a and PA12-d30a increased almost linearly with particle areal weight. The ply slip resistance of PA6-d13r samples was much higher than the other particles. On the other hand, the PA12-d10s and PA12-d5s showed much less influence on the F_C at lower particle areal weights, and the F_C increased when the particle amount was greater than 5 g/m^2. The same phenomenon was observed in measuring the interply friction of T700/M21, which is a commercial prepreg with thermoplastic particles within the surface resin layer [1].

For the polyester nonwoven veil, F_C was much higher than most of the particles, which could be due to the random distribution of short fibres, which might have caused fibre interlocking between the two contacted surfaces under compaction pressure.

4.2.4 Surface morphology

The images in Figure 4-19 shows the prepreg surface coated with the largest PA12-d30a and the smallest PA12-d5s particles. After particle deposition, the particles were adhered to the surface resin layer and held in place by the tacky resin (Figure 4-19a). In the room temperature compaction, e.g. debulking, the applied force pushes the particles further into the resin layer. As shown in Figure 4-19b, the diameter of PA12-d30a particles was far greater than the thickness of resin layer, and only a small part of each particle was embedded in the resin layer, while most of the particle surface was still exposed, which could form a dry surface. On the other hand, the PA12-d5s particles (Figure 4-19c, d), which have very small particle diameter, provided a similar deposition behaviour, but it was observed that the particles can embed more deeply into the surface resin by fitting into the gaps between fibres.

Figure 4-19e and Figure 4-19f show samples that were heated by a heat gun while compressing the sample with a flat substrate, which led to squeezing out more resin from the internal fibre bed layer to the surface. It is clear that a greater volume of the

PA12-d30a particles, as shown in Figure 4-19e, was embedded in the resin layer due to the reduced resin viscosity, but the resin couldn't fully cover the particle surfaces. In contrast, the PA12-d5s particles were completely pushed into the surface resin, only a very small part of particles exposed on the resin surface (Figure 4-19f).

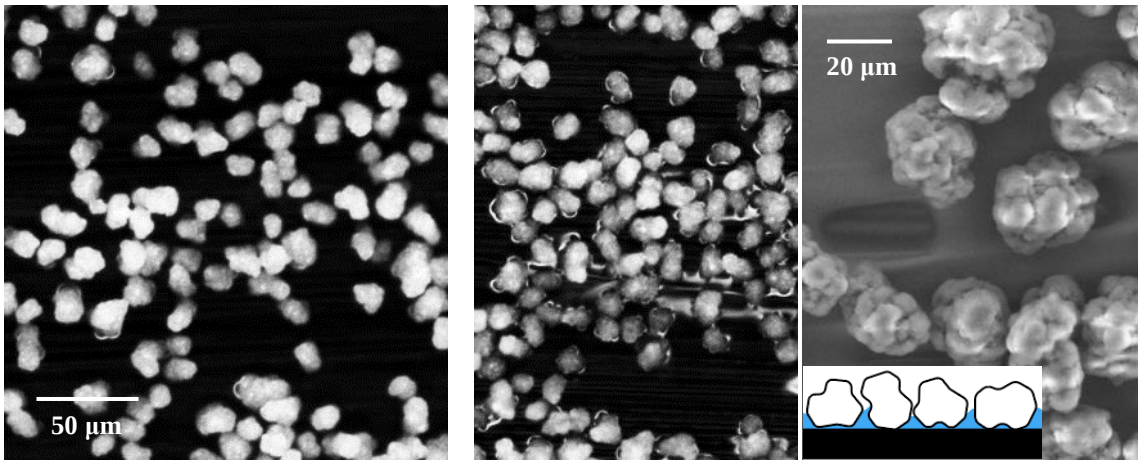

(a) PA12-d30a, 6 g/m^2, before press (b) PA12-d30a, 6 g/m^2, after press

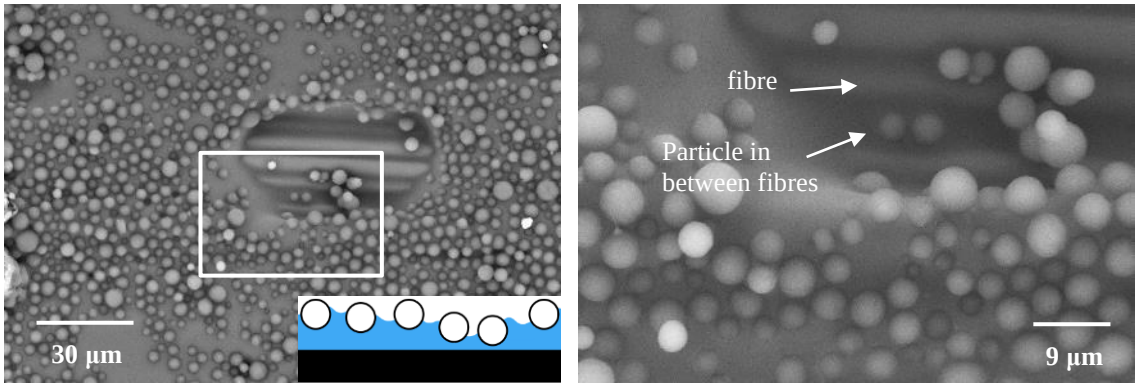

(c) PA12-d5s, 2 g/m^2, after press (d) PA12-d5s, 2 g/m^2, after press

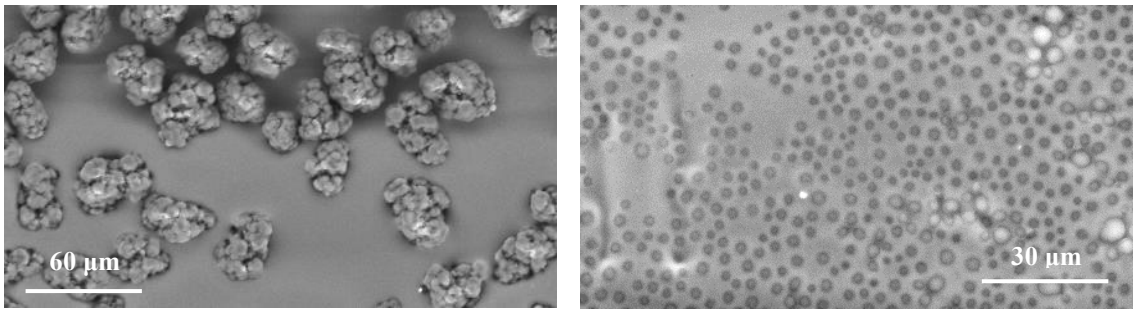

(e) PA12-d30a, 6 g/m^2 (f) PA12-d5s, 2 g/m^2

Figure 4-19 Before and after press of single ply surface with particles

4.3 Discussion

The interply friction is related to the surface condition of the prepreg, which usually refers to the fibre architecture and the included particle toughenners [1,43,107]. However, most of the previous studies on interply friction have focused on the wet friction due to the exposed surface covered by the uncured resin. Potter [87] have reported that thermoplastic particles spread on the prepreg sheet could reduce the required force to deform a stack of prepregs due to the reduced surface tack, but the underlying mechanism have not yet been well investigated. This work demonstrated that the friction behaviour can be significantly affected by the physical features of the particle (i.e. size and shape) and the amount. The observed surface morphology of prepreg could explain the trends of the test results.

4.3.1 Effect of particle size and areal weight

The interleaving particle size affected the interply friction differently in the low and high normal pressure conditions. At 6 kPa (Figure 4-18a), when comparing the PA12-d30a, PA6-d16a, PA12-d10s and PA12-d5s, the average critical friction force (F_C) was reduced as the particle size increased. A possible explanation could be that the particle layer separated the resin interface, which causes less slip resistance coming from shearing the resin layer. In this case, the large particles would be more effective than smaller particles, as the particle diameter would be much greater than the thickness of the surface resin layer (Figure 4-19b); this condition would result in a dry particle-particle dominated interface. The additional particles wouldn't affect the resin layer further, therefore the F_C would be almost unchanged.

In the 0.1 MPa test, the applied high pressure would push the particles against the fibre bed, which increased direct particle-fibre contact without a good wet lubrication effect from the resin, thus the interply friction would be increased in general. However, an interesting observation was that the PA12-d5s and PA12-d10s particles exhibited almost no obvious change of F_C at low particle areal weight (<5 g/m^2). The size of these particles is close to the fibre diameter, as shown in Figure 4-19d, so that the PA12-d5s particles can be located between fibres. Therefore, at low areal weights, the particles

could be pushed into the fibre bed, and the interface could be dominated by the fibres and resin (Figure 4-20a). When the amount of particles is enough to fully cover the prepreg surface, the friction behaviour would become close to a dry friction condition (Figure 4-20b).

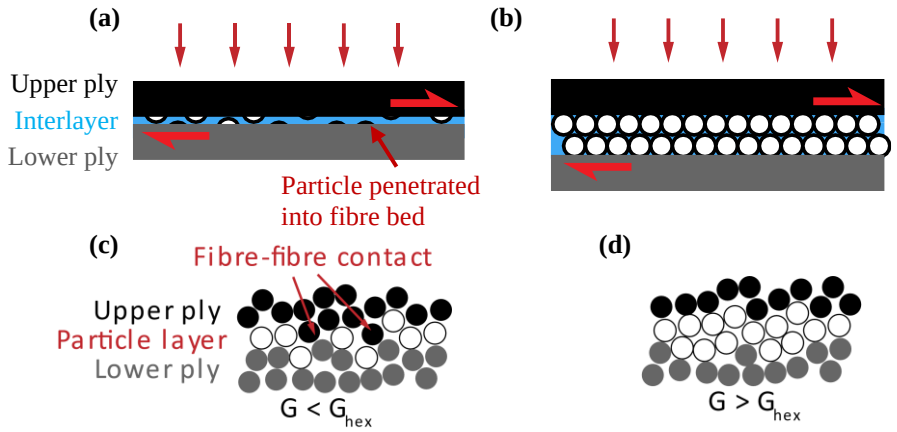

Figure 4-20 Interlayer condition between low and high particle areal weight

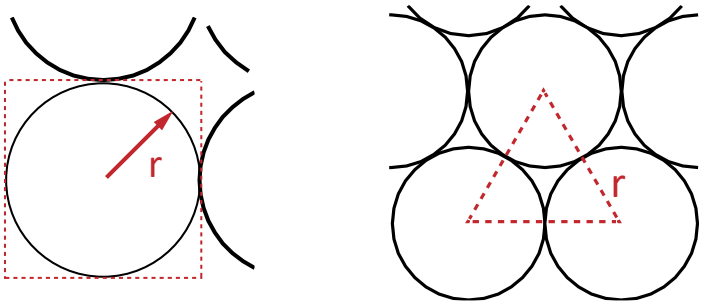

Figure 4-21 Top view of single particle layer in different packing arrangement

This transition characteristic could be explained by calculating the theoretical 2D particle packing density. Figure 4-21 schematically shows the unit area of a single particle layer in close and hexagonal particle packing structures.

The equation to calculate particle areal weight, *G*, is:

$$G = \frac{W}{A} \qquad \textbf{Equation 4-1}$$

Where the W is the total particle weight and A is the total coated area of the prepreg. Assuming that each particle has a radius of r and the density of particle material is ρ, the required particle areal weights to form a single particle layer with close packing and hexagonal packing arrangements can be described as:

$$G_{close} = \frac{\frac{4}{3}\pi r^3 \rho}{4r^2} = \frac{\pi r \rho}{3} \qquad \textbf{Equation 4-2}$$

$$G_{hex} = \frac{\frac{4}{3}\pi r^3 \rho}{2\sqrt{3}r^2} = \frac{2\pi r \rho}{3\sqrt{3}} \qquad \textbf{Equation 4-3}$$

When considering that the average diameter of PA12-d5s is 5 μm, the G_{close} and G_{hex} are 2.67 g/m^2 and 3.08 g/m^2, respectively. This means another particle layer could be formed when the particle amount is greater than those values.

The calculated results agreed with surface analysis shown in Figure 4-22, which are the prepreg surfaces coated with different amounts of PA12-d5s particles and compressed at an elevated temperature. At 1.2 g/m^2 (Figure 4-22a), distinct particle and resin regimes were seen. When the amount was increased to 2.9 g/m^2 (Figure 4-22b), the particles formed a high density single particle layer in the surface resin layer. Further increase of the areal weight to 5.7 g/m^2 (Figure 4-22c) resulted in particles stacked on top of each other.

This different particle coverage significantly affected the interply friction behaviour as shown in Figure 4-16. The stage 2 exhibited an ascending trend in the 2 and 3 g/m^2 samples, suggesting that their friction behaviour was less effected by particle-particle friction at the interface due to the particle penetration into the fibre bed. Thus, the gradually increasing fibre-fibre contact as the test progressed was still observed (Figure 4-20c), as described in Section 4.2.1. When further increasing the particle areal weight to 5.3 g/m^2 and 6.6 g/m^2, the trend in stage 2 became stable, which was attributed to the interlayer successfully separated by the particle layers. In addition, the F_C of 5.3 g/m^2 and 6.6 g/m^2 was slightly higher than the 2 and 3 g/m^2 cases, which could imply the increased dry friction. This agrees with the calculation result from $G_{hex} = \frac{\frac{4}{3}\pi r^3 \rho}{2\sqrt{3}r^2} = \frac{2\pi r \rho}{3\sqrt{3}}$

Equation 4-3 4-3. Interestingly, such transition in stage 2 was not observed with slightly larger PA12-d10s particles and the others, which might be due to their size that is too big to fit between fibres, as a result, the fibre-fibre interaction could be avoided even with a small amount of particles (Figure 4-23).

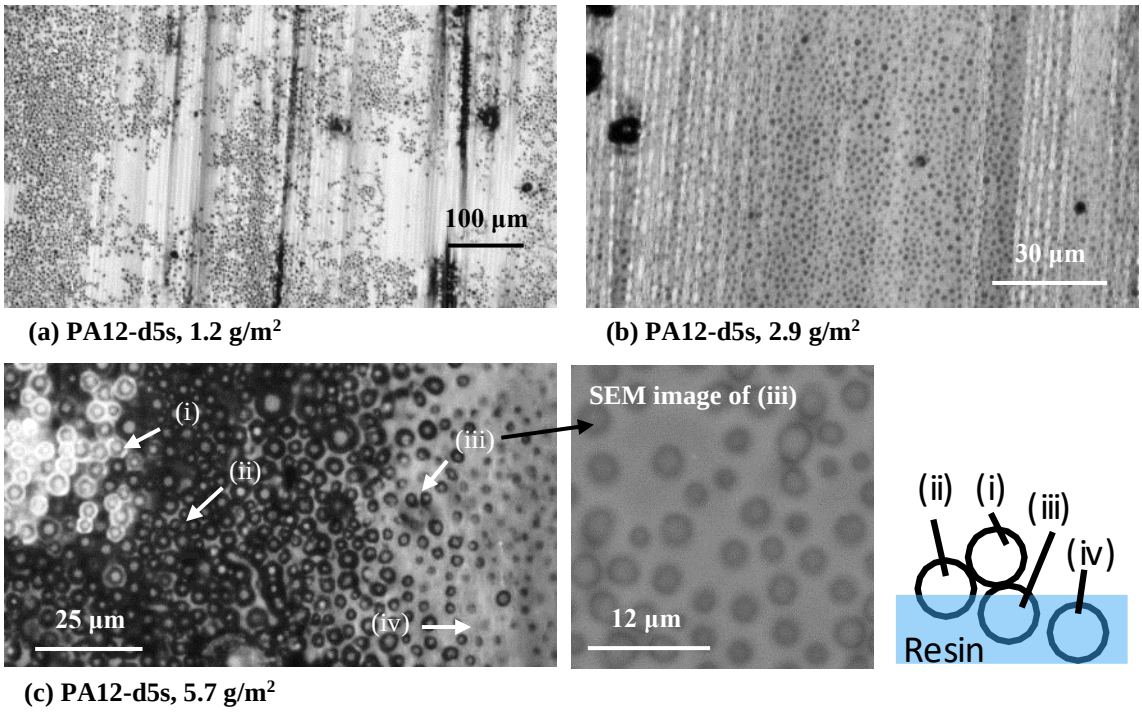

(a) PA12-d5s, 1.2 g/m^2 **(b) PA12-d5s, 2.9 g/m^2**

(c) PA12-d5s, 5.7 g/m^2

Figure 4-22 Single ply pressed at an elevated temperature

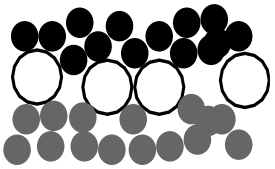

Figure 4-23 Schematic show the fibre beds are separated by a small amount of large particles

When further increasing the amount of the PA12-d5s to 12.8 g/m^2 in Figure 4-16, the interply friction increased, potentially due to the greater contact area between the dry particles. An interesting finding here is that the order of magnitude of the F_C was similar to that in the Coulomb friction of solid polyamide materials. When considering the normal force applied to the contact surface in the test was 160 N, usually the friction

coefficient of polyamide is in a range from 0.15 to 0.25 yields a theoretical frictional force between 24 N and 40 N. The peak force of the 12.8 g/m^2 sample was 27 N, which falls into this range. This could explain that the initial friction was close to dry friction condition.

4.3.2 Effect of particle shape and surface morphology

Apart from shear deformation of the interlayer resin, the particles between fibre plies might move and rotation to facilitate interply slippage. Therefore, the mobility of particles would be important, which can be affected by the surface roughness of particles.

Although the PA12-d10s and PA6-d13r are in similar size, their different surface morphology is significantly different. As shown in Figure 4-18, the friction forces of PA6-d13r were generally higher than the PA12-d10s. At the low normal pressure test, the smooth surface particle could easily slip over other particles due to the low surface friction (Figure 4-24a). However, this might be difficult to happen for rough surface particles. Thus, the sliding ply could drag the rough particles in resin layer that generated high resistance (Figure 4-24b).

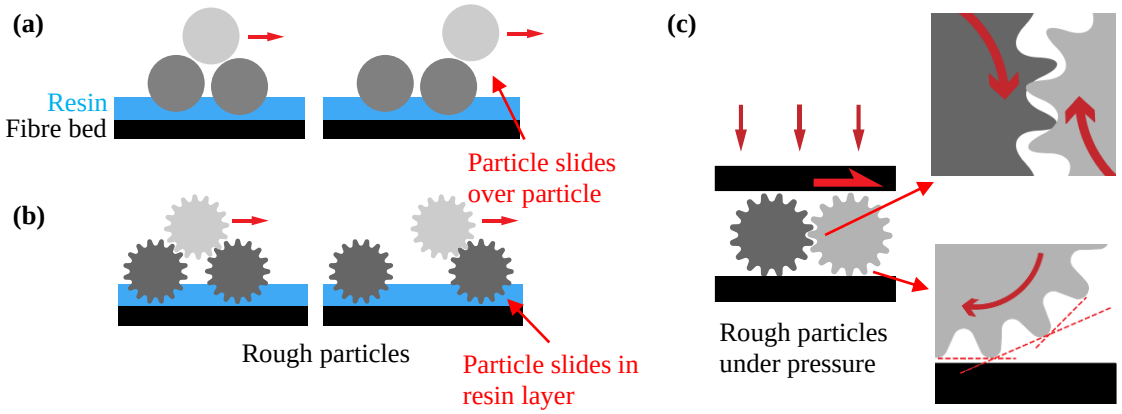

Figure 4-24 Interparticle movement between smooth and rough surface particles

In contrast, in the high pressure test, although the pressure increases direct contact between particles and fibre bed, the smooth PA12-d10s and rounded particles could

easily slide and roll on fibre bed. However, the PA6-d13r particle could create high fiction due to the rough particle surface, and the surface geometry could prevents particle rolling (Figure 4-24c).

4.3.3 Effect of temperature

The main difference between tests at room temperature and an elevated temperature is the effect of the resin matrix. Since the resin viscosity is very high at room temperature, ply slippage causes significantly high frictional force. The toughening particles generally form a dry surface, which reduces the surface tackiness on both sides of a prepreg. This is similar to the separation effect of resin layers discussed in Section 4.3.1. Because the high viscosity resin at room temperature may not allow particles to roll and move easily, the interply slippage could mainly occur at the interface between the coated particle layer on each side.

Figure 4-25 shows the interply friction of samples interleaved with different interleaving materials, tested under 6 kPa pressure at 25°C. The reference sample exhibited the highest force. The peak force was not observed; there wasn't a clear transition region due to the long relaxation of resin matrix. For the samples interleaved with the other three particles, the PA6-d13r sample showed the highest peak force over the other two particles, which could be due to its rough surface. The PA12-d30a was more effective in reducing the interply friction force, which was probably due to its larger particle size separating the ply interfaces more easily. Additionally, the larger particle creating bigger gaps between the plies might have made the resin more difficult to flow into the contact region at room temperature; thus, the effect of surface tackiness was minimal. Such a hypothesis could explain why the polyester veil showed the lowest friction force at room temperature; even the veil used in this work was the thinnest grade available in the commercial market, the thickness of a single sheet was approximately 30 μm.

Therefore, the nonwoven veil exhibited a very low friction; PA12-d10s and PA12-d30a showed less significant effect. The rough PA6-d13r particle has the higher friction among the samples with interleaving materials.

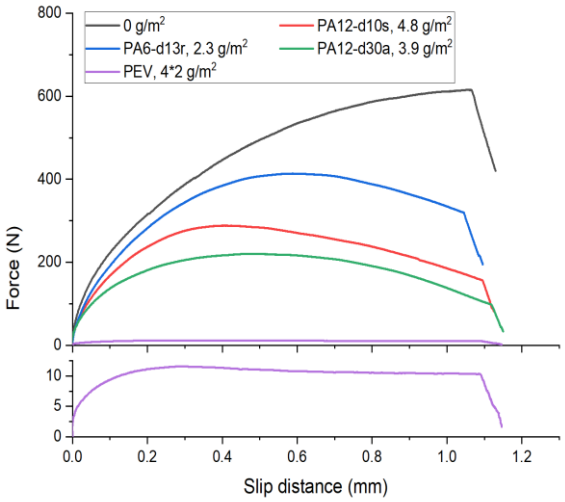

Figure 4-25 Load-slip distance curves of samples with different coating materials tested at 6 kPa, 25°C

4.3.4 Impact on processability

In principle, the interply friction is a useful indicator of formability as it directly impacts the level of compressive stress on the fibre plies located at the inner radius, when manufacturing a curved composite part. Thus, the primary criteria should be avoiding high interply friction when designing a forming process.

From the presented results, the ply slippage can be affected by many parameters of the particle coated on the prepreg surface; the particle size, shape, areal weight, and surface morphology after coating showed considerable influence on the interply friction, as well as the friction behaviours in the transition region and second stage.

For a single diaphragm forming case, since almost no significant external pressure is applied to the area requiring interply slippage until the forming process is completed, the inclusion of particle layer can reduce the interply friction effectively, which could minimise the ply slip resistance during forming. It was found that larger particles and nonwoven veil are more effective.

In a double diaphragm forming scenario, the preform is usually subjected to a compaction pressure applied by vacuum between the diaphragms, which helps to hold the ply position and slightly increase the out-of-plane buckling resistance of plies. Such pressure may have less influence on forming standard prepreg systems, but could

negatively affect the processability if the laminate is interleaved with large or rough particle tougheners. Additionally, some particles such as PA12-d30a at 7.9 g/m^2 and 12.3 g/m^2 exhibited a load drop in transition region (Figure 4-12), which implies the forming process could be less predictable due to sudden loss of ply slip resistance.

As discussed in the introduction, forming a prepreg stack normally requires to be conducted at an elevated temperature to reduce the viscosity of the matrix, which reduces the interply slip resistance but also increases the chance of having more fibre buckling due to the reduced constraint of the fibres by the resin. By coating the ply surface with a particle layer, the ply slippage can be promoted at a low processing temperature, which could maintain the in-plane stability of fibre plies, in other words, decoupling the out-of-plane and in-plane shear stiffness of an uncured prepreg stack.

4.4 Conclusion

This chapter investigated the effect of toughening materials on the interply friction behaviour of uncured prepreg stacks. An in-depth study has been carried out by characterising the interply friction of prepregs interleaved with a range of microparticles and nonwoven veils under different forming conditions. The test results were analysed with visual observation of prepreg surface condition.

For particle tougheners, particle sizes, shapes and applied areal weights showed significant influence on the prepreg interply friction. Certain types of particles were more effective in reducing the interply friction at an elevated temperature, when the normal pressure was low, which could be the separation of the resin layers at ply interface, or increasing ‘dry lubrication effect’, i.e. a dry-contact dominated interface. In the tests to simulate single diaphragm forming case, the samples interleaved with larger particles or nonwoven veils reduced the interply friction, as they were more effective to separate the surface resin on prepreg. The same effect was also found in the 30°C single diaphragm cold forming simulation test.

In contrast, in double diaphragm forming, which has a pressure applied the prepreg surface during the process, particles with smooth surface and smaller diameters were more effective. Especially a small amount (< 5g/m^2) of the smallest PA12-d5s particles

caused a friction force reduction by 45% in the double diaphragm forming simulation test.

The most important finding is that the interply shear and in-plan shear behaviour can be decoupled by coating the toughening particles on the prepreg surface. This is an advantage to minimise the instability of the preform and improve the processability by allowing the processing at a lower temperature in the conventional hot drape forming method.

5 PROCESSABILITY OF CARBON/EPOXY PREPREG LAMINATES INTERLEAVED WITH TOUGHENING MATERIALS IN AUTOCLAVE CURING

The laminate thickness can be affected by the applied temperature and pressure in the different stages in composite manufacturing processes; rolling the material during lay-up, debulking, diaphragm forming and the high pressure in autoclave curing. Such thickness change is mainly caused by the fibre bed compaction and resin squeeze flow in the preform. The interlayer thickness under compaction will be affected when additional materials are included in the interlayers, which will directly affect the overall thickness of the preform during the processes. This chapter studied the bulk factor of a stack of prepregs interleaved with a range of different types of toughening materials, using the test rig developed in this research.

5.1 Experimental

5.1.1 Sample preparation

The prepreg and interleaving particles used were the same as those used in the interply friction test. The details of these materials are presented in Table 2-1 in the Chapter 2

The same polyester nonwoven veil used for the interply friction study in Chapter 4 was also used in this experiment.

In each sample, 20 plies of IM7/8552 prepregs were cut into a size of 60 mm × 60 mm. The particles were directly coated on both sides of each prepreg ply. The particle areal weight was calculated by measuring the weight change of each ply before and after the particle deposition. The stacking sequence was $[0/90]_{10}$ and the top and bottom faces of the stacked preform were covered by a 20 μm thick release film to avoid resin contamination of the test rig. After the 20 plies were laid down, each sample was vacuum debulked for 10 minutes at room temperature. The details of the test set-up and thickness change measurement method are described in Chapter 3.

5.1.2 Test conditions

In the standard curing cycle for IM7/8552 prepreg, the first dwelling stage is at 7 bar pressure at 110°C. Ideally, taking the same processing conditions for test is desirable. However, since the resin viscosity is significantly reduced at such a high temperature, it is not easy to perfectly prevent the resin bleeding during the test; too much resin bleeding would cause difficulty to see the effect of the interleaving materials only. The compaction tests were conducted at 60°C and the analysis was focused on a comparative study between different samples.

Table 5-1 The conditions used for each compaction test

Stage	Pressure	Temperature (°C)	Duration (minutes)
1. Pre-compaction (Debulking)	0.1 MPa	25	5
2. Heating	6 kPa	25 → 60	-
3. Compaction test	0.7 MPa	60	10

In each test, a pre-compaction was conducted for 5 minutes at 25°C under 0.1 MPa for the sample using the pneumatic actuator of the test rig developed in this research

(described in Chapter 3). The applied pressure caused an immediate thickness reduction in a short time, and then reached a transition where the curve started becoming a plateau. The reference thickness (h_1) was measured at the end of this stage, in order to minimise the variability in the sample caused by inconsistency of manual lay-up and focus only on the thickness change during the consolidation process, as shown in Figure 5-1. Then the pressure was removed and the sample was heated to 60°C. At this stage, the force developed by the elastic recovery of the sample was higher than the total resistance of the internal friction of the linear bushing on the moving plate (Chapter 3), and the pneumatic actuator. Thus, the sample thickness started recovering, and then reached a force equilibrium stage where the recovery stopped. After the temperature reached 60°C, a 0.7 MPa pressure was applied, which caused the second decrease of the sample thickness. The high pressure and low resin viscosity resulted in greater thickness reduction in this stage, compared to the pre-compaction stage. Each compaction test was running for 10 minutes, and the thickness at the end (h_2) was used for the calculation of the bulk factor. The sample thickness change in the whole process was recorded, using the measurement method described in Section 3.3.

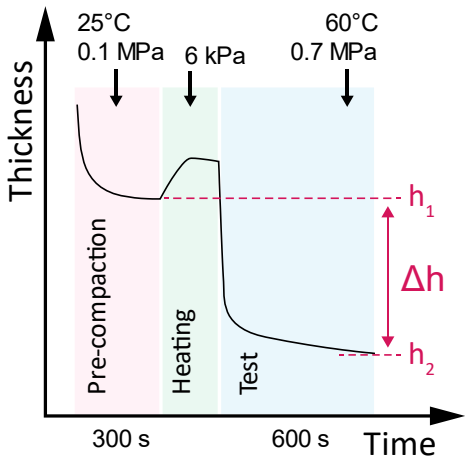

Figure 5-1 The method to determine the thickness change in compaction test

5.2 Results

Figure 5-2 to Figure 5-8 presents the sample thickness change history measured in the test. In each figure, the left plot shows the raw thickness tracking data, and the right plot

does repositioned curves with respect to the thickness at the end of pre-compaction stage (h_1) as a reference point. The Y-axis between different plots are in the same scale, which makes it easy to compare the compaction behaviour at different conditions.

In the three reference samples shown in Figure 5-2, although the REF-3 was about 0.5 mm thicker than the other samples, their trends showed a good agreement in the repositioned plot, which well demonstrated the accuracy of the test and measurement method used.

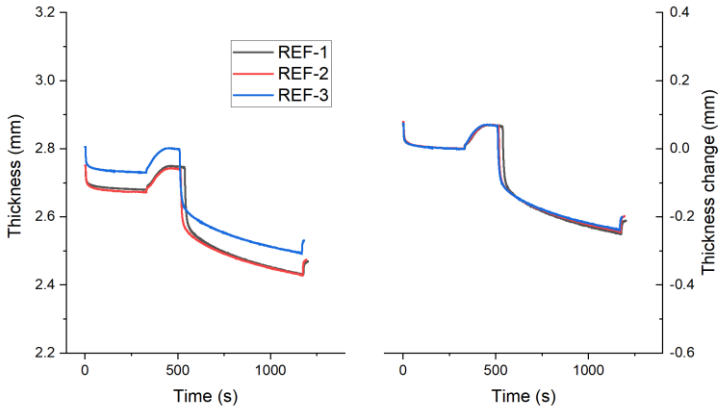

Figure 5-2 The thickness change history of reference samples under 0.7 MPa at 60°C.

From Figure 5-3 to Figure 5-8 shows all the samples interleaved with different particles and one type of non-woven veil at a range of areal weights. The dotted line in the graphs on the right indicates the average thickness change (9%) of the reference samples. It was found that different particles affect the compaction behaviour differently. Figure 5-3 shows the compaction behaviour of the sample interleaved with the PA12-d30a particles, which has the largest diameter among the particles tested. The thickness reduction both in the pre-compaction and test stage were more obvious than the reference case. In contrast, the PA6-d16a (Figure 5-4) and PA12-d5s (Figure 5-7) caused no effect on the compaction behaviour. Furthermore, interestingly, the PA6-d13r and PA12-d10s particles reduced the thickness change (Figure 5-5 and Figure 5-6), rather than increasing it. The sample interleaved with polyester nonwoven veils (Figure 5-8) showed the biggest thickness change with the compaction pressure.

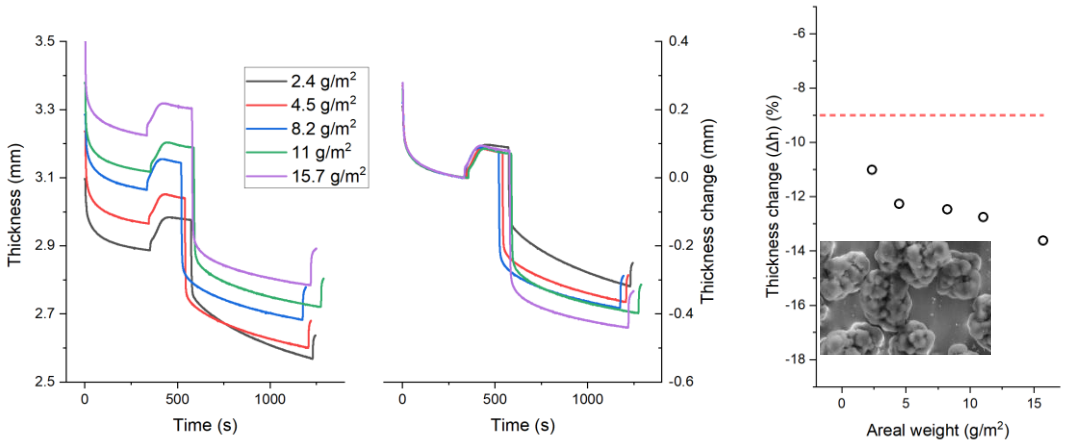

Figure 5-3 The thickness change history of samples interleaved with PA12-d30a particles under 0.7 MPa at 60°C.

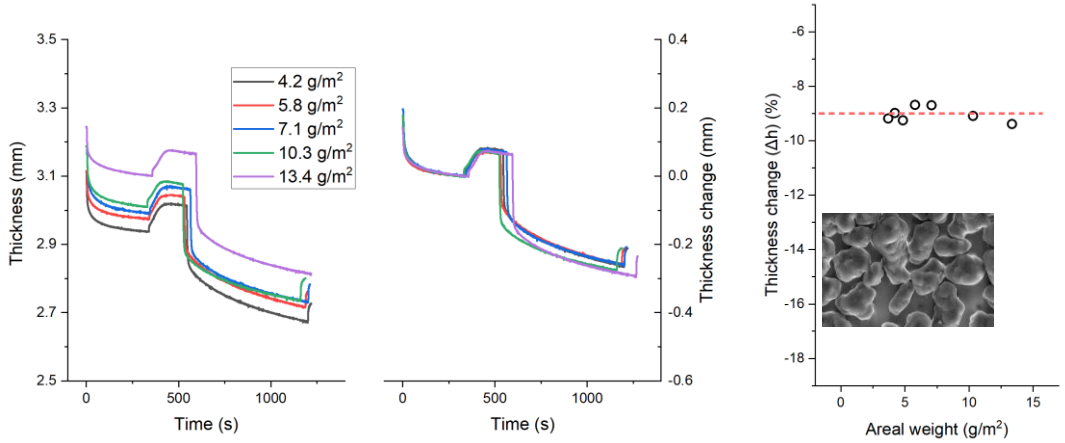

Figure 5-4 The thickness change history of samples interleaved with PA6-d16a particles under 0.7 MPa at 60°C

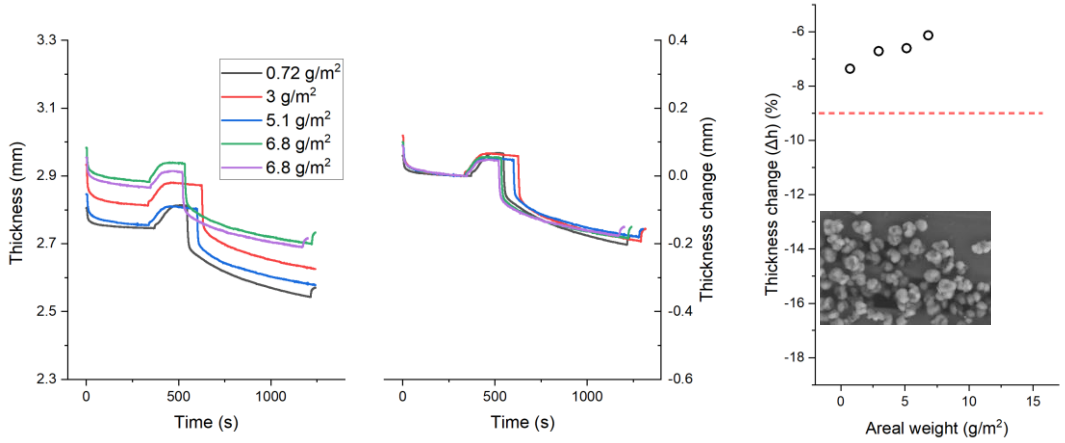

Figure 5-5 The thickness change history of samples interleaved with PA6-d13r particles under 0.7 MPa at 60°C

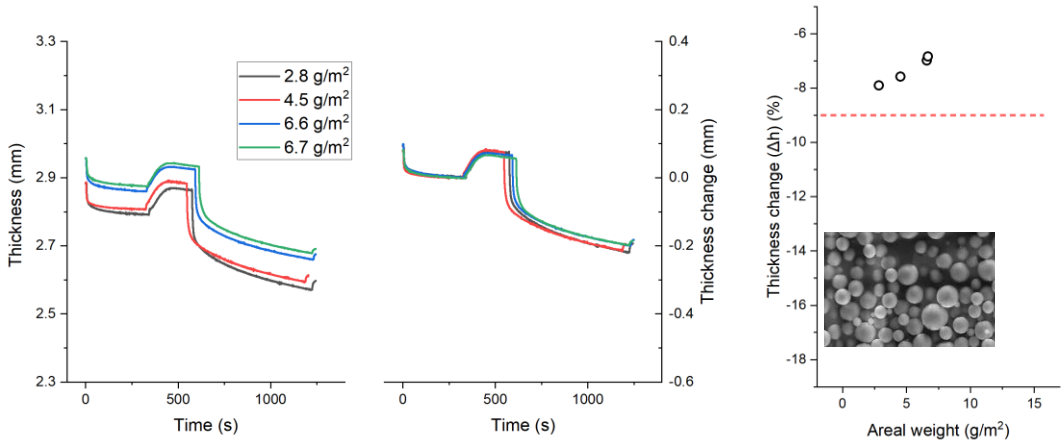

Figure 5-6 The thickness change history of samples interleaved with PA12-d10s particles under 0.7 MPa at 60°C

5.3 Discussion

5.3.1 Thickness reduction

In general, interleaving a laminate with toughening materials inevitably thickens the interlayer between the plies, which increases the overall thickness of the laminate. Figure 5-9a and Figure 5-9b show the thicknesses of the 20-ply laminates at the end of pre-compaction stage (h_1) and the end of test (h_2), respectively. The trends show that the thickness increase is almost proportional to the areal weight of the interleaving material. As discussed in the Chapter 2, laminate thickening caused by the increased interlayer thickness can impact the modulus of composites, which has to be considered when choosing the particle type and amount.

The thickness change, Δh, of the samples interleaved with different particles is shown in Figure 5-9c (the dotted line indicates the Δh of 9%, which is the thickness reduction of the sample without interleaving particles). Generally, the test results show three different trends. The PA12-d5s and PA6-d16a exhibited no significant effect on Δh when varying the areal weight. The preforms interleaved with PEV (Polyester veil) and PA12-d30a were more 'compressible' compared to the other cases; 8 g/m^2 PEV (interleaving two layers of 4 g/m^2 PEV, which is the thinnest non-woven veil

commercially available) reduced Δh by 17.8%, which was the highest among all the samples. For PA12-d30a, the Δh was more outstanding at the low areal weight range, and further increase of particle amount led to a slight reduction of Δh. In contrast, the PA12-d10s and PA6-d13r behaved in the opposite way; their Δh were less than that of the reference sample. Interleaving the preform with 0.7 g/m^2 of PA6-d13r particles yielded a 7.3% thickness reduction, which is nearly 1/5 less than that of the reference sample. PA12-d10s showed a slightly smaller effect, the Δh at 2.8 g/m^2 was 7.9%, which is about 1/10 less than the reference value.

A few mechanisms could be involved when a preform is under compression. The first is evacuation of the trapped air between plies during lay-up. Removing the air decreases the total volume of preform, which causes an immediate thickness change at the initial pre-compaction stage. Second, once most of the trapped air is removed, the compaction force would start acting on the uncured resin both within the interlayer and intralayer, causing a resin squeeze flow. This behaviour depends on the temperature due to the change of resin viscosity. Third, the fibre bed also deforms with the applied force. These are the general compaction mechanisms in the reference samples (Figure 5-2) [108,109].

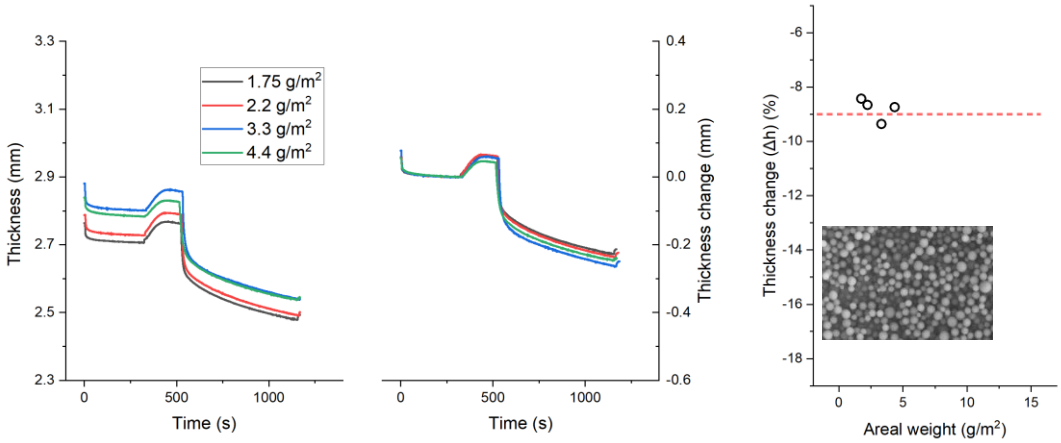

Figure 5-7 The thickness change history of samples interleaved with PA12-d5s particles under 0.7 MPa at 60°C

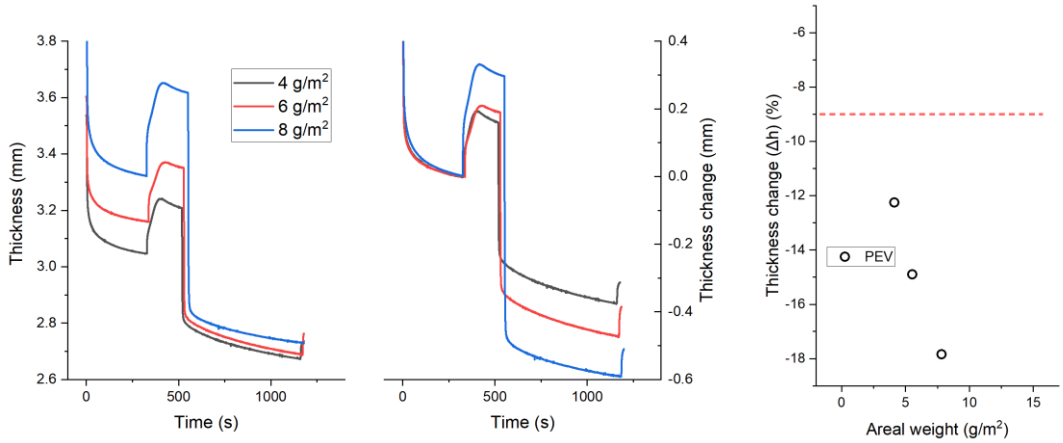

Figure 5-8 The thickness change history of samples interleaved with polyester nonwoven veils under 0.7 MPa at 60°C

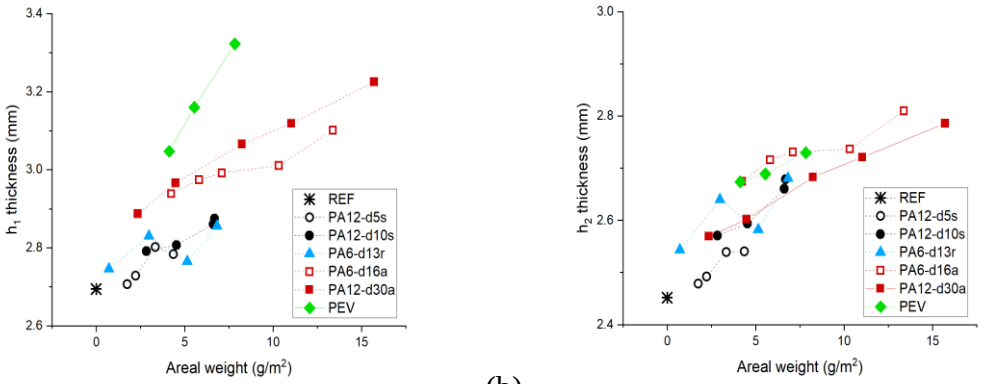

(a) (b)

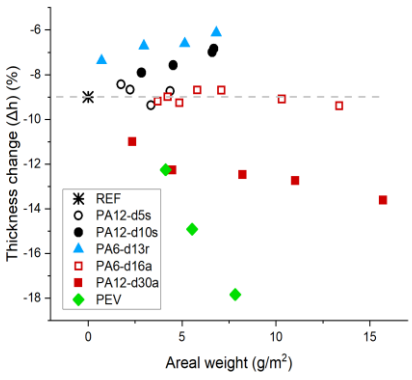

(C)

Figure 5-9 (a) The sample thickness at the end of pre-compaction (h_1). (b) Sample thickness at the end of test (h_2). (c) Sample thickness reductions in percentage.

When the sample includes the particle layers, interaction between the fibre beds within adjacent plies could be suppressed by the particles [2]; the particle rearrangement within the interlayer under compaction would become more significant than the overall compaction response. This behaviour can be affected by the particle sizes, shape and surface morphology**.** One plausible explanation about this would be that in the case where the particles are rather spherical, the particle rearrangement would be relatively easy to occur, which results in a greater interlayer thickness change, as shown in Figure 5-10. The fact that the sample interleaved with PA12-d30a has the highest bulk factor among the tested particles could be an example (Figure 5-9c).

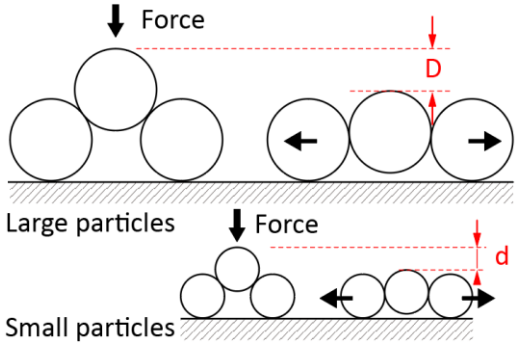

Figure 5-10 Thickness change between compress large particle layer and small particle layer (D > d)

On the other hand, the probability of such particle rearrangement would be dependent on the easiness of interparticle movement, which could be related to the particle surface roughness. Both PA12-d10s and PA6-d13r resulted in a lower Δh than the reference sample, as shown in Figure 5-9c. The PA12-d10s has a smooth surface, which could easily form a dense packing at a low pressure. Therefore, it was inferred that the compaction in the test stage did not cause a large thickness change, as most of the particle rearrangement would have happened in the pre-compaction. In addition, the dense particle packing could impede the resin infiltration within the particle layer [110], which means that further thickness reduction by resin redistribution was difficult to happen. For PA6-d13r particles, which has a smaller diameter to PA12-d10s, the poor interparticle mobility due to their high surface roughness could result in a low Δh. This difference can be found in the cross-section view of the toughened layer in the cured

DCB samples presented in Chapter 2 (Figure 2-6); it can be seen that the interparticle space in the PA12-d10s toughened specimen is generally smaller than in the PA6-d13r.

The Δh for PA12-d5s and PA6-d16a was similar to that of the reference samples. As discussed in Chapter 4, PA12-d5s particle is small enough to penetrate into the fibre bed under pressure. In addition, according to the ideal particle packing structure discussed in Section 4.3.1, the range of tested particle areal weights was not enough to form multilayer of particle at ply interface. Thus, the thickness reduction was difficult to occur. For the PA6-d16a with a broader particle size distribution and a slightly higher aspect ratio (Figure 5-4), once the particles settled down to a stable position (e.g. lay down), further particle rearrangement could not easily happen compared to more spherical particles. Therefore, the thickness change was not obvious.

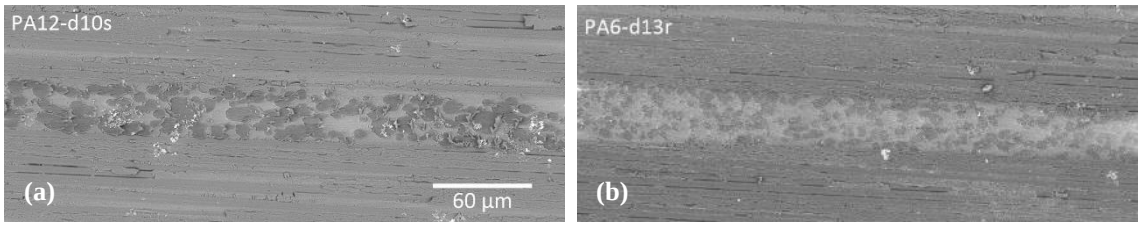

Figure 5-11 Cross-section view of the particle layer in the DCB sample

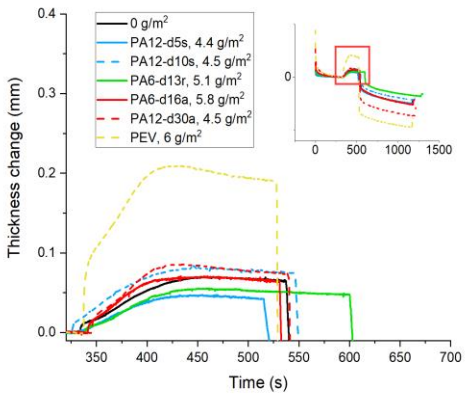

Figure 5-12 The thickness change history in the heating stage during tests, data have been offset based on t_1 as the zero point

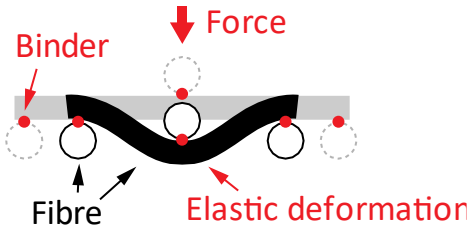

Figure 5-13 Veil fibre elastic deformation

For the samples interleaved with nonwoven veils, the randomly distributed short fibres form loose fibre contacts. Although a binding agent is applied to fix the fibre positions, there is plenty of freedom for the fibres to bend and deform when the veil is under a compaction pressure.

5.3.2 Preform thickness recovery

Another interesting sample behaviour found in the compaction test was the thickness recovery during the heating stage without compaction pressure. Figure 5-12 shows the heating stage of different toughening materials at similar areal weights. The thickness recovery of the reference, PA12-d10s, PA6-d16a and PA12-d30a samples were between 65 and 75 μm; that of PA12-d5s and PA6-d13r were 42 μm and 49 μm, respectively. The sample interleaved with polyester veils showed the greatest thickness recovery, which was approximately 210 μm.

The thickness recovery could be related to the possibility of rearrangement of the interleaving materials. In the case where the particle is small and spherical, applying pressure to particle layers would increase the particle packing density and such a change is irreversible (Figure 5-10); the particles would stay at the changed position even when the pressure is removed, and the recovery behaviour would mainly come from the fibre beds in prepreg. For nonwoven veils, the short fibres are interlaced and fixed with a binder material, therefore, the thickness reduction during compaction is mainly caused by elastic deformation of the fibres (Figure 5-13), which is recoverable if the applied pressure is removed. As a result, the samples interleaved with veils exhibited the highest thickness recovery among the samples.

5.4 Discussion

In general, the bulk factor is not very important to thin or flat laminates in terms of the manufacturing quality. However, for curved laminates, the thickness reduction by the consolidation pressure can significantly impact the manufacturing quality. As the number of plies increases, the laminate thickness change at the corner becomes greater, increasing the risk of ply wrinkling. Therefore, in the laminates with polyester veil and PA12-d30a, shown in Figure 5-9, could have much higher risk of generating out-of-plane wrinkles in autoclave curing, compared to the reference, PA12-d5s and PA6-d16a samples. Even the reference sample may cause wrinkling if the laminate is thick and curved. In this case, interleaving 'less compressible' materials such as PA12-d10s and PA6-d13r could minimise the wrinkling defect due to their smaller thickness change. The thickness recovery of preform after compaction is also critical to the processes. This could affect the stability of preform after debulking and may cause handling issue. In these respects, particles seem to have an advantage over the nonwoven veil in terms of processability, which could be a more suitable material type for interlaminar toughening.

5.5 Conclusion

This chapter experimentally studied the compaction behaviour of prepreg stacks interleaved with a range of different toughening materials. The particle sizes, shapes and areal weights all showed different level of influence on the sample thickness change under compaction at an elevated temperature.

For the preform interleaved with particles, the compaction behaviour was mainly affected by the particle size and shape. The smaller particles showed no obvious difference, or an even lower bulk factor than the reference sample. Rough particles were effective to reduce the bulk factor, due to the poor interparticle mobility resulting in less compressibility. However, such poor compressibility could cause considerable thickening effect of the interlayers, which reduces the fibre volume fraction of the

laminate. In contrast, large particles and nonwoven veils led to increasing the bulk factor, which could generate wrinkles on the preform in autoclave curing.

The thickness recovery of the samples was another interesting finding in this chapter. This preform behaviour could be important to the conventional manufacturing processes, because usually the preform is not subjected to a compaction force at the stage between vacuum debulking and curing. Therefore, a greater thickness recovery can deteriorate the preform stability and cause undesirable quality issue in curing.

6 L-BEAM MANUFACTURING QUALITY

The behaviour of the uncured resin layer at the interlaminar region has a crucial influence on the forming and curing characteristics. The previous chapters experimentally investigated the interply friction and compaction of prepreg stack. In this chapter, a few toughening materials used in the previous chapters were selected as interleaving tougheners in manufacturing L-shaped beams for demonstration of their impact on the manufacturing quality. The L-beam shape was created by using a single diaphragm forming method at 30°C and then cured in autoclave.

The forming temperature of 30°C rather than 60°C, which might be closer to the actual diaphragm forming condition, was selected except for the reference sample (formed at both room and an elevated temperatures) for the following reason. At a low normal pressure condition (single diaphragm forming condition), as discussed in Chapter 4, the toughening materials reduced the interply friction even down to that of the reference sample tested at room temperature; therefore, no significant forming-induced defects were envisaged at an elevated temperature. However, the main driving factor for the defects was the thickness change during curing, which was why the effect of the preform thickness change at an elevated temperature was able to be separately assessed from the forming quality. In addition, through the forming test at 30°C, the feasibility of cold forming was able to be evaluated.

The level of fibre waviness and ply wrinkling after curing were investigated by observing cross-section of these samples. The wrinkle generation mechanisms were discussed based on the characterisation results from the previous chapters.

6.1 Experimental

6.1.1 Sample preparation

The curved beams were manufactured using single diaphragm forming and autoclave curing. IM7/8552 prepregs were cut into the size of 200 mm × 30 mm and manually laid up to create a flat laminate with a stacking sequence of $[-45/0/45/90]_{5s}$. The toughening particles were applied on all the prepreg surfaces except the 20 mm long area at the top of the tool, which is to ease positing of each ply during lay-up and to force ply slippage to occur only at the lateral surface of the tool where the interleaving materials were introduced (Figure 6-1). 15 minutes debulking was applied to every 20 plies. In order to make the laminate edge flush, about 2 mm length at the free-end of the laminate edge was trimmed off after finishing the lay-up, as shown in Figure 6-1. This created a reference for the initial position of each layer before forming, which was used to analyse the ply slippage after forming by visual observation.

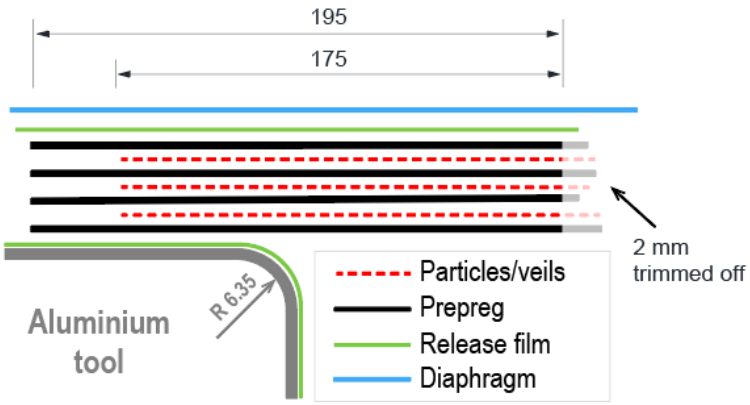

Figure 6-1 Schematic drawing of the laminate with particle layers, and the set-up for diaphragm forming (not scaled)

6.1.2 Manufacturing conditions

A rectangular aluminium tube with a wall-thickness of 6.35 mm and a corner radius of 6.35 mm was used as the tool. The laid laminate was placed on top of the tool, and both were then placed in an in-house developed single diaphragm forming rig (Figure 6-2). The diaphragm material used was a high elongation vacuum bag (Stretchlon®700, Airtech, US) designed to minimise bag bridging on sharp corner during curing. The forming was carried out in an oven at 30°C. Thermocouples were attached on top and bottom sides of the free-hanging part of the preform (Figure 6-2b) to ensure the material temperature reaches the forming temperature. Once the temperature reached the target, the air in the sealed forming rig was evacuated by a vacuum pump, and then the flat laminate was formed into a L-shaped preform. The forming rate was controlled to be completed in 10-15 seconds.

After forming, multiple L-shaped preforms were vacuum bagged on the same aluminium tool with silicone rubber dams to prevent resin bleed from the lateral surfaces (Figure 6-3). The interleaving tougheners and forming conditions of the L-beam specimens are listed in Table 6-1. Curing conditions were the same as the samples manufactured for the interlaminar fracture toughness tests in Chapter 2; 1 hour dwelling at 110°C and 2 hours curing at 180°. The cured L-beams were then cut in half to check the cross-section and investigate the formation of ply wrinkling.

Table 6-1 Overview of the manufacturing conditions of L-beams

Toughener type	ID	Areal weight	Forming temperature
-	REF50	-	50°C
-	REF30	-	30°C
PA12-d10s	PA12-d10s	5.5-6.5 g/m^2	30°C
PA12-d30a	PA12-d30a	5.5-6.5 g/m^2	30°C
PA6-d13r	PA6-d13r	5.5-6.5 g/m^2	30°C
Polyester veil	PEV	8 g/m^2	30°C

It is worth mentioning that during the lay-up, the prepreg surface tack can be reduced by the coated toughening materials. It was found that the tackiness can be recovered by applying pressure during lay-up; e.g. using roller, or compact laminate by debulking, because the pressure pushes the particles into the surface resin layer, which makes some resin squeezed out to the interface and promote the ply adhesion, as shown in Figure 6-4. However, if the formed particle layer is too thick (e.g. large particle such as PA12-d30a, nonwoven veils or high areal weight), the surface tack would not be easy recovered due to lack of resin flow to the interface.

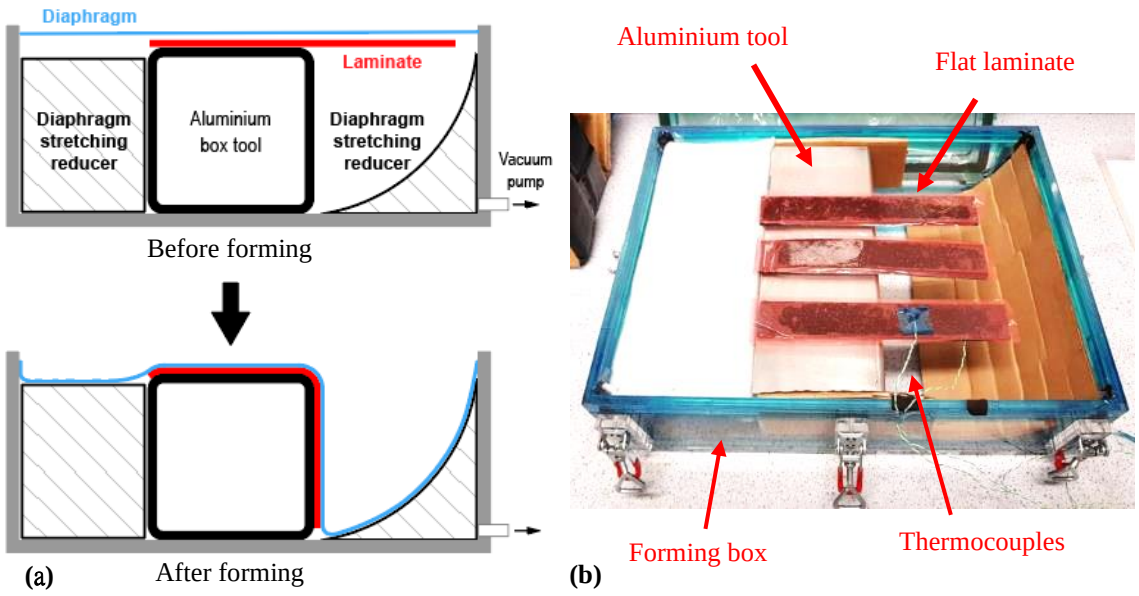

Figure 6-2 (a) Schematic drawing of diaphragm forming process. (b) The configuration of forming rig.

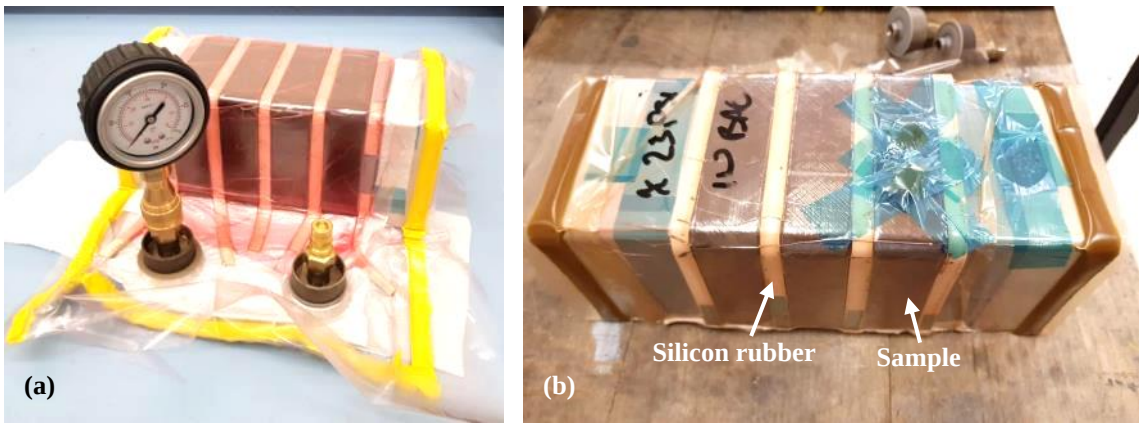

Figure 6-3 Before (a) and after cured (b) L- beams

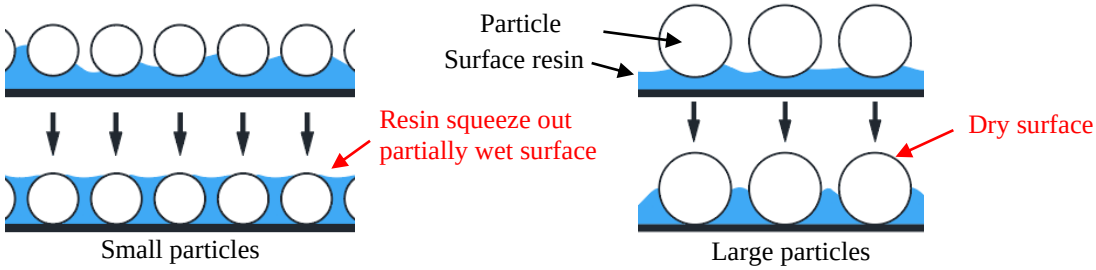

Figure 6-4 Schematic drawing of the uncured prepreg surface condition coated with different sized particles

6.1.3 Identify of defect types

Figure 6-5 shows the locations and typical compression induced defects observed in this experiment. The compressive stress can be generated by different processes. For forming, the insufficient ply slippage causes compression close to the tool side, as shown in Figure 6-5a. Curing induced wrinkle generally occurs at the outside corner, as the reduced laminate thickness also decreases the corner arc length, as shown in Figure 6-5b. In some cases where the compressive stress is developed but not enough to cause these out-of-plane ply buckling, the fibres form in-plane waviness, as shown in Figure 6-5c. This type of defect can be observed by the changed fibre pattern at the cross-section of 0° plies.

6.2 Results

Table 6-2 shows listed the locations of ply wrinkles and fibre waviness found in the cured L-beam samples.

To easily describe where the defects were found in the L-beams, the four locations were noted, as shown in Figure 6-5c; A and C are the inner and outer corners, B and D are on each side of the flat region. The defects generated at Location A and B were mainly caused by forming, while those at Location C and D were due to high compaction pressure during consolidation.

Table 6-2 Summary of the defect types and locations

ID	Forming temperature	Wrinkle starts location*	0° fibre waviness location*
REF50	50°C		A, C, D
REF30	30°C	A	A, B, C, D
PA12-d10s	30°C		A, B, C, D
PA12-d30a	30°C	C	A, C, D
PA6-d13r	30°C	A, B	A, B, C
PEV	30°C	C	A, C

* Locations showed in Figure 6-5d

6.2.1 Effect of forming temperature

Figure 6-6 shows the cross-section of reference L-beams formed at 30°C and 50°C. For REF30 sample, an obvious out-of-plane wrinkle occurred at Location A (Figure 6-6a, b), which was on the side facing to the tool surface, while the cured surface was smooth (Figure 6-6e). Out-of-plane wrinkles were also developed on the side in contact with the vacuum bag at the Location C, which seemed to be affected by the wrinkle developed at the Location A. REF50 showed no obvious wrinkle on Location C and D.

The in-plane fibre waviness was observed both in the REF30 and REF50 from the microscopy images. This type of defect was found at the Location A, C and D in the REF50 sample, while in the REF30 sample, the fibre waviness was observed on both inner and outer corners (Location A and C) and both sides of the flat regions (Location B and D), as shown in Figure 6-6a-c.

The REF30 generated more severer wrinkle and fibre waviness close to the tool side due to the insufficient ply slippage, as shown in the cross-section of the preform edge in Figure 6-6d; the two plies labelled with 0°-A and 0°-B showed no clear length difference compared to the rest of 0° plies, and these two plies also exhibited severe out-of-plane wrinkles at the corner, as shown in Figure 6-6b.

Although the REF50 sample formed at 50°C showed a much better quality, some fibre waviness was still observed at Location A. The compressive stress was still developed

in the sample during forming, as the interply friction was not completely removed at this temperature. However, such compressive stress was not high enough to generate large out-of-plane ply buckling so that the fibre deformation turned into small in-plane waviness.

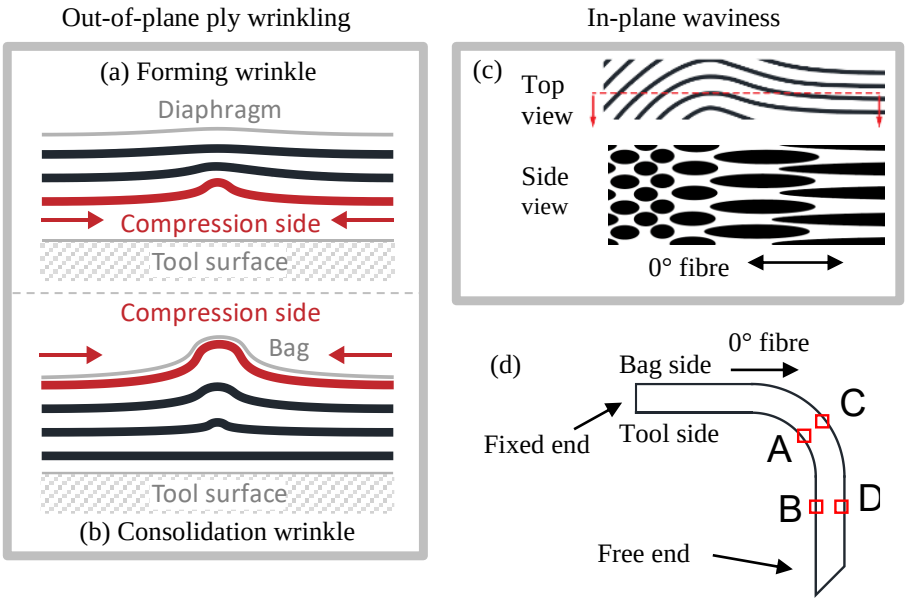

Figure 6-5 (a) and (b) Out-of-plane ply wrinkling. (c) In-plane 0° fibre waviness pattern. (d) Wrinkle locations

Defects caused by thickness reduction are usually generated close to the outer surface [106], which is Location C and D in a composite L-beam. The outer plies must fit over a shorter length than the ideal length due to the thickness change, which compresses the plies and causes wrinkle. From the compaction test results in Chapter 5, the reference sample showed about 9% of thickness reduction under high compaction pressure at 60°C. Therefore, it is reasonable that both reference samples produced fibre waviness at Location C and D, because they have the same bulk factor.

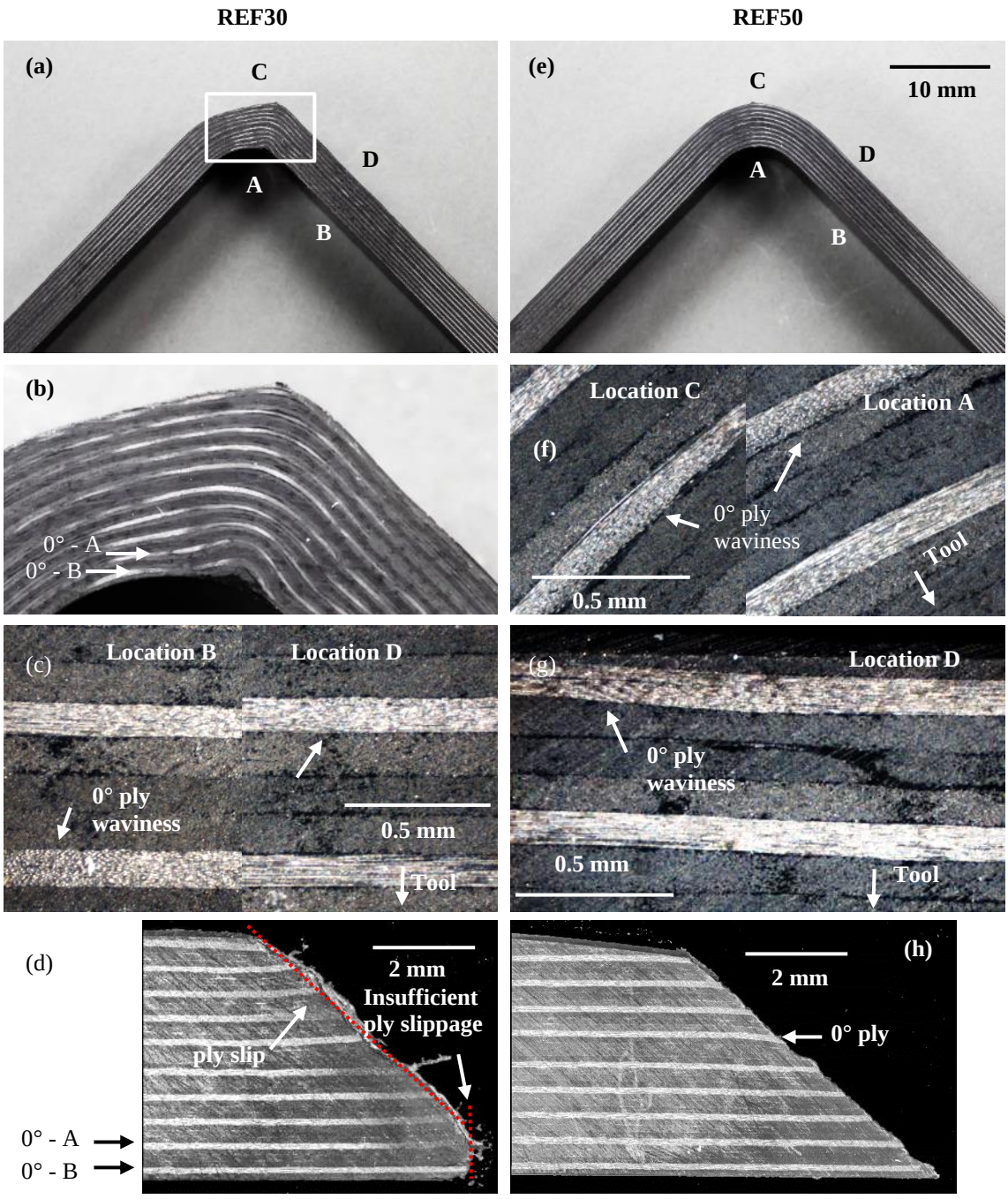

Figure 6-6 Cross-section images of reference samples formed at 30°C (left) and 50°C (right)

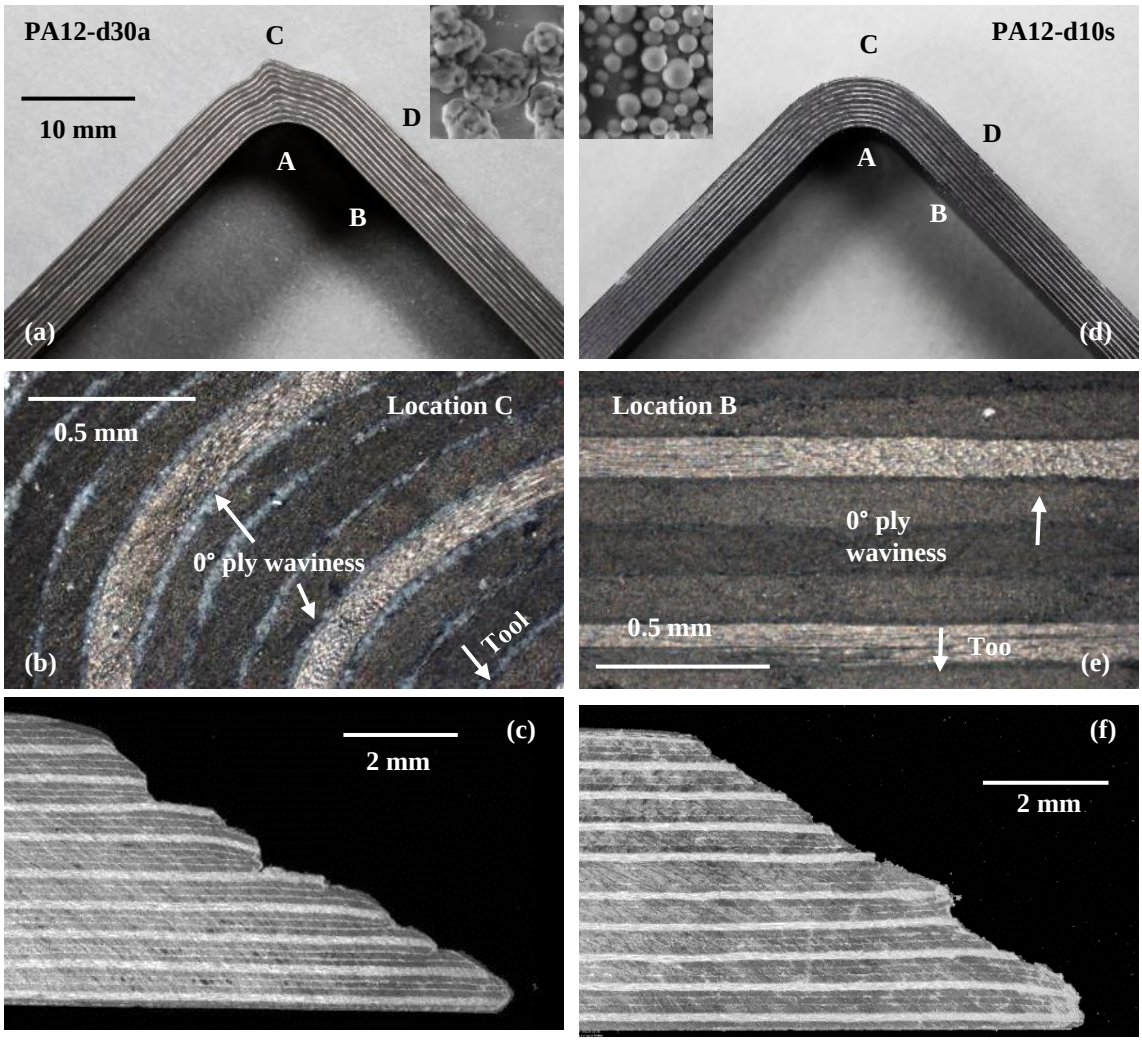

Figure 6-7 Cross-section images of sample interleaved with PA12-d30a (left) and PA12-d10s (right)

6.2.2 Effect of particle diameter

Figure 6-7 shows the cross-section images of the L-beams interleaved with PA12-d30a and PA12-d10s particles. The PA12-d30a produced a considerably large out-of-plane wrinkle at the outer corner Location C (Figure 6-7a), while PA12-d10s shows no obvious out-of-plane wrinkle (Figure 6-7d). Minor fibre waviness was also found at Location A, C and D in the PA12-d30a sample, and Location A, B, C and D in the PA12-d10s sample, which were almost equivalent to that observed in the REF50 sample formed at 50°C.

In general, both samples showed good ply slippage at the free-ends of the samples (Figure 6-7c, f), which correlates well with the interply friction test results (Figure 4-18a) where both particles exhibited a lower interply friction than the reference sample at room temperature. Thus, no obvious ply wrinkle at the Location A and B in these two cases. However, comparing the friction results of both particles in Figure 4-18a, the PA12-d10s exhibited slightly higher critical friction force than the PA12-d30a. This could explain why some minor 0° fibre ply waviness was generated at the Location A and B in the PA12-d10s sample.

The main difference between PA12-d10s and PA12-d30a is the bulk factor (Figure 5-9c), which are approximately 7.5% and 12.5%, respectively. The significant thickness reduction of the PA12-d30a particles led to developing a severe out-of-plane wrinkle at Location C, accompanying with fibre waviness at Location C and D (Figure 6-7b). Whilst in the L-beam interleaved with PA12-d10s, since the thickness reduction was much less than the PA12-d30a, only minor in-plane fibre waviness observed along the outer 0° plies (Figure 6-7e).

In summary, the interleaving particle layers were effective to improve the diaphragm forming quality. However, if the interlayer of the preform contains a particle layer with a high bulk factor, severe wrinkles can still be generated during consolidation.

6.2.3 Effect of particle morphology

Figure 6-8 shows the cross-section images of the L-beam interleaved with PA6-d13r particles, which has a much higher surface roughness than the other particles. Multiple out-of-plane wrinkles were found at the corner (Location A) and the flat region (Location B) on the side close to tool surface, which suggests high interply friction developed during forming. 0° fibre ply waviness was also found at those two locations and at Location C.

High surface friction is the main characteristic of PA6-d13r toughened prepreg due to its high surface roughness, which means that facilitating particle movement is more difficult than smooth particles such as PA12-d10s, which negatively affects the formability. This resulted in a shorter end ply length of the first few 0° plies on the tool side (Figure 6-8c). It was also found that the fibres in 45° plies filled the space created

by the buckling of adjacent 0° ply (Figure 6-8d, e), resulting in an ununiform ply thickness.

6.2.4 Nonwoven veils

Figure 6-9 shows the cross-section images of the L-beam interleaved with the low friction but high bulk factor polyester veils. A significant out-of-plane wrinkle was produced at the outer corner (Location C) in Figure 6-9a. Microscopy images also show 0° fibre waviness both on the Location A and C (Figure 6-9b, c). The polyester nonwoven veils exhibited low interply friction in a single diaphragm forming condition, as presented in Figure 4-18a. No ply wrinkle was found in the L-beam on the side close to the tool surface. The nicely stacked plies at the free-end of the L-beam was the evidence of good ply slippage during forming process (Figure 6-9d). The main reason for ply wrinkle at Location C was the high bulk factor of sample interleaved with polyester veils. The in-plane compressive stress was developed within almost all the layers, which caused many 0° fibre ply waviness, even at the tool side. Resin rich and void areas were also observed.

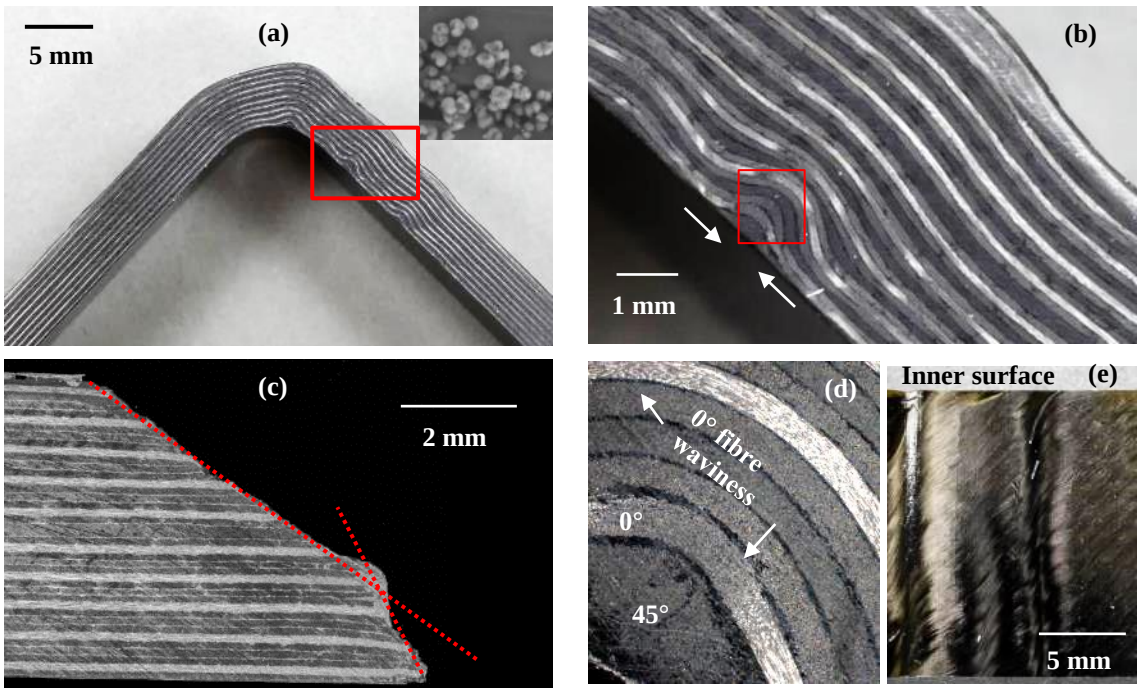

Figure 6-8 Cross-section images of sample interleaved with PA6-d13r particles

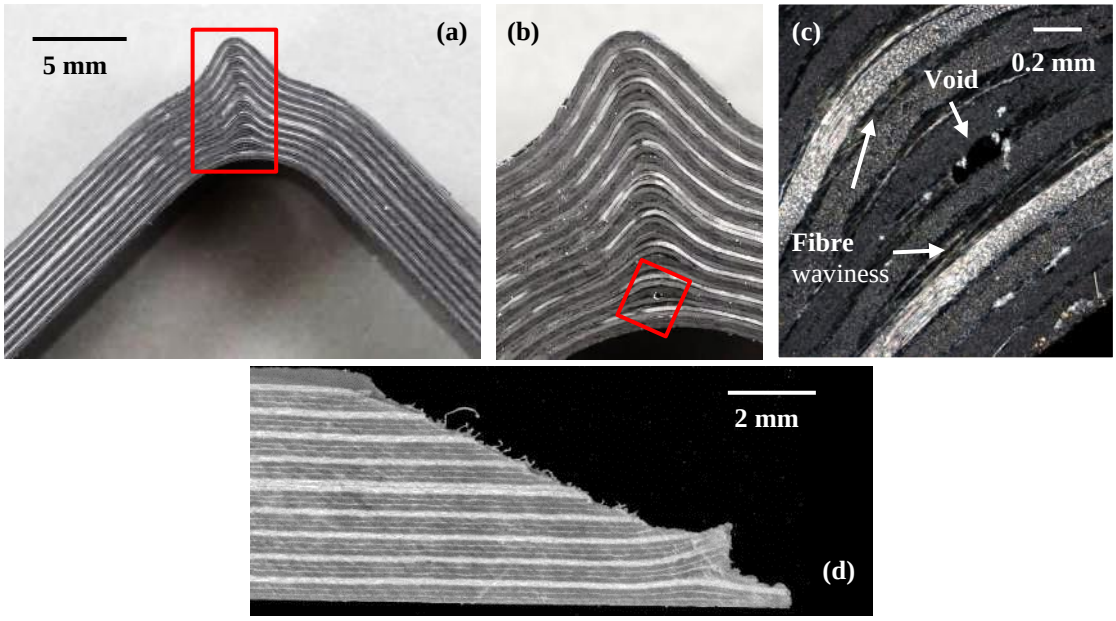

Figure 6-9 Cross-section images of sample interleaved with polyester nonwoven veils

6.3 Conclusion

This chapter experimentally investigated the manufacturing quality of L-shaped beams interleaved with different toughening materials applied by using a direct particle deposition method. In general, the observation of the L-beams' quality showed a reasonable agreement with the interply friction and compaction test results presented in Chapter 4 and Chapter 5. The 6 g/m^2 of PA12-d30a, PA12-d10s and 8 g/m^2 of polyester nonwoven veils all improved the single diaphragm forming quality processed at 30°C, while the beam interleaved with rough surface particle PA6-d13r produced considerable forming induced ply wrinkling. However, the high compressible materials such as the nonwoven veils and PA12-d30a particles produced ply wrinkles in consolidation because they increased the bulk factor of preform. Those two materials may not be ideal as interlaminar tougheners.

Another finding that needs to be addressed is the prepreg surface tack can be affected by the toughening materials. Therefore, creating thinner toughener layer on prepreg surface

and then recovering the surface tack by applying deposition pressure during lay-up would be recommended.

The demonstrated work showed the potential of using toughening materials to improve the diaphragm forming and autoclave curing quality of laminated composites. Especially, the L-beams manufactured with the finest toughening particles showed no significant forming defects at 30°C, which is the temperature that cannot be used in conventional hot drape forming methods.

In selection of a suitable toughening material, the microparticles offered a greater advantage over the polyester nonwoven veil, showing less impact on the preform bulk factor, which minimises the risk of defects generation in consolidation. However, it is important to choose suitable particle type to achieve high manufacturing quality. Based on the finding in this chapter, the smooth and spherical particle was the most ideal one.

7 CONCLUSION AND FUTURE WORK

The presented research investigated the effect of direct deposition of interleaving materials on the interlaminar fracture toughness of a commercially available carbon/epoxy prepreg system, and their impact on the processability under different processing conditions. The interlaminar toughening effect of composites was experimentally investigated using a Mode-I interlaminar fracture toughness test method using double-cantilever beam specimens, and the material processability was evaluated by using an in-house developed test rig, which is able to measure both the prepreg interply friction and the preform compaction behaviours. The impact of the material processability on the manufacturing quality was evaluated using L-shaped composite beams interleaved with different toughening materials, which were formed using single diaphragm forming method and cured in autoclave.

7.1.1 Mode-I fracture Toughness

The results showed that the Mode-I interlaminar fracture toughness and the failure behaviour were highly dependent on the characteristic of the interleaving materials, which include the type of materials, their sizes, shapes and amounts. However, the most important parameter is the processing temperature and the melting point of the toughening materials. In the two curing temperatures used in the experiment, the 180°C cured samples showed crack went through the polyamide 12 particles, while for the 140°C cured ones exhibited particle-matrix debonding. The G_{IC} improvement for the 180°C cured samples were increased with particle amount, the highest G_{IC} was approximately 500% higher than the reference samples. However, for the 140°C cured samples, the G_{IC} was not affected by varying the particle areal weight. This result was similar to the samples interleaved with polyamide 6 particles, which has a higher melting point (210°C) than polyamide 12 particles. These observations suggested that

the particle-matrix bonding has to be developed in the curing processes, which is important to absorb the crack propagation energy by the ductile failure of thermoplastic particles.

Although the direct particle coating method allows the flexibility of changing the prepreg systems and toughening particles, the priority should aim to promote sufficient interfacial bonding strength between the particles and the matrix to enhance the interlaminar toughness, which could be based on choosing suitable processing temperature and the chemical compatibility between the two materials. Additionally, the fact that the interleaving material caused thickening effect should be considered, as the laminate fibre volume fraction can be reduced by the thicker interlayer, which can affect the mechanical properties of the composite.

7.1.2 Interply friction and forming

The interply friction test results in this work provided a useful guidance when forming a prepreg system toughened with interleaving materials. In a single diaphragm forming case, in which the preform is not subjected to a compaction pressure during forming, the toughening materials directly deposited on prepreg surface can be used to promote ply slippage due to the separation of resin layers on interface, or dry lubrication effect, which minimises the risk of forming defects. From the interply friction test results, the friction reduction was dependent on the size of toughening particles, as the interleaving materials separated resin layer at the ply interface. Therefore, the largest PA12-d30a particles was the most effective particle, which causes 70% of reduction of the friction force at 60°C. Other smaller particles also provided approximate 60% of reduction. For the test at room temperature, although the measured friction force was high, the effect was still dependent on the size of particles. This conclusion was validated by the high forming quality of few thick L-shaped composite beams interleaved with particles and veils; it is worth addressing that the single diaphragm forming process was conducted at 30°C. This showed the possibility of cold forming.

For double diaphragm forming process, a compaction pressure applied to the preform during forming pushes the particles into the fibre bed at the interlayer, or causes fibre-fibre entanglement when nonwoven veils were used. The contact areas between the

plies could have insufficient wet resin lubrication, resulting in a higher interply friction. Large and rough surface particles caused a high interply friction, and the friction was increased with particle areal weight, which is disadvantageous in forming process. However, it was found such an issue can be minimised by using smooth and spherical particles (PA12-d5s) of which the size is similar to the fibre diameter, which allows some particles to penetrate into the fibre bed without affecting the sliding plies, and consequently, the friction was close to the reference sample. It was also found that the PA12-d5s particle amount required to fully cover the prepreg surface was like a threshold level from which the friction force increased with particle areal weight. Interleaving composites with such small particles has potential for maintaining forming quality as well as improving the interlaminar fracture toughness. Although these findings were not fully validated by manufacturing trials of double diaphragm forming in this work, they provided some useful guidance for future studies.

7.1.3 Compaction behaviour and autoclave curing

The thickness variation under high pressure was found to have a strong relationship with the interleaving materials. It was found the large PA12-d30a and nonwoven veils may not be ideal interlaminar tougheners for thick composite parts with sharp corners, as they significantly increase the bulk factor. The potential reason is that the loose particle arrangement and short fibre architecture made them more compressible.

However, the other particles tested in this work such as PA12-d5s and PA6-d16a had no influence, and the PA6-d13r and PA12-d10s made the prepreg preform even less compressible than the reference sample. In the former case, the possible reason is that the particles were difficult to be rearranged by pressure due to either their rough surface (PA6-d13r) or irregular particle shape (PA6-d16a). And the latter case might be because the particles were easy to form a dense particle packing under low compaction pressure due to the smooth surface and spherical shape (PA12-d5s and PA12-d10s). An effective interleaving toughener should have less impact or even reduce the preform bulk factor, which could be achieved by using small and smooth surface particles.

7.1.4 Selective particle deposition

The direct particle deposition method used in this work has several advantages over conventional toughening methods. First, a composite part could have different structural requirements depending the regions. Direct particle deposition can selectively apply toughening particles at the regions where require higher toughness, without affecting the other regions that need a high fibre volume fraction for modulus or strength. Second, when forming a complex composite part, some areas may require a higher interply slip distance to achieve final geometry without forming defects. The particles that exhibit low friction can be deposited onto those regions to facilitate the forming. Third, corner thinning is a common issue when curing composite parts with sharp corners using a male tool. The particles could be deposited at those areas requiring a low bulk factor to produce high curing quality, by minimising the thinning effect during autoclave curing.

7.1.5 Conclusion and future work suggestions

In summary, the present study showed that direct deposition of toughening particles on prepreg surface can achieve high fracture toughness, and improve the manufacturing quality in composite forming and autoclave curing. In order to maximise the material processiblity as well as the toughening effect, it is important to select suitable particle size, shape, surface morphology and particle areal weight, and use an optimal curing temperature. In the processability characterisation, the test rig and test set-up can significantly affect the accuracy of load-ply slippage measurement, which needs to be considered carefully.

Some suggestions for future works are suggested below:

- Interply friction between the particle-toughened plies with different ply orientations

  The friction tests done in this work were mainly for the contact between two unidirectional plies with the same fibre orientation. However, such a stacking sequence is not common in most of composite applications. At a low compaction pressure, the effect of fibre orientation would be minimal. However, it is known

that fibre-fibre contact which occurs at a high compaction pressure could significantly affect the friction behaviour. It is unknown how the particle tougheners introduced at the ply interface would affect the friction in such a contact condition.

- Complex shapes forming with particle layer

  The main advantage of forming processes is that they can achieve a high production rate when manufacturing relatively simple composite parts, which mainly require interply slippage and compaction within the preform. The forming processes often need to be used to produce parts with complex features (e.g. a spar with recess areas) requiring considerable amount of in-plane shear deformation. It was envisaged that the direct particle method would have an advantage of decoupling the in-plane and out-of-plane shear deformation characteristics; i.e. only the interply friction could be controlled without affecting the in-plane shear behaviour. However, due to the time constraint, only a simple L-beam shape was used in the forming trials. Further investigate the forming quality of more complex parts such as doubly curved surfaces would be valuable.

- Particle deposition method

  This research has focused more on scientific analysis on the effect of the toughening particles rather than technical development of the direct particle deposition method. And the stamping and scraping methods was useful for small-sized samples. However, in order to conduct a large-scale forming test, which could be closer to the industrial applications, an automated particle deposition process needs to be developed. This could be a scope of a more industrial application-oriented research project.

- Different prepreg systems

  Different prepreg systems could affect the lubrication effect of coated particle layers, due to the resin content and viscoelastic behaviour. It would be worth to further study the interply shear behaviour of particles coated on different types of prepregs.

REFERENCE

[1] Y.R.Larberg, M.Åkermo, On the interply friction of different generations of carbon/epoxy prepreg systems, Composites Part A: Applied Science and Manufacturing. 42 (2011) 1067–1074. doi:10.1016/j.compositesa.2011.04.010.

[2] O.Nixon-Pearson, J.-H.Belnoue, D.Ivanov, K.Potter, S.Hallett, An experimental investigation of the consolidation behaviour of uncured prepregs under processing conditions, Journal of Composite Materials. 51 (2017) 1911–1924. doi:10.1177/0021998316665681.

[3] A.P.Mouritz, Review of z-pinned composite laminates, Composites Part A: Applied Science and Manufacturing. 38 (2007) 2383–2397. doi:10.1016/j.compositesa.2007.08.016.

[4] G.Dell'Anno, J.W.G.Treiber, I.K.Partridge, Manufacturing of composite parts reinforced through-thickness by tufting, Robotics and Computer-Integrated Manufacturing. 37 (2016) 262–272. doi:10.1016/j.rcim.2015.04.004.

[5] K.T.Faber, A.G.Evans, Crack deflection processes-II. Experiment, Acta Metallurgica. 31 (1983) 577–584. doi:10.1016/0001-6160(83)90047-0.

[6] K.T.Faber, A.G.Evans, Crack deflection processes-I. Theory, Acta Metallurgica. 31 (1983) 565–576. doi:10.1016/0001-6160(83)90046-9.

[7] Y.Nakamura, M.Yamaguchi, M.Okubo, T.Matsumoto, Effect of particle size on the fracture toughness of epoxy resin filled with spherical silica, Polymer. 33 (1992) 3415–3426. doi:10.1016/0032-3861(92)91099-N.

[8] S.Y.Fu, X.Q.Feng, B.Lauke, Y.W.Mai, Effects of particle size, particle/matrix interface adhesion and particle loading on mechanical properties of particulate-polymer composites, Composites Part B: Engineering. 39 (2008) 933–961. doi:10.1016/j.compositesb.2008.01.002.

[9] J.N.Sultan, F.J.McGarry, Effect of rubber particle size on deformation mechanisms in glassy epoxy, Polymer Engineering and Science. 13 (1973) 29–34. doi:10.1002/pen.760130105.

[10] A.C.Garg, Y.-W.Mai, Failure mechanisms in toughened epoxy resins—A review, Composites Science and Technology. 31 (1988) 179–223. doi:10.1016/0266-

3538(88)90009-7.

[11] J.K.Kim, R.E.Robertson, Toughening of thermoset polymers by rigid crystalline particles, Journal of Materials Science. 27 (1992) 161–174. doi:10.1007/BF00553852.

[12] R.A.Pearson, A.F.Yee, Toughening mechanisms in thermoplastic-modified epoxies: 1. Modification using poly(phenylene oxide), Polymer. 34 (1993) 3658–3670. doi:10.1016/0032-3861(93)90051-B.

[13] R. a.Pearson, Toughening Epoxies Using Rigid Thermoplastic Particles, in: Toughened Plastics, 1993: pp. 405–425. doi:10.1021/ba-1993-0233.ch017.

[14] W.D.Bascom, R.L.Cottington, R.L.Jones, P.Peyser, The fracture of epoxy- and elastomer-modified epoxy polymers in bulk and as adhesives, Journal of Applied Polymer Science. 19 (1975) 2545–2562. doi:10.1002/app.1975.070190917.

[15] N.Sela, O.Ishai, L.Banks-Sills, The effect of adhesive thickness on interlaminar fracture toughness of interleaved cfrp specimens, Composites. 20 (1989) 257–264. doi:10.1016/0010-4361(89)90341-8.

[16] O.Ishai, H.Rosenthal, N.Sela, E.Drukker, Effect of selective adhesive interleaving on interlaminar fracture toughness of graphite/epoxy composite laminates, Composites. 19 (1988) 49–54. doi:10.1016/0010-4361(88)90543-5.

[17] M.R.Groleau, Y.-B.Shi, A.F.Yee, J.L.Bertram, H.J.Sue, P.C.Yang, Mode II fracture of composites interlayered with nylon particles, Composites Science and Technology. 56 (1996) 1223–1240. doi:10.1016/S0266-3538(96)00080-2.

[18] M.Yasaee, I.P.Bond, R.S.Trask, E.S.Greenhalgh, Mode I interfacial toughening through discontinuous interleaves for damage suppression and control, Composites Part A: Applied Science and Manufacturing. 43 (2012) 198–207. doi:10.1016/j.compositesa.2011.10.009.

[19] E.N.Gilbert, B.S.Hayes, J.C.Seferis, Interlayer toughened unidirectional carbon prepreg systems: effect of preformed particle morphology, Composites Part A: Applied Science and Manufacturing. 34 (2003) 245–252. doi:10.1016/S1359-835X(02)00141-0.

[20] R.W.Hillermeier, J.C.Seferis, Interlayer toughening of resin transfer molding composites, Composites Part A: Applied Science and Manufacturing. 32 (2001) 721–729. doi:10.1016/S1359-835X(00)00088-9.

[21] M.Hojo, S.Matsuda, M.Tanaka, S.Ochiai, A.Murakami, Mode I delamination fatigue properties of interlayer-toughened CF/epoxy laminates, Composites Science and Technology. 66 (2006) 665–675. doi:10.1016/j.compscitech.2005.07.038.

[22] S.Zeng, M.Hoisington, J.C.Seferis, Particulate interlayer toughening of dicyanate matrix composites, Polymer Composites. 14 (1993) 458–466. doi:10.1002/pc.750140603.

[23] B.J.Cardwell, A.F.Yee, Toughening of epoxies through thermoplastic crack bridging, Journal of Materials Science. 33 (1998) 5473–5484. doi:doi.org/10.1023/A:100442712.

[24] H.Kishi, K.Uesawa, S.Matsuda, A.Murakami, Adhesive strength and mechanisms of epoxy resins toughened with pre-formed thermoplastic polymer particles, Journal of Adhesion Science and Technology. 19 (2005) 1277–1290. doi:10.1163/156856105774784402.

[25] M.E.Nichols, R.E.Robertson, The toughness of epoxy-poly(butylene terephthalate) blends, Journal of Materials Science. 29 (1994) 5916–5926. doi:10.1007/BF00366876.

[26] S.Kim, J.Kim, S.H.Lim, W.H.Jo, C.R.Choe, Effects of mixing temperatures on the morphology and toughness of epoxy/polyamide blends, Journal of Applied Polymer Science. 72 (1999) 1055–1063. doi:10.1002/(SICI)1097-4628(19990523)72:8<1055::AID-APP10>3.0.CO;2-8.

[27] B.Y.Park, S.C.Kim, B.Jung, Interlaminar Fracture Toughness of Carbon Fiber/Epoxy Composites using Short Kevlar Fiber and/or Nylon-6 Powder Reinforcement, Polymers for Advanced Technologies. 8 (1997) 371–377. doi:10.1002/(SICI)1099-1581(199706)8:6<371::AID-PAT658>3.0.CO;2-I.

[28] C.Paris, Etude et Modélisation de la Polymérisation Dynamique de Composites à Matrice Thermodurcissable, Universite of Toulouse, 2011. http://oatao.univ-toulouse.fr/6966/1/paris_partie_1_sur_2.pdf%0Ahttp://ethesis.inp-toulouse.fr/archive/00001787/01/paris_partie_1_sur_2.pdf.

[29] C.Hunt, J.Kratz, I.K.Partridge, Cure path dependency of mode I fracture toughness in thermoplastic particle interleaf toughened prepreg laminates, Composites Part A: Applied Science and Manufacturing. 87 (2016) 109–114.

doi:10.1016/j.compositesa.2016.04.016.

[30] I.Gawin, B.J.Swetlin, Damage tolerant composites containing infusible particles, Composites Manufacturing. 1 (2008) 265. doi:10.1016/0956-7143(90)90081-7.

[31] A.Maranci, S.L.Peake, S.S.Kaminski, Advance composites with thermoplastic particles an the interface between layers, US 4957801, 1990. https://patents.google.com/patent/US5057353.

[32] Y.He, Q.Li, T.Kuila, N.H.Kim, T.Jiang, K.Lau, J.H.Lee, Micro-crack behavior of carbon fiber reinforced thermoplastic modified epoxy composites for cryogenic applications, Composites Part B: Engineering. 44 (2013) 533–539. doi:10.1016/j.compositesb.2012.03.014.

[33] F.Gao, G.Jiao, R.Ning, L.Zhixian, Damage resistance of the composite laminates with interlayer thermoplastic particles, Acta Materiae Compositae Sinica. 2 (2005).

[34] B.S.Hayes, J.C.Seferis, Preformed particle toughening of epoxy-based film adhesive systems: The effect of particle size and chemistry, Polymer Composites. 23 (2002) 418–424. doi:10.1002/pc.10443.

[35] P.T.McGrail, S.D.Jenkins, Some aspects of interlaminar toughening: reactively terminated thermoplastic particles in thermoset composites, Polymer. 34 (1993) 677–683. doi:10.1016/0032-3861(93)90347-D.

[36] F.Gao, G.Jiao, Z.Lu, R.Ning, Mode II Delamination and Damage Resistance of Carbon/Epoxy Composite Laminates Interleaved with Thermoplastic Particles, Journal of Composite Materials. 41 (2007) 111–123. doi:10.1177/0021998306063356.

[37] K.Potter, B.Khan, M.Wisnom, T.Bell, J.Stevens, Variability, fibre waviness and misalignment in the determination of the properties of composite materials and structures, Composites Part A: Applied Science and Manufacturing. 39 (2008) 1343–1354. doi:10.1016/j.compositesa.2008.04.016.

[38] S.Mukhopadhyay, M.I.Jones, S.R.Hallett, Tensile failure of laminates containing an embedded wrinkle; numerical and experimental study, Composites Part A: Applied Science and Manufacturing. 77 (2015) 219–228. doi:10.1016/j.compositesa.2015.07.007.

[39] S.Mukhopadhyay, M.I.Jones, S.R.Hallett, Compressive failure of laminates

containing an embedded wrinkle; experimental and numerical study, Composites Part A: Applied Science and Manufacturing. 73 (2015) 132–142. doi:10.1016/j.compositesa.2015.03.012.

[40] D.Bhattacharyya, Composite Sheet Forming, Elsevier, Netherlands, 1997.

[41] T.G.Gutowski, G.Dillon, S.Chey, H.Li, Laminate wrinkling scaling laws for ideal composites, Composites Manufacturing. 6 (1995) 123–134. doi:10.1016/0956-7143(95)95003-H.

[42] F.N.Cogswell, Thermoplastic Aromatic Polymer Composites: A Study of the Structure, Processing and Properties of Carbon Fibre Reinforced Polyetheretherketone and Related Materials, Butterworth-Heinemann Ltd, Oxford, 1992.

[43] U.Sachs, Friction and bending in thermoplastic composites forming processes, University of Twente, 2014. doi:10.3990/1.9789462594838.

[44] R.K.Pandey, C.T.Sun, Mechanisms of wrinkle formation during the processing of composite laminates, Composites Science and Technology. 59 (1999) 405–417. doi:10.1016/S0266-3538(98)00080-3.

[45] S.Erland, T.J.Dodwell, R.Butler, Characterisation of inter-ply shear in uncured carbon fibre prepreg, Composites Part A: Applied Science and Manufacturing. 77 (2015) 210–218. doi:10.1016/j.compositesa.2015.07.008.

[46] R.H.W.tenThije, R.Akkerman, M.Ubbink, L.van derMeer, A lubrication approach to friction in thermoplastic composites forming processes, Composites Part A: Applied Science and Manufacturing. 42 (2011) 950–960. doi:10.1016/j.compositesa.2011.03.023.

[47] Y.Larberg, M.Åkermo, In-plane deformation of multi-layered unidirectional thermoset prepreg – Modelling and experimental verification, Composites Part A: Applied Science and Manufacturing. 56 (2014) 203–212. doi:10.1016/j.compositesa.2013.10.005.

[48] S.P.Haanappel, R.H.W.tenThije, U.Sachs, B.Rietman, R.Akkerman, Formability analyses of uni-directional and textile reinforced thermoplastics, Composites Part A: Applied Science and Manufacturing. 56 (2014) 80–92. doi:10.1016/j.compositesa.2013.09.009.

[49] K.Potter, Bias extension measurements on cross-plied unidirectional prepreg,

Composites - Part A: Applied Science and Manufacturing. 33 (2002) 63–73. doi:10.1016/S1359-835X(01)00057-4.

[50] Y.R.Larberg, M.Åkermo, M.Norrby, On the in-plane deformability of cross-plied unidirectional prepreg, Journal of Composite Materials. 46 (2012) 929–939. doi:10.1177/0021998311412988.

[51] J.Sjölander, P.Hallander, M.Åkermo, Forming induced wrinkling of composite laminates: A numerical study on wrinkling mechanisms, Composites Part A: Applied Science and Manufacturing. 81 (2016) 41–51. doi:10.1016/j.compositesa.2015.10.012.

[52] S.Chen, O.P.L.McGregor, A.Endruweit, M.T.Elsmore, D.S.A.DeFocatiis, L.T.Harper, N.A.Warrior, Double diaphragm forming simulation for complex composite structures, Composites Part A: Applied Science and Manufacturing. 95 (2017) 346–358. doi:10.1016/j.compositesa.2017.01.017.

[53] S.Haanappel, Forming of UD fibre reinforced thermoplastics : a critical evaluation of intra-ply shear, University of Twente, 2013. doi:10.3990/1.9789036535014.

[54] P.Boisse, N.Hamila, E.Vidal-Sallé, F.Dumont, Simulation of wrinkling during textile composite reinforcement forming. Influence of tensile, in-plane shear and bending stiffnesses, Composites Science and Technology. 71 (2011) 683–692. doi:10.1016/j.compscitech.2011.01.011.

[55] G.Lebrun, M.N.Bureau, J.Denault, Evaluation of bias-extension and picture-frame test methods for the measurement of intraply shear properties of PP/glass commingled fabrics, Composite Structures. 61 (2003) 341–352. doi:10.1016/S0263-8223(03)00057-6.

[56] Y.R.Larberg, M.Åkermo, in-Plane Properties of Cross-Plied Unidirectional Prepreg, in: 16th International Conference on Composite Materials, 2007: pp. 1–7.

[57] A.M.Murtagh, J.J.Lennon, P.J.Mallon, Surface friction effects related to pressforming of continuous fibre thermoplastic composites, Composites Manufacturing. 6 (1995) 169–175. doi:10.1016/0956-7143(95)95008-M.

[58] C.J.Martin, J.C.Seferis, M.A.Wilhelm, Frictional resistance of thermoset prepregs and its influence on honeycomb composite processing, Composites Part

A: Applied Science and Manufacturing. 27 (1996) 943–951. doi:10.1016/1359-835X(96)00037-1.

[59] G.Lebrun, M.N.Bureau, J.Denault, Thermoforming-Stamping of Continuous Glass Fiber/Polypropylene Composites: Interlaminar and Tool–Laminate Shear Properties, Journal of Thermoplastic Composite Materials. 17 (2004) 137–165. doi:10.1177/0892705704035411.

[60] C.Pasco, M.Khan, J.Gupta, K.Kendall, Experimental investigation on interply friction properties of thermoset prepreg systems, Journal of Composite Materials. 53 (2019) 227–243. doi:10.1177/0021998318781706.

[61] J.Sun, Y.Gu, M.Li, X.Ma, Z.Zhang, Effect of forming temperature on the quality of hot diaphragm formed C-shaped thermosetting composite laminates, Journal of Reinforced Plastics and Composites. 31 (2012) 1074–1087. doi:10.1177/0731684412453778.

[62] X.X.Bian, Y.Z.Gu, J.Sun, M.Li, W.P.Liu, Z.G.Zhang, Effects of Processing Parameters on the Forming Quality of C-Shaped Thermosetting Composite Laminates in Hot Diaphragm Forming Process, Applied Composite Materials. 20 (2013) 927–945. doi:10.1007/s10443-012-9310-7.

[63] T.A.Martin, D.Bhattacharyya, I.F.Collins, Bending of fibre-reinforced thermoplastic sheets, Composites Manufacturing. 6 (1995) 177–187. doi:10.1016/0956-7143(95)95009-N.

[64] R.Scherer, K.Friedrich, Inter- and intraply-slip flow processes during thermoforming of cf/pp-laminates, Composites Manufacturing. 2 (1991) 92–96. doi:10.1016/0956-7143(91)90185-J.

[65] M.Åkermo, Y.R.Larberg, J.Sjölander, P.Hallander, Influence of interply friction on the forming of stacked UD prepreg, 19th International Conference on Composite Materials. (2013) 919–928.

[66] S.Erland, T.J.Dodwell, R.Butler, Viscoelastic inter-ply slip in uncured laminates - experiemntal characterisation and modelling, 20th International Conference on Composite Materials. (2015).

[67] P.Hallander, J.Sjölander, M.Åkermo, Forming of composite spars including interlayers of aligned, multiwall, carbon nanotubes: An experimental study, Polymer Composites. 39 (2018) 181–191. doi:10.1002/pc.23918.

[68] P.HUBERT, A.POURSARTIP, Aspects of the Compaction of Composite Angle Laminates: An Experimental Investigation, Journal of Composite Materials. 35 (2001) 2–26. doi:10.1106/X8D7-PR9V-U6F2-0JEK.

[69] J.P.-H.Belnoue, O.J.Nixon-Pearson, A.J.Thompson, D.S.Ivanov, K.D.Potter, S.R.Hallett, Consolidation-Driven Defect Generation in Thick Composite Parts, Journal of Manufacturing Science and Engineering. 140 (2018) 071006. doi:10.1115/1.4039555.

[70] S.R.Hallett, J.P.-H.Belnoue, O.J.Nixon-Pearson, T.Mesogitis, J.Kratz, D.S.Ivanov, I.K.Partridge, K.D.Potter, Understanding and Prediction of Fibre Waviness Defect Generation, in: Proceedings of the American Society for Composites - 31st Technical Conference, ASC 2016, Lancaster, 2016.

[71] M.Brillant, Out-of-Autoclave Manufacturing of Complex Shape Composite Laminates, McGill University, 2010.

[72] T.J.Dodwell, R.Butler, G.W.Hunt, Out-of-plane ply wrinkling defects during consolidation over an external radius, Composites Science and Technology. 105 (2014) 151–159. doi:10.1016/j.compscitech.2014.10.007.

[73] B.Chen, E.J.Lang, T.-W.Chou, Experimental and theoretical studies of fabric compaction behavior in resin transfer molding, Materials Science and Engineering: A. 317 (2001) 188–196. doi:10.1016/S0921-5093(01)01175-3.

[74] R..Saunders, C.Lekakou, M..Bader, Compression in the processing of polymer composites 1. A mechanical and microstructural study for different glass fabrics and resins, Composites Science and Technology. 59 (1999) 983–993. doi:10.1016/S0266-3538(98)00137-7.

[75] Y.R.Kim, S.P.McCarthy, J.P.Fanucci, Compressibility and relaxation of fiber reinforcements during composite processing, Polymer Composites. 12 (1991) 13–19. doi:10.1002/pc.750120104.

[76] T.Grieser, P.Mitschang, Investigation of the compaction behavior of carbon fiber NCF for continuous preforming processes, Polymer Composites. 38 (2017) 2609–2625. doi:10.1002/pc.23854.

[77] P.Hubert, A.Poursartip, A Review of Flow and Compaction Modelling Relevant to Thermoset Matrix Laminate Processing, Journal of Reinforced Plastics and Composites. 17 (1998) 286–318. doi:10.1177/073168449801700402.

[78] M.Li, Y.Gu, Z.Zhang, Z.Sun, A simple method for the measurement of compaction and corresponding transverse permeability of composite prepregs, Polymer Composites. 28 (2007) 61–70. doi:10.1002/pc.20255.

[79] K.Hall, C.; Ward, C.; Ivanov, D.S.; Potter, The compaction of uncured toughened prepreg laminates in relation to automated forming, in: 15th European Conference on Composite Materials, Venice, 2012.

[80] J.P.-H.Belnoue, O.J.Nixon-Pearson, D.Ivanov, S.R.Hallett, A novel hyper-viscoelastic model for consolidation of toughened prepregs under processing conditions, in: 17th European Conference on Composite Materials, Elsevier Ltd, 2016: pp. 118–134. doi:10.1016/j.mechmat.2016.02.019.

[81] J.P.-H.Belnoue, Predicting Wrinkle Formation in Components Manufactured From Toughened UD Prepreg, in: 17th European Conference on Composite Materials, 17th European Conference on Composite Materials, Munich, 2016.

[82] P.Hallander, J.Sjölander, M.Petersson, M.Åkermo, Interface manipulation towards wrinkle-free forming of stacked UD prepreg layers, Composites Part A: Applied Science and Manufacturing. 90 (2016) 340–348. doi:10.1016/j.compositesa.2016.07.013.

[83] S.B.Truslow, Permanent Press, No Wrinkles: Reinforced Double Diaphragm Forming of Advanced Thermoset Composites, Harvard University, 2000.

[84] K. j.Johnson, R.Butler, E. g.Loukaides, C.Scarth, A. t.Rhead, Stacking sequence selection for defect-free forming of uni-directional ply laminates, Composites Science and Technology. 171 (2019) 34–43. doi:10.1016/j.compscitech.2018.11.048.

[85] J.S.Lightfoot, M.R.Wisnom, K.Potter, A new mechanism for the formation of ply wrinkles due to shear between plies, Composites Part A: Applied Science and Manufacturing. 49 (2013) 139–147. doi:10.1016/j.compositesa.2013.03.002.

[86] P.Hallander, M.Åkermo, C.Mattei, M.Petersson, T.Nyman, M.Akermo, C.Mattei, M.Petersson, T.Nyman, An experimental study of mechanisms behind wrinkle development during forming of composite laminates, Composites Part A: Applied Science and Manufacturing. 50 (2013) 54–64. doi:10.1016/j.compositesa.2013.03.013.

[87] K.Potter, In-plane and out-of-plane deformation properties of unidirectional

preimpregnated reinforcement, Composites Part A: Applied Science and Manufacturing. 33 (2002) 1469–1477. doi:10.1016/S1359-835X(02)00138-0.

[88] Y.-S.Wang, Y.-J.Wu, Epoxy resins with improved burn properties, US 8039109B2, 2011. https://patents.google.com/patent/US20100087582.

[89] Hexcel, HexPly® 8552 Epoxy Matrix - Product Data, n.d. http://www.hexcel.com/Resources/DataSheets/Prepreg-Data-Sheets/8552_us.pdf.

[90] D5528, Standard Test Method for Mode I Interlaminar Fracture Toughness of Unidirectional, ASTM International. (2007). doi:10.1520/D5528-01R07E03.

[91] HexTow ® IM7 Carbon Fiber - Product data sheet, (n.d.). https://www.hexcel.com/user_area/content_media/raw/IM7_HexTow_DataSheet.pdf.

[92] Hexcel, HexPly ® M21 - Product Data Sheet, (n.d.). https://www.hexcel.com/user_area/content_media/raw/HexPly_M21_global_DataSheet.pdf.

[93] H.Y.Sohn, C.Moreland, The effect of particle size distribution on packing density, The Canadian Journal of Chemical Engineering. 46 (1968) 162–167. doi:10.1002/cjce.5450460305.

[94] E.Clarkson, Hexcel 8552 IM7 Unidirectional Prepreg 190 gsm & 35 % RC Qualification Statistical Analysis Report, Wichita, 2011.

[95] G115, Standard Guide for Measuring and Reporting Friction Coefficients, ASTM International. 10 (2018) 1–12. doi:10.1520/G0115-10R18.2.

[96] D.J.Groves, A characterization of shear flow in continuous fibre thermoplastic laminates, Composites. 20 (1989) 28–32. doi:10.1016/0010-4361(89)90678-2.

[97] K.J.Chan, Investigation of Processing Conditions and Viscoelastic Properties on Frictional Sliding Behavior of Unidirectional Carbon Fiber Epoxy Prepreg, Virginia Polytechnic Institute and State University, 2018. https://vtechworks.lib.vt.edu/handle/10919/86444.

[98] J.L.Gorczyca-Cole, J. a.Sherwood, J.Chen, A friction model for thermostamping commingled glass–polypropylene woven fabrics, Composites Part A: Applied Science and Manufacturing. 38 (2007) 393–406. doi:10.1016/j.compositesa.2006.03.006.

[99] D1894, Standard Test Method for Static and Kinetic Coefficients of Friction of Plastic Film and Sheeting, ASTM International. (2001) 2. doi:10.1520/D1894-14.2.

[100] S.R.Morris, C.T.Sun, An investigation of interply slip behaviour in AS4/PEEK at forming temperatures, Composites Manufacturing. 5 (1994) 217–224. doi:10.1016/0956-7143(94)90136-8.

[101] U.Sachs, R.Akkerman, K.Fetfatsidis, E.Vidal-Sallé, J.Schumacher, G.Ziegmann, S.Allaoui, G.Hivet, B.Maron, K.Vanclooster, S.V.Lomov, Characterization of the dynamic friction of woven fabrics: Experimental methods and benchmark results, Composites Part A: Applied Science and Manufacturing. 67 (2014) 289–298. doi:10.1016/j.compositesa.2014.08.026.

[102] K.Vanclooster, Forming of Multilayered Fabric Reinforced Thermoplastic Composites, Katholieke Universiteit Leuven, 2009.

[103] P.Hubert, A.Poursartip, A method for the direct measurement of the fibre bed compaction curve of composite prepregs, Composites Part A: Applied Science and Manufacturing. 32 (2001) 179–187. doi:10.1016/S1359-835X(00)00143-3.

[104] D.Ivanov, Y.Li, C.Ward, K.Potter, Transitional Behaviour of Prepregs in Automated Fibre Deposition Processes, in: 19Th International Conference on Composite Materials Transitional, n.d.

[105] D.H.-J.A.Lukaszewicz, K.Potter, Through-thickness compression response of uncured prepreg during manufacture by automated layup, Proceedings of the Institution of Mechanical Engineers, Part B: Journal of Engineering Manufacture. 226 (2012) 193–202. doi:10.1177/0954405411411817.

[106] P.Hubert, Aspects of flow and compaction of laminated composite shapes during cure, The University of British Colubmia, 1996.

[107] S.Erland, T.J.Dodwell, R.Butler, The Influence of Fibre Angle and Resin Properties on Uncured Interply Shear, in: 17th European Conference on Composite Materials, 2016.

[108] T.G.Gutowski, T.Morigaki, Zhong Cai, The Consolidation of Laminate Composites, Journal of Composite Materials. 21 (1987) 172–188. doi:10.1177/002199838702100207.

[109] T.G.Gutowski, Z.Cai, S.Bauer, D.Boucher, J.Kingery, S.Wineman, Consolidation

Experiments for Laminate Composites, Journal of Composite Materials. 21 (1987) 650–669. doi:10.1177/002199838702100705.

[110] N.Delhaye, A.Poitou, M.Chaouche, Squeeze flow of highly concentrated suspensions of spheres, Journal of Non-Newtonian Fluid Mechanics. 94 (2000) 67–74. doi:10.1016/S0377-0257(00)00130-0.